DISCRETE FIELD STABILITY ANALYSIS OF RIBBED PLATES

A THESIS

Presented to

The Faculty of the Division of

Graduate Studies

By

Dieter Bounin

In Partial Fulfillment

of the Requirements for the Degree

Doctor of Philosophy

in the School of Civil Engineering

Georgia Institute of Technology

August, 1975

DISCRETE FIELD STABILITY ANALYSIS OF RIBBED PLATES

Approved:

R. R. Avent, Chairman

L. Z. Emkin

D. C. Perry

B. J. Goodno

J. A. Aberson

Date approved by Chairman: 8/19/75

ACKNOWLEDGMENTS

The author wishes to express his sincere appreciation to his thesis advisor, Dr. R. R. Avent, for his continued interest, guidance, and encouragement in the completion of this dissertation, as well as for his careful reading and the many important suggestions.

He would also like to thank the members of the reading committee, Dr. L. Z. Emkin, Dr. D. J. Goodno, Dr. D. C. Perry, and Dr. J. A. Aberson, for reading this dissertation and for their valuable suggestions.

The author is deeply indebted to Dr. D. L. Dean, Professor and Head, Civil Engineering Department, North Carolina State University, for his many important suggestions, in particular with respect to the summation of infinite series.

Finally, the author extends his sincere thanks to his wife for her continued understanding, support, and patience during the hard years of graduate study and the writing of this dissertation.

TABLE OF CONTENTS

LIST OF TABLES

LIST OF ILLUSTRATIONS

SUMMARY

Discrete field analyses are used to derive formulas from which the elastic buckling behavior of ribbed plates subjected to uniform longitudinal compression can be determined. The problem is treated by two methods, termed here a micro and macro analysis, respectively. The two methods lead to dissimilar types of equations that have identical numerical solutions.

In the micro analysis the equilibrium and compatibility equations for a typical interior plate-rib juncture element are utilized to generate sets of difference-differential equations. Using infinite Fourier series solutions in the longitudinal direction the dependent variables associated with the x and y coordinates are uncoupled. The rib line forces are expressed in terms of the rib line deformations by boundary force-deformation relations. For the solution to the rib line deformations in the transverse direction finite Fourier series are used. To account for the inhomogeneous boundary conditions in the case of flexible beam boundaries, the equilibrium equations at the boundary rib line are used. In addition, algebraic terms must be added to the finite series solutions for the rib line deformations.

In the macro analysis the compatibility of plate and rib deformations along the rib lines is used to generate sets of summation-integral equations. Continuous plate deformations are found for unit concentrated loads. In the transverse direction these continuous kernel functions are transformed into finite series valid only at the

rib lines. To account for flexible beam side boundaries, the compatibility of plate edge and boundary beam deflections due to total boundary shears is used. The total boundary shears are obtained from deformation solutions for the side simply supported plate plus deformations due to the boundary deflections.

Both types of analyses are utilized for three different mathematical models. The two simple models, the non-composite flexural and the composite membrane analyses, consider out-of-plane and in-plane effects, respectively, and the corresponding plate-rib interactive forces. The third model, the composite membrane-flexural analysis, includes the effects of both simpler models, that is, both flexural and membrane plate action along with complete interaction between plate and ribs.

For both types of analyses the stability equations are in terms of the coefficients of the finite series solutions. The relatively simple stability equations are numerically solved for critical buckling loads. The form and complexity of these equations are independent of the number of ribs in the system. Results are graphically illustrated to show effects of various problem parameters on ribbed plate stability.

CHAPTER I

INTRODUCTION

Interest in ribbed plate structures has been widespread in recent years due to the economic and structural advantages of such systems. Ribbed plate structures are efficient, economical, functional, and readily constructed of most common materials. Applications range from box girder bridges to large-scale roof systems, and from ships to airplanes (see Figure 1).

A typical cross-section of a box girder bridge is shown in Figure 1a. The cross-section will be subjected to bending and torsional moments, shear, and, in the case of a cable stayed bridge (see Figure 1b), to high axial compression. With good approximation the top and bottom flanges, along with the stiffeners of those flanges, will be in uniform compression at points of positive and negative bending moments, respectively. The longitudinal center and boundary beams and the diaphragms, in particular at the ends and at points of intermediate supports, will subdivide the box girder into several segments. Within each of these segments the compression flanges can be treated as ribbed plates simply supported at the ends and having either simple or flexible supports along the sides.

Figure 1c shows the cross-section of another box girder where the stiffeners connect top and bottom flanges. This cross-section can also be analyzed as a ribbed plate subjected to axial compression by modifying the stiffener properties, that is, using symmetric and

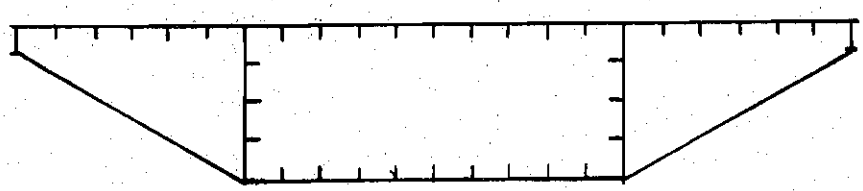

(a) Cross Section of Box Girder Bridge

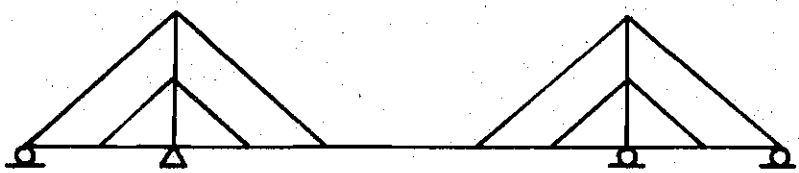

(b) Cable Stayed Bridge

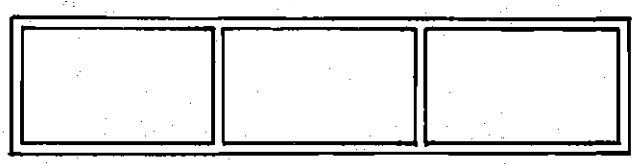

(c) Tubular Box Girder

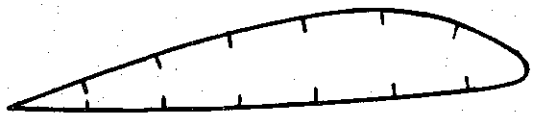

(d) Airplane Wing

Figure 1. Typical Ribbed Plate Structures

anti-symmetric behavior.

A cross-section of an airplane wing is shown in Figure 1d. The skin is stiffened by longitudinal ribs. Despite the curved surface of the skin the analysis of the compression flange as a ribbed plate will serve as a good model for its behavior when the wing is subjected to bending.

The object of this dissertation is to provide a rational stability analysis of ribbed plate structures like those discussed above.

Several methods of analysis are presently available to the design engineer. Most common are approximate methods, for example the orthotropic plate theory, and numerical methods, for example the finite element analysis.

In the orthotropic plate theory the properties of the ribs, like cross-sectional area, eccentricity, bending and torsional stiffnesses, are smeared out with the plate properties, which results in an equivalent continuum. The process of smearing out the rib properties lacks a rational basis. It will be shown in this dissertation, for example, that present assumptions of rib eccentricities and effective bending stiffnesses overestimate the actual ribbed plate properties. Orthotropic plate theory is also unable to predict local behavior, particularly at the plate-rib juncture.

The finite element method requires an amount of preparation and computation which is at least an order of magnitude greater than either the discrete field or the orthotropic plate theory analyses. In addition, there is the same difficulty, as in the orthotropic plate theory, of predicting local behavior, even with a fine mesh. A change of an

important problem parameter, like the number of ribs, would involve a substantial effort of redefining the node points and elements.

Exact analyses of ribbed plates in open and closed form are also available. However, all of these are severely limited in their applications. The exact analyses of the open form approaches require computational efforts that are dependent on the number of ribs in the system. For a large number of ribs they simply become cumbersome and unattractive, that is, their application is limited to a small number of ribs.

The exact closed form analyses presently available are limited to lower order models that do not include membrane effects and that also make restricting assumptions of the effective rib properties. With few exceptions the available methods are restricted to simple side supports.

The purpose of this thesis is to avoid the above cited difficulties and approximations by presenting formulas from which the exact elastic buckling behavior or ribbed plate structures can be determined. The only assumptions are those associated with classical plate and beam theories along with uniform rib spacing and uniform properties of the interior ribs. It should be noted that the equations of this dissertation, while limited to the stability analysis of ribbed plates, can easily be modified for the analysis of forces and deflections of such structures.

1.1 Approach to Solution

Two discrete field stability analyses are formulated, the micro and macro solutions.

Micro Analysis

In the micro solution the equilibrium equations are developed at the typical interior rib-plate juncture. Using a stiffness analysis, the plate and rib panel forces at the rib lines are expressed as functions of the rib line deformations. After consideration of the compatibility of the panel deformations at the rib lines and uncoupling these equations by the use of infinite Fourier series solutions in the longitudinal direction, sets of governing difference equations are developed.

The total solution for the rib line deformations in the transverse direction is obtained through superposition of the solutions for simple side supports and for imposed boundary deformations. For simple side supports these solutions are in the form of finite Fourier series. For imposed boundary deflections, simple algebraic terms must be added to the finite series solution in order to satisfy the inhomogeneous boundary conditions. Before completing the solution for imposed boundary deflections, these algebraic terms are developed into matching finite series.

The total solutions for the rib line deformations are in the form of finite-infinite series, where the continuous variable designates distance along the rib lines and the discrete variable designates the rib line under consideration.

Substitution of the solution series into the governing and boundary equations leads to sets of algebraic equations in terms of the series coefficients. The stability equations are obtained from the resulting eigenvalue problem by setting the determinants of

coefficients of these equations equal to zero. The relatively simple stability equations can easily be solved for buckling loads. The form and complexity of the stability equations are independent of the number of ribs in the system and of the boundary conditions. This enables large systems to be evaluated as easily as small systems.

Macro Analysis

In the macro solution the compatibility of plate and rib deformations at the rib lines is used to generate sets of summation-integral equations. Continuous plate and rib deformations are developed for unit concentrated loads, that is, in the form of kernel function solutions. In the transverse direction the continuous functions for plate deformations have to be transformed into discrete functions, valid only at the rib lines, before they can be substituted into the compatibility equations. Using orthogonality properties of infinite and finite series the summation-integral equations are simplified to sets of algebraic equations.

For the case of flexible beam boundaries another set of algebraic equations is found by matching the deflections at the panel edges. The edge beams are loaded by the total edge shears resulting from the sides simply supported and the imposed boundary deflection cases.

The stability equations for the macro analysis are of similar form as those for the micro analysis, that is, in terms of the coefficients of the series solutions for plate and rib deflections. The transformation of the series solutions from doubly infinite to finite-infinite is achieved by open form summations. For several series a closed form expression can be found. The open form summations converge

rapidly and the numerical sensitivities encountered are as a rule no greater than those in the micro analysis.

For both the micro and macro analyses three different structural models of the ribbed plate are presented. The first two models are special cases of the more complex third model and include only flexural, or out-of-plane, and membrane, or in-plane, plate effects, respectively, and neglect the corresponding plate-rib interactive forces. The third model includes both flexural and membrane plate effects and also complete interaction between plate and ribs.

1.2 Review of Literature

A number of papers have appeared which address the subject of ribbed plate elastic stability. They may be broadly divided into four categories: approximate, open form, finite element, and closed form.

Of the approximate analyses, one approach has been to utilize orthotropic plate theory (16). This method is based on the replacement of the ribbed plate by an equivalent continuum obtained by "smearing out" the rib properties. The resulting non-isotropic continuum model is then solved for critical buckling loads. Since the step of replacing the discrete-continuous system with a continuum lacks a rational basis, significant errors may result especially for configurations with widely spaced ribs.

Various authors have investigated ribbed plate stability by approximating the actual system with a simplified model. Examples of such works include assuming an infinitely wide plate (17), considering only limited buckling modes (15), or similar approximations.

Another approach is to utilize a stiffness or flexibility

analysis to develop a set of simultaneous equations, the number of which is proportional to the number of ribs in the system. For more than two ribs, an open form analysis of this nature requires such complex numerical procedures as to be untenable, even utilizing computers. Timoshenko (19), Barbré (1), and Bleich (2) utilized this approach for simple cases of one or two ribs. However, only non-composite flexural behavior was considered. Wittrick (21) utilized the stiffness method to generate a recursive relationship at a typical rib line which included composite flexural-membrane effects. In each of the above, the large number of simultaneous equations lead to large and complex stability determinants for all but the simplest cases, i.e., one, two, or three-rib systems. The computational difficulties associated with large systems make this procedure impractical for general application.

Another approach in which the same difficulties are encountered is the finite element method (11). While having great freedom with respect to sizes, dimensions, and boundary conditions, the computational difficulties associated with the large number of equations suggests its application only where other solutions are not available.

For regular ribbed plate systems, the most effective approach is a closed form solution. However, only two instances of such a method have been found in the literature. Lokshin (15) developed a difference equation formulation and obtained buckling solutions for a simplified model. He considered only flexural plate action, neglected rib eccentricity and torsion, and considered simply supported boundaries on all sides. Wah (20) extended Lokshin's solution by including torsional rib stiffness and more effectively treating all possible

buckling modes. These results are for very simplified models which do not include effects of rib eccentricity, composite membrane rib-plate interaction, and general side boundary conditions.

Bounin (3) extended the state of the art by developing a more general micro discrete field analysis for axially loaded ribbed plates. While considering the simplified models of a non-composite flexural and a composite membrane solution, effects of rib eccentricity and general side boundary conditions were incorporated into the solution. However, the most general case of a composite membrane-flexural analysis has not been investigated.

The micro approach utilized in this dissertation was developed by Dean and Omid'varan (8) for a deformation analysis of ribbed plates. The more recent macro approach for deformation analyses has been presented by Dean and Abdel-Malek (5), Dean and Avent (6), and Dean and GangaRao (7) considering various aspects of ribbed plate behavior.

1.3 Purpose of Investigation

As illustrated by the review of literature, relatively few investigations have been initiated using exact elastic field analysis techniques for the stability of ribbed plates. In addition, available studies are for simplified mathematical models only. Therefore, the main objectives of this dissertation are threefold: (1) to extend the current state of the art by developing a general composite membrane-flexural micro stability analysis; (2) to introduce, as an alternative, a macro stability analysis for composite membrane-flexural ribbed plates; and (3) to illustrate through numerical studies the effects on stability of various parameters such as rib eccentricity, rib

torsional stiffness, boundary rib effects, rib lateral stiffness, and number of stiffeners, along with an evaluation of the simple and complex models utilized.

A secondary objective is to compare and evaluate the micro and macro solutions as to efficiency and ease of use.

The exact stability analysis of ribbed plate systems presented here using discrete field mechanics techniques is quite general with respect to membrane and flexural plate and rib behavior, rib-plate interaction and side boundary conditions. The analysis is no more complex than approximate procedures in which the actual system is replaced with an equivalent continuum. In addition, the discrete field analysis does not increase in complexity or amount of computations required as the number of ribs are increased. It is believed that the analysis presented here is the first general discrete field stability analysis presented for space structures of any type and that it will have applications in many areas of structural analysis.

1.4 Organization of Presentation

The discrete field stability analyses are presented in four chapters. Chapters II and III treat the micro stability analysis with the basic boundary force-deformation relations for plate and rib panels developed in Chapter II. These relations are required in the micro analysis of Chapter III in which the stability equations for three different structural models of the ribbed plate are derived. Chapters IV and V treat the macro stability analysis. In Chapter IV kernel function and imposed boundary deformation solutions are found for the deflections and edge shears of plates and ribs. These solutions are

used in Chapter V to develop the compatibility equations of plate and rib deformations that lead to the stability equations of the macro approach.

Numerical illustrations of the stability equations are presented in Chapter VI along with detailed explanations of the numerical methods required in their applications.

Along with Chapter VII, which contains the conclusions, two appendices list the symbols used in this dissertation and present some formulas required in the summation of infinite series.

CHAPTER II

MICRO ANALYSIS--BOUNDARY FORCE-DEFORMATION RELATIONS FOR AXIALLY LOADED PLATE AND RIB PANELS

For the discrete field micro analysis of ribbed plates, sets of solutions relating the panel edge forces to the panel edge displacements are needed. These stiffness analyses are performed for panels treated by flexural plate theory as well as by membrane plate theory. Special solutions are found for ribs treated as flat strips with one free edge. Alternate solutions for the ribs are presented based on ordinary beam theory.

2.1 Flexural Plate Panels

For a structure containing flat rectangular panels, the analysis for out-of-plane action requires a set of coefficients relating out-of-plate edge forces to edge deformations. In this section the coefficients are found by performing a flexural plate analysis including axial loading and evaluating the boundary moments and shears for imposed edge displacements.

The plate panel under consideration is shown in Figure 2. The classical governing differential equation for the plate subjected to a uniform longitudinal compression resultant, N, and zero transverse loads is, see Timoshenko (19)

$$\{D_{\sim x}^4 + 2D_{\sim x}^2 D_{\sim y}^2 + (D_{\sim y}^2 + \frac{1}{D} N) D_{\sim y}^2\} w(x,y) = 0 \qquad (1a)$$

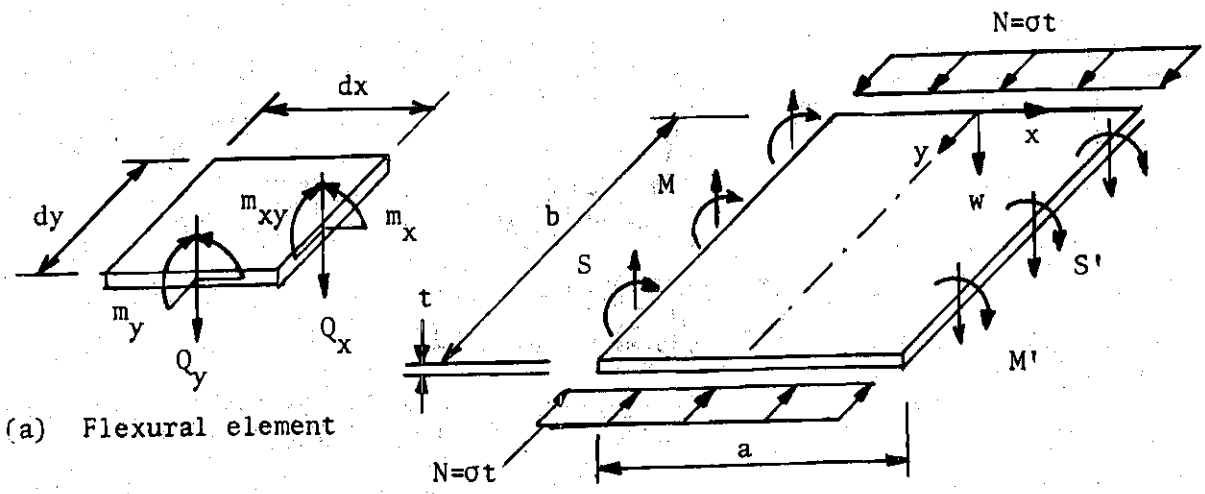

(a) Flexural element

(b) Plate panel

Figure 2. Flexural Plate Panel and Element

where

$$D = \frac{Et^3}{12(1-\nu^2)} \tag{1b}$$

The panel is simply supported out-of-plane at the extremities of the y-coordinate or

$$w(x,\overset{0}{b}) = m_y(x,\overset{0}{b}) = 0 \tag{2a,b}$$

A Levy type solution satisfying these boundary conditions and general boundary conditions along the sides, that is at $x = \pm \frac{a}{2}$, can be expressed as

$$w(x,y) = \sum_{j=1}^{\infty} X_j(x) \sin \bar{\alpha}_j y \tag{3a}$$

where

$$\bar{\alpha}_j = \frac{j\pi}{b} \tag{3b}$$

Substitution of Equation 3 into Equation 1 leads to an ordinary differential equation

$$[D_{\sim x}^4 - 2\bar{\alpha}_j^2 D_{\sim x}^2 + \bar{\alpha}_j^2(\bar{\alpha}_j^2 - \frac{1}{D} N)]X_j(x) = 0 \tag{4}$$

which can be solved for $X_j(x)$ in the following form

$$X_j(x) = \bar{A}_j e^{m_1 x} + \bar{B}_j e^{m_2 x} + \bar{C}_j e^{m_3 x} + \bar{D}_j e^{m_4 x} \tag{5a}$$

where

$$m_{1,2} = \pm \bar{\alpha}_j \sqrt{1 + \frac{1}{\bar{\alpha}_j}\sqrt{\frac{N}{D}}} \quad ; \quad m_{3,4} = \pm \bar{\alpha}_j \sqrt{1 - \frac{1}{\bar{\alpha}_j}\sqrt{\frac{N}{D}}} \tag{5b,c}$$

As can be seen the roots may be either real or imaginary for various values of N. However, the range of N for which buckling occurs is always

$$N > \bar{\alpha}_j^2 D$$

For this case there are pairs of real and imaginary roots and

$$X_j(x) = A_j \sinh(m_1 x) + B_j \cosh(m_1 x) + C_j \sin(m_3 x) + D_j \cos(m_3 x) \tag{6a}$$

where

$$m_{1,3} = \bar{\alpha}_j \sqrt{\frac{1}{\bar{\alpha}_j}\sqrt{\frac{N}{D}} \pm 1} \tag{6b}$$

For $N = \bar{\alpha}_j^2 D$ there are two pairs of real double roots,

$$m_{1,2} = \pm \sqrt{2}\,\bar{\alpha}_j \quad ; \quad m_{3,4} = 0 \tag{7a}$$

and

$$X_j(x) = A_j \sinh(\sqrt{2}\,\bar{\alpha}_j) + B_j \cosh(\sqrt{2}\,\bar{\alpha}_j) + C_j + D_j x \tag{7b}$$

For $N < \bar{\alpha}_j^2 D$ there are four real roots and

$$X_j(x) = A_j \sinh(m_1 x) + B_j \cosh(m_2 x) + C_j \sinh(m_3 x) + D_j \cosh(m_4 x) \tag{8}$$

where m_1 through m_4 are defined in Equation 5.

For the case where there are no axial loads on the plate, the roots are simply

$$m_{1,2,3,4} = \pm \bar{\alpha}_j \tag{9a}$$

and

$$X_j(x) = A_j \sinh(\bar{\alpha}_j x) + B_j \cosh(\bar{\alpha}_j x) + C_j \bar{\alpha}_j x \sinh(\bar{\alpha}_j x) + D_j \bar{\alpha}_j x \cosh(\bar{\alpha}_j x) \tag{9b}$$

The interest here is in obtaining relations between boundary forces and displacements which are related to the displacement function $w(x,y)$. These forces and moments along the panel edges and the panel edge deformations (see Figure 1) also vary sinusoidally and with the same half-wave length b/j as the deflections $w(x,y)$. They can be

expressed as infinite series with respect to the y-coordinate as follows

$$\begin{Bmatrix} \underset{\sim}{D}_x w(-\frac{a}{2},y) \\ \frac{1}{a} w(-\frac{a}{2},y) \\ \underset{\sim}{D}_x w(\frac{a}{2},y) \\ \frac{1}{a} w(\frac{a}{2},y) \end{Bmatrix} = \begin{Bmatrix} \theta(y) \\ W(y) \\ \theta'(y) \\ W'(y) \end{Bmatrix} = \sum_{j=1}^{\infty} \begin{Bmatrix} \theta \\ W \\ \theta' \\ W' \end{Bmatrix}_j \sin \bar{\alpha}_j y \tag{10a}$$

$$\begin{Bmatrix} m_x(-\frac{a}{2},y) \\ Q_x(-\frac{a}{2},y) + \underset{\sim}{D}_y m_{xy}(-\frac{a}{2},y) \\ -m_x(\frac{a}{2},y) \\ Q_x(\frac{a}{2},y) + \underset{\sim}{D}_y m_{xy}(\frac{a}{2},y) \end{Bmatrix} = \begin{Bmatrix} M(y) \\ S(y) \\ M'(y) \\ S'(y) \end{Bmatrix} = \sum_{j=1}^{\infty} \begin{Bmatrix} M \\ S \\ M' \\ S' \end{Bmatrix}_j \sin \bar{\alpha}_j y \tag{10b}$$

where the panel edge moment and shear resultants are, see Timoshenko (19)

$$m_{xy} = D(1-\nu)\underset{\sim}{D}_x \underset{\sim}{D}_y w \tag{10c}$$

$$m_x = -D(\underset{\sim}{D}_x^2 + \nu \underset{\sim}{D}_y^2)w \tag{10d}$$

$$Q_x = -D\underset{\sim}{D}_x(\underset{\sim}{D}_x^2 + \nu \underset{\sim}{D}_y^2)w \tag{10e}$$

$$S_x = -D\underset{\sim}{D}_x[\underset{\sim}{D}_x^2 + (2-\nu)\underset{\sim}{D}_y^2]w \tag{10f}$$

The force-deformation relations for all values of the compression resultant N can be expressed in the following form

$$\begin{Bmatrix} M \\ aS \\ M' \\ aS' \end{Bmatrix}_j = \frac{D}{a} \begin{bmatrix} d_{11} & d_{12} & d_{13} & -d_{14} \\ -d_{12} & -a^2\bar{\alpha}_j^2 d_{22} & -d_{14} & a^2\bar{\alpha}_j^2 d_{24} \\ d_{13} & d_{14} & d_{11} & -d_{12} \\ -d_{14} & -a^2\bar{\alpha}_j^2 d_{24} & -d_{12} & a^2\bar{\alpha}_j^2 d_{22} \end{bmatrix}_j \begin{Bmatrix} \theta \\ W \\ \theta' \\ W' \end{Bmatrix}_j \tag{11}$$

where the Euler coefficients are obtained by use of the side boundary conditions. The stiffness coefficients for the various values of N are:

1. $N > \bar{\alpha}_j^2 D$ (12a)

$$d_{11} = \frac{1}{J_j}(\psi^2 + \zeta^2)(\psi\cosh\psi \sin\zeta - \zeta\sinh\psi \cos\zeta) \tag{12b}$$

$$d_{12} = \frac{1}{J_j}\{(1-\nu)\psi\zeta(\psi^2 - \zeta^2)(\cosh\psi \cos\zeta - 1) + [2\psi^2\zeta^2 + \frac{\nu}{2}(\psi^2 - \zeta^2)^2]\sinh\psi \sin\zeta\} \tag{12c}$$

$$d_{13} = \frac{1}{J_j}(\psi^2 + \zeta^2)(\zeta\sinh\psi - \psi\sin\zeta) \tag{12d}$$

$$d_{14} = \frac{1}{J_j}(\psi^2 + \zeta^2)\psi\zeta(\cosh\psi - \cos\zeta) \tag{12e}$$

$$a^2\bar{\alpha}_j^2 d_{22} = \frac{1}{J_j}(\psi^2 + \zeta^2)\psi\zeta(\psi\sinh\psi \cos\zeta + \zeta\cosh\psi \sin\zeta) \tag{12f}$$

$$a^2\bar{\alpha}_j^2 d_{24} = \frac{1}{J_j}(\psi^2 + \zeta^2)\psi\zeta(\psi\sinh\psi + \zeta\sin\zeta) \tag{12g}$$

$$J_j = (\psi^2 - \zeta^2)\sinh\psi\sin\zeta + 2\psi\zeta(1 - \cosh\psi\cos\zeta) \tag{12h}$$

$$\psi = m_1 a \; ; \; \zeta = m_3 a \qquad (12i,j)$$

where m_1 and m_3 are defined in Equation 6.

2. $N = \bar{\alpha}_j^2 D$ (13a)

$$d_{11} = \frac{1}{J_j} \psi^2(\psi^2 \cosh\psi - \sinh\psi) \qquad (13b)$$

$$d_{12} = \frac{1}{J_j} \psi^3[(1-\nu)(\cosh\psi-1) + \frac{\nu}{2} \psi \sinh \psi] \qquad (13c)$$

$$d_{13} = \frac{1}{J_j} \psi^2(\sinh\psi - \psi) \qquad (13d)$$

$$d_{14} = \frac{1}{J_j} \psi^3(\cosh\psi - 1) \qquad (13e)$$

$$a^2\bar{\alpha}_j^2 d_{22} = a^2\bar{\alpha}_j^2 d_{24} = \frac{1}{J_j} \psi^4 \sinh\psi \qquad (13f,g)$$

$$J_j = \psi^2 \sinh\psi + 2\psi(1 - \cosh\psi) \qquad (13h)$$

where $\psi = \sqrt{2}\, a\bar{\alpha}_j$ (13i)

3. $N < \bar{\alpha}_j^2 D$ (14a)

$$d_{11} = \frac{1}{J_j} (\psi^2 - \zeta^2)(\psi\sinh\zeta \cosh\psi - \zeta\sinh\psi \cosh\zeta) \qquad (14b)$$

$$d_{12} = \frac{1}{J_j} \{\psi\zeta(\psi^2 + \zeta^2)(1-\nu)(\cosh\psi \cosh\zeta - 1) - [2\psi^2\zeta^2 - \frac{\nu}{2} (\psi^2 + \zeta^2)^2]\sinh\psi \sinh\zeta\} \qquad (14c)$$

$$d_{13} = \frac{1}{J_j} (\psi^2 - \zeta^2)(\zeta\sinh\psi - \psi\sinh\zeta) \qquad (14d)$$

$$d_{14} = \frac{1}{J_j} (\psi^2 - \zeta^2)\psi\zeta(\cosh\psi - \cosh\zeta) \qquad (14e)$$

$$a^2\bar{\alpha}_j^2 d_{22} = \frac{1}{J_j}(\psi^2 - \zeta^2)\psi\zeta(\psi\sinh\psi\cosh\zeta - \zeta\sinh\zeta\cosh\psi) \quad (14f)$$

$$a^2\bar{\alpha}_j^2 d_{24} = \frac{1}{J_j}(\psi^2 - \zeta^2)\psi\zeta(\psi\sinh\psi - \zeta\sinh\zeta) \quad (14g)$$

$$J_j = (\psi^2 + \zeta^2)\sinh\psi\sinh\zeta + 2\psi\zeta(1 - \cosh\psi\cosh\zeta) \quad (14h)$$

$$\psi = m_1 a \quad ; \quad \zeta = m_3 a \quad (14i,j)$$

where m_1 and m_3 are defined in Equation 5.

4. For N = 0, the stiffness coefficients as found in reference (8) are

$$d_{22},\ d_{11} = \frac{2\beta_j}{J_j}(\sinh 4\beta_j \pm 4\beta_j) \quad (15a,b)$$

$$d_{24},\ d_{13} = \frac{4\beta_j}{J_j}(2\beta_j\cosh 2\beta_j \pm \sinh 2\beta_j) \quad (15c,d)$$

$$d_{12} = \frac{4\beta_j^2}{J_j}[4(1-\nu)\beta_j^2 + (1+\nu)\sinh^2 2\beta_j] \quad (15e)$$

$$d_{14} = \frac{16}{J_j}\beta_j^3\sinh 2\beta_j \quad (15f)$$

$$J_j = \sinh^2 2\beta_j - 4\beta_j^2 \quad (15g)$$

and $\beta_j = a\bar{\alpha}_j/2$ (15h)

This completes the derivation of the boundary force-deformation equations for flexural plates.

3.2 Membrane Plate Panels

To consider a structure containing flat rectangular panels, an analysis for in-plane action requires a set of coefficients relating

the membrane edge forces to the edge displacements. In order to include axial load effects, the in-plane deformed geometry must be considered thereby leading to a nonlinear differential equation model. Wittrick (21) developed the nonlinear model and by using a linearizing procedure, obtained the desired force-deformation coefficients. A summary of these results are presented in this section.

A plate panel is shown in Figure 3 subjected to membrane forces and axial loads.

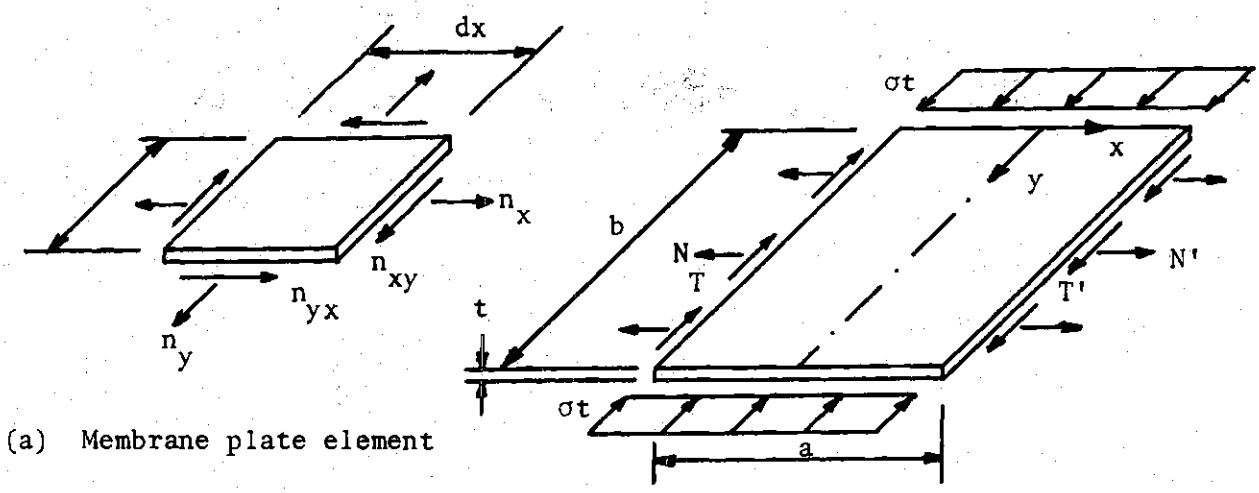

(a) Membrane plate element

(b) Plate panel

Figure 3. Membrane Plate Panel and Element

The set of governing partial differential equations including axial effects and zero in-plane loadings is

$$\begin{bmatrix} 2D_{\sim x}^2 + (1-\nu)\lambda^2 D_{\sim y}^2 & (1+\nu)D_{\sim x}D_{\sim y} \\ (1+\nu)D_{\sim x}D_{\sim y} & (1-\nu)D_{\sim x}^2 + 2\phi^2 D_{\sim y}^2 \end{bmatrix} \begin{Bmatrix} u(x,y) \\ v(x,y) \end{Bmatrix} = \begin{Bmatrix} 0 \\ 0 \end{Bmatrix} \qquad (16a)$$

where

$$\phi^2 = 1 - (1 - \nu^2)\varepsilon \tag{16b}$$

$$\lambda^2 = 1 - 2(1 + \nu)\varepsilon \tag{16c}$$

$$\varepsilon = \frac{\sigma}{E} \tag{16d}$$

and σ is the uniform longitudinal compressive stress in the undeformed state. Note that neglecting ε with respect to unity in Equation 16 would reduce it to the classic linear equation and would mean the entire loss of the destabilizing effect of the compressive stress, σ.

Here the concern is with panels that are simply supported in the plane at the extremities of the y-coordinate, hence a partial statement of the boundary conditions is

$$u(x,\overset{0}{b}) = 0 \quad ; \quad n_y(x,\overset{0}{b}) = -\sigma t \tag{17a,b}$$

Thus, a Levy type solution that satisfies these boundary conditions and that is general with respect to the boundary conditions at $x = \pm \frac{a}{2}$ can be written as

$$u(x,y) = \sum_{j=1}^{\infty} U_j(x) \sin\bar{\alpha}_j y \tag{18a}$$

$$v(x,y) = \sum_{j=0}^{\infty} V_j(x) \cos\bar{\alpha}_j y \tag{18b}$$

Substitution of Equation 18 into Equation 16 yields two ordinary simultaneous differential equations in $U_j(x)$ and $V_j(x)$

$$\begin{bmatrix} \bar{\alpha}_j(1+\nu)D_{\sim x} & (1-\nu)D_{\sim x}^2 - 2\phi^2\bar{\alpha}_j^2 \\ 2D_{\sim x}^2 - (1-\nu)\lambda^2\bar{\alpha}_j^2 & -(1+\nu)\bar{\alpha}_j D_{\sim x} \end{bmatrix} \begin{Bmatrix} U_j(x) \\ V_j(x) \end{Bmatrix} = \begin{Bmatrix} 0 \\ 0 \end{Bmatrix} \tag{19}$$

Utilizing a stress function, $F_j(x)$, defined as

$$U_j(x) = [(1-\nu)D_{\sim x}^2 - 2\phi^2\bar{\alpha}_j^2]F_j(x) \tag{20a}$$

$$V_j(x) = -\bar{\alpha}_j(1+\nu)D_{\sim x}F_j(x) \tag{20b}$$

and substituting the above into Equation 19, results in a scalar equation in the form

$$\{2(1-\nu)D_{\sim x}^4 - [4\phi^2 + (1-\nu)^2\lambda^2 - (1+\nu)^2]\bar{\alpha}_j^2 D_{\sim x}^2 + 2(1-\nu)\lambda^2\phi^2\bar{\alpha}_j^4\}F_j(x) = 0 \tag{21}$$

which is an ordinary differential equation of the fourth order with the same form of the general solution as given in Equation 5 for the flexural plate analysis.

This solution to Equation 21 is substituted into Equations 20a and 20b which in turn are substituted into Equations 19 and 18. Substitution of these displacements into the stress strain relationships results in expressions for the stresses in terms of the integration coefficients A_j through D_j. The stress-strain relationships for these additional stresses and displacements during buckling are identical with those of the linear elastic theory. The equations for n_x and n_{xy} are

$$n_x = K(\underset{\sim}{D}_x u + \nu \underset{\sim}{D}_y v) \tag{22a}$$

$$= K \sum_{j=1}^{\infty} \{-[1 - (1+\nu)\varepsilon](A_j \cosh\phi\bar{\alpha}_j x + C_j \sinh\phi\bar{\alpha}_j y)$$

$$+ \lambda(B_j \cosh\lambda\bar{\alpha}_j x + D_j \sinh\lambda\bar{\alpha}_j y)\}\bar{\alpha}_j \sin\bar{\alpha}_j y \tag{22b}$$

$$n_{xy} = \frac{1-\nu}{2} K(\underset{\sim}{D}_y u + \underset{\sim}{D}_x v) \tag{22c}$$

$$= K \sum_{j=1}^{\infty} \{\phi(A_j \sinh\phi\bar{\alpha}_j x + C_j \cosh\phi\bar{\alpha}_j y)$$

$$- [1 - (1+\nu)\varepsilon](B_j \sinh\lambda\bar{\alpha}_j x + D_j \cosh\lambda\bar{\alpha}_j x)\}\bar{\alpha}_j \cos\bar{\alpha}_j y \tag{22d}$$

where

$$K = \frac{Et}{1-\nu^2} \tag{22e}$$

The integration coefficients have to be evaluated for the general boundary conditions at $x = \pm \frac{a}{2}$. These boundary conditions are expressed in infinite series form and shown below

$$\frac{1}{a}\begin{Bmatrix} u(-\frac{a}{2},y) \\ u(\frac{a}{2},y) \end{Bmatrix} = \begin{Bmatrix} U(y) \\ U'(y) \end{Bmatrix} = \sum_{j=1}^{\infty} \begin{Bmatrix} U_j \\ U'_j \end{Bmatrix} \sin\bar{\alpha}_j y \tag{23a,b}$$

$$\frac{1}{a}\begin{Bmatrix} v(-\frac{a}{2},y) \\ v(\frac{a}{2},y) \end{Bmatrix} = \begin{Bmatrix} V(y) \\ V'(y) \end{Bmatrix} = \sum_{j=0}^{\infty} \begin{Bmatrix} V_j \\ V'_j \end{Bmatrix} \cos\bar{\alpha}_j y \tag{23c,d}$$

$$\begin{Bmatrix} n_x(-\frac{a}{2},y) \\ n_x(\frac{a}{2},y) \end{Bmatrix} = \begin{Bmatrix} N(y) \\ N'(y) \end{Bmatrix} = \sum_{j=1}^{\infty} \begin{Bmatrix} N_j \\ N'_j \end{Bmatrix} \sin\bar{\alpha}_j y \tag{23e,f}$$

$$\begin{Bmatrix} n_{xy}(-\frac{a}{2},y) \\ n_{xy}(\frac{a}{2},y) \end{Bmatrix} = \begin{Bmatrix} T(y) \\ T'(y) \end{Bmatrix} = \sum_{j=0}^{\infty} \begin{Bmatrix} T_j \\ T'_j \end{Bmatrix} \cos\bar{\alpha}_j y \qquad (23g,h)$$

At this point it is convenient to represent the forces and displacements of the panel edges by their symmetric and anti-symmetric components

$$N_j^s = (N_j' + N_j)/2 \qquad N_j^a = (N_j' - N_j)/2 \qquad (24a,b)$$

$$T_j^s = (T_j' - T_j)/2 \qquad T_j^a = (T_j' + T_j)/2 \qquad (24c,d)$$

$$U_j^s = (U_j' - U_j)/2 \qquad U_j^a = (U_j' + U_j)/2 \qquad (24e,f)$$

$$V_j^s = (V_j' + V_j)/2 \qquad V_j^a = (V_j' - V_j)/2 \qquad (24g,h)$$

Evaluating the integration constants at the boundaries and using the symmetric and anti-symmetric components of edge forces and displacements leads to the following force-deformation relations

$$\begin{Bmatrix} N \\ T \\ N' \\ T' \end{Bmatrix}_j = K \begin{bmatrix} -b_{11} & b_{12} & b_{13} & -b_{14} \\ b_{12} & -b_{22} & b_{14} & b_{24} \\ -b_{13} & -b_{14} & b_{11} & b_{12} \\ b_{14} & -b_{24} & b_{12} & b_{22} \end{bmatrix}_j \begin{Bmatrix} U \\ V \\ U' \\ V' \end{Bmatrix}_j \qquad (25a)$$

where

$$b_{11},b_{13} = \lambda\beta_j [\frac{1}{I_j} \cos\phi\beta_j \cosh\lambda\beta_j \pm \frac{1}{I_j'} \sinh\phi\beta_j \sinh\lambda\beta_j] \qquad (25b)$$

$$b_{22},b_{24} = \pm \phi\beta_j [\frac{1}{I_j} \sinh\phi\beta_j \sinh\lambda\beta_j \pm \frac{1}{I_j'} \cosh\phi\beta_j \cosh\lambda\beta_j] \qquad (25c)$$

$$-b_{12} = \beta_j \left[\frac{1}{I_j} \cosh\phi\beta_i \sinh\lambda\beta_i + \frac{1}{I_j'} \sinh\phi\beta_i \cosh\lambda\beta_i - 2(1-\nu)\right] \quad (25d)$$

$$b_{14} = \beta_j \left[\frac{1}{I_j} \cosh\phi\beta_j \sinh\lambda\beta_j - \frac{1}{I_j'} \sinh\phi\beta_j \cosh\lambda\beta_j\right] \quad (25e)$$

$$I_j = (\cosh\phi\beta_j \sinh\lambda\beta_j - \phi\lambda\sinh\phi\beta_j \cosh\lambda\beta_j) \frac{1}{\varepsilon(1-\nu^2)} \quad (25f)$$

$$I_j' = (\sinh\phi\beta_j \cosh\lambda\beta_j - \phi\lambda\cosh\phi\beta_j \sinh\lambda\beta_j) \frac{1}{\varepsilon(1-\nu^2)} \quad (25g)$$

For the case where there are no axial loads on the plate, the above relations can be reduced to a simplified form as found by Dean and Omid'varan (8) to be

$$b_{11}, b_{22} = \frac{1}{G_j} [(3-\nu)\sinh 4\beta_j \pm 4(1+\nu)\beta_j] \quad (26a,b)$$

$$b_{13}, b_{24} = \frac{1}{G_j} [2(3-\nu)\sinh 2\beta_j \pm 4(1+\nu)\beta_j \cosh 2\beta_j] \quad (26c,d)$$

$$b_{12} = \frac{1}{G_j} [(3-\nu)(1-\nu)\sinh^2 2\beta_j - 4(1+\nu)^2\beta_j^2] \quad (26e)$$

$$b_{14} = \frac{1}{G_j} [4(1+\nu)\beta_j \sinh 2\beta_j] \quad (26f)$$

$$G_j = \frac{1}{2(1-\nu)\beta_j} [(3-\nu)^2\sinh^2 2\beta_j - 4(1+\nu)^2\beta_j^2] \quad (26g)$$

2.3 Rib Formulas

Rib Formulas for Out-of-plane Loads

Flat ribs can be considered either as flexural plates with one free edge or as ordinary engineering beams. Both cases will be

considered here and compared numerically in Chapter VI.

Ribs as Flexural Plates. For axially loaded flexural plates with one free edge the force-deformation relations of section 2.1 can be modified by setting $M_j' = S_j' = 0$ in Equation 11. In that case, θ_j' and W_j' can also be eliminated from the same equation which yields

$$\begin{Bmatrix} M \\ aS \end{Bmatrix}_j = \frac{D}{a} \begin{bmatrix} e_{11} & e_{12} \\ -e_{12} & e_{22} \end{bmatrix}_j \begin{Bmatrix} \theta \\ W \end{Bmatrix}_j \tag{27a}$$

where

$$\begin{bmatrix} e_{11} & e_{12} \\ -e_{12} & e_{22} \end{bmatrix}_j = \begin{bmatrix} d_{11} & d_{12} \\ -d_{12} & -4\beta^2 d_{22} \end{bmatrix}_j - \begin{bmatrix} d_{13} & -d_{14} \\ -d_{14} & 4\beta^2 d_{24} \end{bmatrix}_j \begin{bmatrix} d_{11} & -d_{12} \\ -d_{12} & 4\beta^2 d_{22} \end{bmatrix}_j^{-1} \begin{bmatrix} d_{13} & d_{14} \\ -d_{14} & -4\beta^2 d_{24} \end{bmatrix}_j \tag{27b}$$

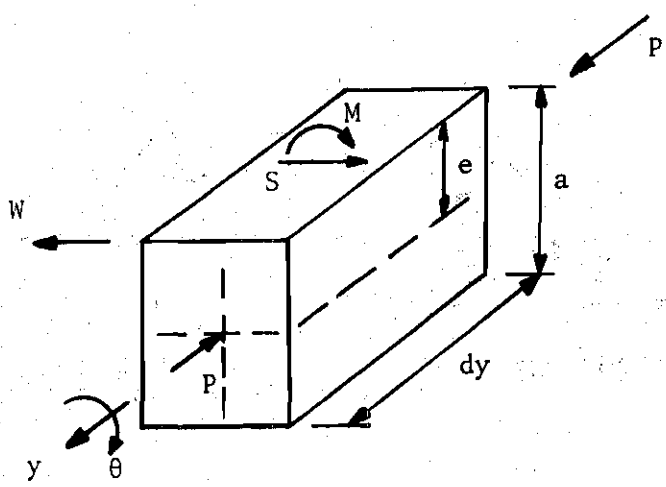

Figure 4. Beam Element for Out-of-plane Loads

Ribs as Ordinary Engineering Beams. Comparable out-of-plane stiffness coefficients for ribs treated by elementary beam theory (see Figure 4) can be derived from the following governing differential equation, see reference (3).

$$\begin{bmatrix} [e^2(B'\underset{\sim}{D}_y^2 + P) - GJ]\underset{\sim}{D}_y^2 & ea(B'\underset{\sim}{D}_y^2 + P)\underset{\sim}{D}_y^2 \\ -ea(B'\underset{\sim}{D}_y^2 + P)\underset{\sim}{D}_y^2 & -a^2(B'\underset{\sim}{D}_y^2 + P)\underset{\sim}{D}_y^2 \end{bmatrix} \begin{Bmatrix} \theta(y) \\ W(y) \end{Bmatrix} = \begin{Bmatrix} M(y) \\ aS(y) \end{Bmatrix} \tag{28}$$

where B' is the flexural rigidity about the minor axis, GJ is the torsional rigidity, e and a are the eccentricity and rib depth respectively, and P is the resultant compressive force.

Substitution of the series solutions for $\theta(y)$, $W(y)$, $M(y)$, and $S(y)$ from Equations 10a,b into Equation 28 and solving for M_j and S_j, the relations from Equation 27a are valid with the following new definitions of the coefficients:

$$e_{11} = e^2(\bar{\alpha}_j^2 B' - P) + GJ \tag{29a}$$

$$e_{12} = ae(\bar{\alpha}_j^2 B' - P) \tag{29b}$$

$$e_{22} = -a^2(\bar{\alpha}_j^2 B' - P) \tag{29c}$$

$$D = a\bar{\alpha}_j^2 \tag{29d}$$

Ribs Subjected to Torsional Moments or Lateral Loads Only. In this case Equation 27a must be modified by setting $S = 0$ and $M = 0$ respectively. Elimination of the appropriate deformation coefficients yields

$$M_j = \frac{D}{a} \frac{e_{11}e_{22} + e_{12}^2}{e_{22}} \theta_j \tag{30a}$$

and

$$S_j = \frac{D}{a^2} \frac{e_{11}e_{22} + e_{12}^2}{e_{11}} W_j \tag{30b}$$

Rib Formulas for In-plane Loads

Again, the ribs will be treated in two ways, as membranes with one free edge and as ordinary beams loaded in the plane of their minor axis (see Figure 5).

Ribs as Membranes. For axially loaded membranes with one free edge the force-deformation relations of section 2.2 can be modified by setting $N_j' = T_j' = 0$ in Equation 25a. Elimination of U_j' and V_j' from the same equations yields

$$\begin{Bmatrix} N \\ T \end{Bmatrix}_j = K \begin{bmatrix} c_{11} & c_{12} \\ c_{12} & c_{22} \end{bmatrix}_j \begin{Bmatrix} U \\ V \end{Bmatrix}_j \tag{31a}$$

where

$$\begin{bmatrix} c_{11} & c_{12} \\ c_{12} & c_{22} \end{bmatrix}_j = \begin{bmatrix} -b_{11} & b_{12} \\ b_{12} & -b_{22} \end{bmatrix}_j - \begin{bmatrix} b_{13} & -b_{14} \\ b_{14} & b_{24} \end{bmatrix}_j \begin{bmatrix} b_{11} & b_{12} \\ b_{12} & b_{22} \end{bmatrix}_j^{-1} \begin{bmatrix} -b_{13} & -b_{14} \\ b_{14} & -b_{24} \end{bmatrix}_j \tag{31b}$$

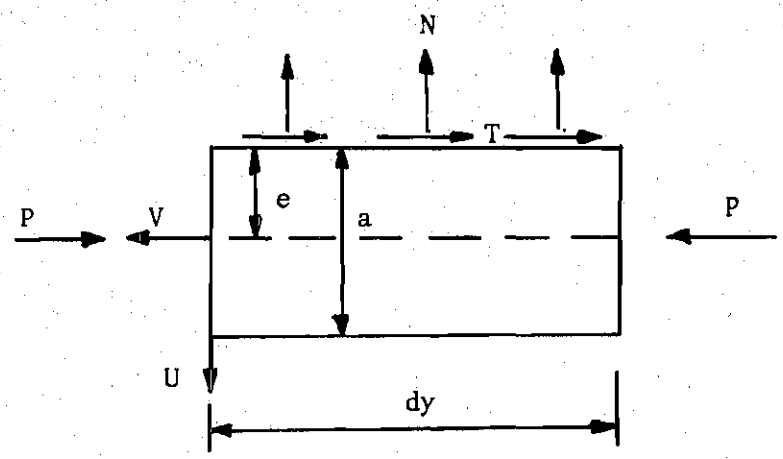

Figure 5. Beam Element for In-plane Loads

Ribs as Ordinary Engineering Beams. Comparable in-plane stiffness coefficients for ribs treated by elementary beam theory (see Figure 5) can be derived from the following governing differential equation, see reference (3)

$$a\begin{bmatrix} -(\rho^2 + e^2)EAD_{\sim y}^4 - PD_{\sim y}^2 & eEAD_{\sim y}^3 \\ eEAD_{\sim y}^3 & -EAD_{\sim y}^2 \end{bmatrix} \begin{Bmatrix} U(y) \\ V(y) \end{Bmatrix} = \begin{Bmatrix} N(y) \\ -T(y) \end{Bmatrix} \tag{32}$$

where P, a, and e are as defined in Equation 28, ρ is the rib radius of gyration about the major axis, and A is the cross sectional area. Substitution of the series solutions for U(y), V(y), N(y), and T(y) from Equation 23 into Equation 32 and solving for N_j and T_j, the relations from Equation 31 are valid with the following new definitions of the coefficients:

$$c_{11} = [-(\rho^2 + e^2)\bar{\alpha}_j^2 + \frac{\sigma}{E}](1-\nu^2)a\bar{\alpha}_j^2 \frac{A}{t} \tag{33a}$$

$$c_{12} = (1-\nu^2)ea\bar{\alpha}_j^3 \frac{A}{t} \tag{33b}$$

$$c_{22} = (1-\nu^2)a\bar{\alpha}_j^2 \frac{A}{t} \tag{33c}$$

Ribs Subjected to Vertical or Longitudinal Loads Only. In this case Equation 31a has to be modified by setting T = 0 and N = 0 respectively. Elimination of the appropriate coefficients yields

$$N_j = K \frac{c_{11}c_{22} - c_{12}^2}{c_{22}} U_j \tag{34a}$$

and

$$T_j = K \frac{c_{11}c_{22} - c_{12}^2}{c_{11}} V_j \tag{34b}$$

This completes the formulas for ribs subjected to out-of-plane and in-plane loads.

CHAPTER III

MICRO STABILITY ANALYSIS OF RIBBED PLATES

The micro stability analysis is the first of the two methods developed in this dissertation. The object is to arrive at simple stability equations for three types of ribbed plate structures: (1) flexural plates stiffened by ribs subjected to vertical and torsional plate-rib interactive forces, neglecting the T-beam or in-plane effects of the plate-rib interaction as well as membrane plate behavior; (2) membrane plates stiffened by ribs subjected to lateral and longitudinal plate-rib interactive forces but neglecting flexural plate behavior and interactive forces; and (3) plates treated by both flexural and membrane theory and having complete interaction with the stiffening ribs. All three types of plates may be simply supported on their two side boundaries or have flexible boundary ribs.

The method of solution will be to use the equilibrium, compatibility, and continuity equations of a typical interior plate-rib juncture element. The forces and deformations at the discrete rib lines will be related to each other by the stiffness coefficients derived in the preceding chapter for this purpose. The equilibrium equations will lead to sets of difference-differential equations that are uncoupled by the use of infinite Fourier series solutions in the longitudinal direction. The solutions for the rib line deformations in the transverse direction are in the form of finite Fourier series. For the case of flexible beam boundaries, solutions will be derived for the

deformations due to imposed boundary deflections. In order to satisfy the inhomogeneous boundary conditions, algebraic terms must be added to the finite series solutions. The solutions for the imposed boundary deformations are also substituted into the governing difference equations. Matching coefficients requires that the algebraic terms be developed into finite series. The total solution consists of the superposition of the solutions for simple side supports and for imposed boundary displacements.

3.1 Non-composite Flexural Analysis

The non-composite flexural analysis of ribbed plates includes the effects of flexural plate action and the two interactive forces between the plate and the ribs shown in Figure 6, that is, shear forces in the z-direction and moments about the y-axis. The ribs are thus subjected to bending about the major axis and to torsion.

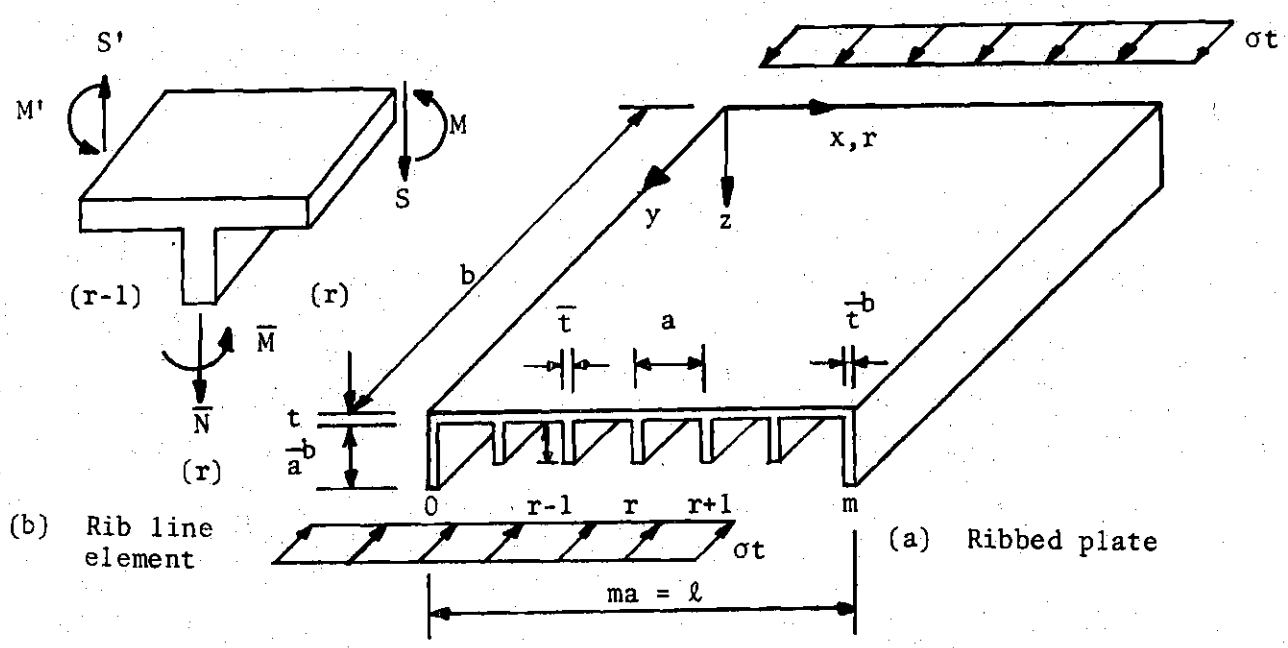

Figure 6. Ribbed Plate Subjected to Axial Compression

Mathematical Model

A stiffness approach is used to express equilibrium of the plate element along the rib lines, as shown in Figure 6a, in terms of the coefficients of rib line rotations and displacements. Equilibrium at the rib line element requires the following relations of the rib line forces

$$M(r,y) + M'(r-1,y) + \bar{M}(r,y) = 0 \tag{35a}$$

$$S(r,y) - S'(r-1,y) + \bar{N}(r,y) = 0 \tag{35b}$$

where $M(r,y)$, $M'(r,y)$, $S(r,y)$, $S'(r,y)$ are the plate boundary moments and shear resultants on the typical panel r between the rib lines r and r+1, and $\bar{M}(r,y)$ and $\bar{N}(r,y)$ are the distributes twisting moments and direct forces transmitted to the rib. These forces are defined in a manner analogous to Equation 10 where they were shown without the discrete variable r, designating the appropriate rib and panel.

$$\begin{Bmatrix} M(r,y) \\ S(r,y) \\ M'(r,y) \\ S'(r,y) \\ \bar{M}(r,y) \\ \bar{N}(r,y) \end{Bmatrix} = \sum_{j=1}^{\infty} \begin{Bmatrix} M(r) \\ S(r) \\ M'(r) \\ S'(r) \\ \bar{M}(r) \\ \bar{N}(r) \end{Bmatrix} \sin\bar{\alpha}_j y \tag{36}$$

Replacement of all quantities in Equations 35a,b by their equivalent series and matching like coefficients results in the following relations between the series coefficients

$$M_j(r) + M'_j(r-1) + \overline{M}_j(r) = 0 \tag{37a}$$

$$S_j(r) - S'_j(r-1) + \overline{N}_j(r) = 0 \tag{37b}$$

The panel force coefficients M_j, M'_j, S_j, S'_j can be expressed in terms of the coefficients of the rib line deflections and rotations by use of the plate stiffness coefficients, Equation 11. The stiffness coefficients used for the ribs, $\overline{M}_j$ and $\overline{N}_j$ are those given by Equations 30a and 34a. Displacement compatibility requires that U_j for the beam in Equation 34a must be replaced by W_j for use in Equation 37b for the rib line, or panel edge deflection, that is

$$\overline{aU}_j(r) = aW_j(r) \tag{38a}$$

whereas

$$\overline{\theta}_j(r) = \theta_j(r) \tag{38b}$$

The necessary relationships are thus:

$$M_j(r) = \frac{D}{a}\left[d_{11}\theta_j(r) + d_{12}W_j(r) + d_{13}\theta_j(r) - d_{14}W'_j(r)\right] \tag{39a}$$

$$M'_j(r-1) = \frac{D}{a}\left[d_{13}\theta_j(r-1) + d_{14}W_j(r-1) + d_{11}\theta'_j(r-1) - d_{12}W'_j(r-1)\right] \tag{39b}$$

$$\overline{M}_j(r) = \frac{\overline{D}}{\overline{a}}\frac{\overline{e}_{11}\overline{e}_{22} + \overline{e}_{12}^{\,2}}{\overline{e}_{22}}\theta_j(r) \tag{39c}$$

$$S_j(r) = \frac{D}{a}\left[-\frac{d_{12}}{a}\theta_j(r) - a\bar{\alpha}_j^2 d_{22} W_j(r) - \frac{d_{14}}{a}\theta_j'(r) + a\bar{\alpha}_j^2 d_{24} W_j'(r)\right] \quad (39d)$$

$$S_j'(r-1) = \frac{D}{a}\left[-\frac{d_{14}}{a}\theta_j(r-1) - a\bar{\alpha}_j^2 d_{24} W_j(r-1) - \frac{d_{12}}{a}\theta_j'(r-1) + a\bar{\alpha}_j^2 d_{22} W_j(r-1)\right] \quad (39e)$$

$$\bar{N}_j(r) = \bar{K}\,\frac{\bar{c}_{11}\bar{c}_{22} - \bar{c}_{12}^{\,2}}{\bar{c}_{22}}\,\frac{a}{\bar{a}}\,W_j(r) \quad (39f)$$

Note also the following expressions of continuity at the rib lines:

$$\theta'(r-1) = \theta(r) \quad (40a)$$

$$W'(r-1) = W(r) \quad (40b)$$

$$\theta'(r) = \theta(r+1) \quad (40c)$$

$$W'(r) = W(r+1) \quad (40d)$$

The set of governing difference equations is obtained by substituting the force deformation equations, Equations 39a-f, into the equilibrium equations, Equations 37a,b, and by introducing Debla, Δ, the second central difference operator, and Multa, $\Box$, the mean difference operator, that is,

$$\Delta_r F(r) = F(r+1) - 2F(r) + F(r-1) \quad (41a)$$

$$\Box_r F(r) = \frac{1}{2}\left[F(r+1) - F(r-1)\right] \quad (41b)$$

The governing difference equations are

$$\begin{bmatrix} d_{13}(\nabla_r - 2\gamma_j) & -2d_{14}\nabla_r \\ -2d_{14}\nabla_r & a^2\bar{\alpha}_j^2 d_{24}(\nabla_r - 2\eta_j') \end{bmatrix} \begin{Bmatrix} \theta_j(r) \\ W_j(r) \end{Bmatrix} = \begin{Bmatrix} 0 \\ 0 \end{Bmatrix} \tag{42a}$$

in which

$$\gamma_j' = -1 - \frac{d_{11}}{d_{13}} - \frac{a\bar{D}}{2\bar{a}Dd_{13}} \cdot \frac{\bar{e}_{11}\bar{e}_{22} + \bar{e}_{12}^2}{\bar{e}_{22}} \tag{42b}$$

$$\eta_j' = -1 + \frac{d_{22}}{d_{24}} - \frac{a\bar{K}}{2\bar{a}\bar{\alpha}_j^2 Dd_{24}} \frac{\bar{c}_{11}\bar{c}_{22} - \bar{c}_{12}^2}{\bar{c}_{22}} \tag{42c}$$

Note that the unbarred quantities refer to plate panel coefficients and that the barred quantities refer to rib panel coefficients.

Solution to the Mathematical Model

The general solution for the non-composite flexural model consists of the superposition of the solution for the simple side support condition and the imposed boundary deflections W(0) and W(m) in the z-direction, which are represented by their symmetric and anti-symmetric components

$$W^s = \frac{1}{2}[W(0) + W(m)] \quad ; \quad W^a = \frac{1}{2}[W(0) - W(m)] \tag{43a}$$

$$W\begin{pmatrix} 0 \\ m \end{pmatrix} = \sum_{j=1}^{\infty} W_j\begin{pmatrix} 0 \\ m \end{pmatrix} \sin\bar{\alpha}_j y \tag{43b}$$

For symmetric and anti-symmetric boundary conditions the total solutions therefore can be written as

$$\begin{Bmatrix} \theta_j^t(r) \\ W_j^t(r) \end{Bmatrix} = \begin{Bmatrix} \theta_j(r) \\ W_j(r) \end{Bmatrix} + W_j^s \begin{Bmatrix} \theta_j^{ws}(r) \\ W_j^{ws}(r) \end{Bmatrix} \tag{44a}$$

and

$$\begin{Bmatrix} \theta_j^t(r) \\ W_j^t(r) \end{Bmatrix} = \begin{Bmatrix} \theta_j(r) \\ W_j(r) \end{Bmatrix} + W_j^a \begin{Bmatrix} \theta_j^{wa}(r) \\ W_j^{wa}(r) \end{Bmatrix} \tag{44b}$$

respectively.

Simple Side Support Boundary Conditions

The first solution will be for all sides simply supported. A statement of the mathematical boundary conditions at y = 0,b is given in Chapter II, Equations 2a,b. For simple supports on the side boundaries the deflection w and the moment resultant m_x must be zero at r = o,m, that is, in terms of the coefficients,

$$W_j(O) = W_j(m) = 0 \tag{45a,b}$$

$$M_j(O) + \bar{M}_j(O) = M_j'(m-1) + \bar{M}_j(m) = 0 \tag{45c,d}$$

Substitution of the appropriate coefficients from Equations 11 and 30a into Equation 45 yields the mathematical statement of the side boundary conditions as

$$d_{13}(\Delta_r - \gamma_j')\theta_j(0) - d_{14}(\Delta_r + \tau_j')W_j(0) = 0 \tag{46a}$$

$$-d_{13}(\nabla_r + \gamma_j')\theta_j(m) - d_{14}(\nabla_r - \tau_j')W_j(m) = 0 \tag{46b}$$

where γ_j' is defined in Equation 42b and

$$\tau_j' = 1 - \frac{d_{12}}{d_{14}} \tag{46c}$$

and

$$\Delta_r F(r) = F(r+1) - F(r) \tag{46d}$$

is the first forward, and

$$\nabla_r F(r) = F(r) - F(r-1) \tag{46e}$$

is the first backward difference operator.

In order to utilize a classical finite series solution form, both the governing and the boundary equations must be conformable. It is thus required that the boundaries be reinforced with ribs whose torsional stiffness is one-half that of the interior ribs, that is, $\bar{M}_j(r)$ in Equation 30a has to be modified to

$$\bar{M}_j\binom{0}{m} = \frac{1}{2}\frac{\bar{D}}{\bar{a}}\frac{\bar{e}_{11}\bar{e}_{22} + \bar{e}_{12}^2}{\bar{e}_{22}}\theta_j\binom{0}{m} \tag{47}$$

The finite Fourier series solutions that satisfy the governing and the boundary equations are

$$\theta_j(r) = \sum_{k=0}^{m} \theta_{jk} \cos \lambda_k r \quad ; \quad \lambda_k = \frac{k\pi}{m} \tag{48a,b}$$

$$W_j(r) = \sum_{k=1}^{m-1} W_{jk} \sin \lambda_k r \tag{48c}$$

Note that the complete expression, for example for $\theta(r,y)$, is a

finite-infinite series as follows:

$$\theta_j(r,y) = \sum_{j=1}^{\infty} \sum_{k=0}^{m} \theta_{kj} \cos \lambda_k r \sin \bar{\alpha}_j y \tag{48d}$$

When substituting Equations 48a,c into Equation 42a, the operators Debla, Δ, and Multa, Ξ, will operate onto the trigonometric terms with the following results

$$\Delta_r \theta_j(r) = -2 \sum_{k=0}^{m} \theta_{jk} \sigma_k \cos \lambda_k r \tag{49a}$$

$$\Delta_r W_j(r) = -2 \sum_{k=1}^{m-1} W_{jk} \sigma_k \sin \lambda_k r \tag{49b}$$

$$\Xi_r \theta_j(r) = - \sum_{k=0}^{m} \theta_{jk} \sin \lambda_k \sin \lambda_k r \tag{49c}$$

$$\Xi_r W_j(r) = \sum_{k=1}^{m-1} W_{jk} \sin \lambda_k \cos \lambda_k r \tag{49d}$$

where

$$\sigma_k = 1 - \cos \lambda_k \tag{49e}$$

Substituting the series expansions for rib line displacements into the governing and boundary equations, Equations 42a and 46a,b, and using the relations of Equations 49a-d, yields, after matching like coefficients,

$$[L^f_{\ell n}] \begin{Bmatrix} \theta_{jk} \\ W_{jk} \end{Bmatrix} = \begin{Bmatrix} 0 \\ 0 \end{Bmatrix} \tag{50a}$$

where

$$[L^f_{\ell n}] = \begin{bmatrix} d_{13}(\sigma_k + \gamma'_j) & d_{14} \sin \lambda_k \\ -d_{14} \sin \lambda_k & a^2\bar{\alpha}_j^2 d_{24}(\sigma_k + \eta'_j) \end{bmatrix} \tag{50b}$$

Buckling Criteria for Sides Simply Supported Case

From Equation 50a, the buckling criteria can be found by solving the eigenvalue problem, i.e., setting the determinant of coefficients equal to zero

$$|L^f_{\ell n}| = a^2\bar{\alpha}_j^2 d_{13}d_{24}(\sigma_k + \gamma'_j)(\sigma_k + \eta'_j) + d_{14}^2\sigma_k(2 - \sigma_k) = 0 \tag{51a}$$

where

$$\sin^2\lambda_k = \sigma_k(2 - \sigma_k) \tag{51b}$$

Equation 51a can be solved for the lowest compressive stress on the ribbed plate. As this critical stress coefficient is included in numerous transcendental terms, an iterative scheme is required. The technique that was found to be both computationally efficient and easy to use was an incremental load procedure. The procedure can be routinely programmed and exhibits no numerical sensitivities, for this case of simply supported sides. Note that the formulation includes the possibility of different axial loads on the plate and ribs.

Special Cases of Ribbed Plates. When the ribs are treated as ordinary beams, the beam stiffness coefficients from Equations 29a-d are used. In that case the buckling criteria $|L^f_{\ell n}| = 0$ can be solved for the axial force on the ribs, P, explicitly, that is,

$$P_{cr} = \left(\frac{j\pi}{b}\right)^2 B + \frac{2D}{a}\left[d_{22} - d_{24}(1 - \sigma_k) - \frac{d_{14}{}^2\sigma_k(2 - \sigma_k)}{a^2\alpha_j^2 d_{13}(\gamma_j' - \sigma_k)}\right] . \quad (52)$$

The first term of this equation is the Euler buckling load of a column with simple end supports. The second term represents the effect of stiffening the ribs by the plate. It reduces to zero as the plate thickness t, and therefore the plate rigidity D, approach zero.

On the other hand, $|L^f_{\ell n}| = 0$ cannot be solved explicitly for the compression resultant N on the plate. However, for negligible rib properties, that is, for an effectively unstiffened plate, one can set $a = \ell$, $W_j = W_j' = 0$, and $\theta_j = -\theta_j'$ in Equation 11. This results in

$$\theta_j = \frac{\ell}{D}\frac{M_j}{d_{11} - d_{13}} \quad (53a)$$

which increases above all bounds for $d_{11} = d_{13}$ or

$$\psi \sin\zeta(\cosh\psi+1) - \zeta \sinh\psi(\cos\zeta+1) = 0 \quad (53b)$$

This equation is satisfied for $\zeta = \pi$ which yields

$$\pi = \ell \frac{j\pi}{b}\sqrt{\frac{1}{\alpha_j}\sqrt{\frac{N}{D}} - 1} \quad (53c)$$

or

$$N_{cr} = K_{cr}\left(\frac{\pi}{\ell}\right)^2 D \tag{53d}$$

where

$$K_{cr} = \left(\frac{b}{j\ell} + \frac{j\ell}{b}\right)^2 \tag{53e}$$

which is the classical solution for the unstiffened, simply supported plate.

Rib Boundaries

An intermediate step required for the case of rib side boundaries is the solution of the ribbed plate system for unknown imposed displacements in the z-direction, $W(^{0}_{m})$, at the boundaries, represented by their symmetric and anti-symmetric components (see Equation 43). The solutions that satisfy the governing equation and the imposed boundary deflection are

$$\theta_j^{ws}(r) = \sum_{k=1,3,\ldots}^{m} \theta_{jk}^{w} \cos \lambda_k r \tag{54a}$$

$$W_j^{ws}(r) = 1 + \sum_{k=1,3,\ldots}^{m-1} W_{jk}^{w} \sin \lambda_k r \tag{54b}$$

$$\theta_j^{wa}(r) = \sum_{k=2,4,\ldots}^{m} \theta_{jk}^{w} \cos \lambda_k r \tag{54c}$$

$$W_j^{wa}(r) = 1 - \frac{2r}{m} + \sum_{k=2,4,\ldots}^{m-1} W_{jk}^{w} \sin \lambda_k r \tag{54d}$$

The Euler coefficients of the displacements can be found by

substituting Equations 54 into Equation 42a. Performing the indicated operations, algebraic terms will arise on the right hand sides which can be expanded into finite series, see Dean (4), as follows:

1. Symmetric terms

$$2(d_{14} - d_{12}) \frac{D}{a^2} (\delta_r^0 - \delta_r^m) = \frac{4}{m} (d_{14} - d_{12}) \frac{D}{a^2} \sum_{k=1,3,\ldots}^{m} \omega_k \cos \lambda_k r \tag{55a}$$

$$2Dd_{24}\eta_j'\bar{\alpha}_j^2 = \frac{4}{m} Dd_{24}\eta_j'\bar{\alpha}_j^2 \sum_{k=1,3,\ldots}^{m-1} \frac{\sin \lambda_k}{\sigma_k} \sin \lambda_k r \tag{55b}$$

2. Anti-symmetric terms

$$(d_{14} - d_{12}) \frac{D}{a^2} (\delta_r^0 + \delta_r^m) - \frac{4}{m} d_{14} \frac{D}{a^2}$$

$$= \frac{4}{m} (d_{14} - d_{12}) \frac{D}{a^2} \sum_{k=0,2,\ldots}^{m} \omega_k \cos \lambda_k r - \frac{4}{m} d_{14} \frac{D}{a^2} \sum_{k=0,2,\ldots}^{m} \delta_k^0 \cos \lambda_k r \tag{55c}$$

$$2Dd_{24}\eta_j'\bar{\alpha}_j^2(1 - \frac{2r}{m}) = \frac{4}{m} Dd_{24}\eta_j'\bar{\alpha}_j^2 \sum_{k=2,4,\ldots}^{m-1} \frac{\sin \lambda_k}{\sigma_k} \sin \lambda_k r \tag{55d}$$

After matching like coefficients the resulting equations for the Euler coefficients of the deformations are

$$[L^f_n] \begin{Bmatrix} \theta^w_{jk} \\ W^w_{jk} \end{Bmatrix} = \frac{4}{m} \begin{Bmatrix} (d_{14} - d_{12})\omega_k \\ a^2\bar{\alpha}_j^2 d_{24}\eta_j' \dfrac{\sin \lambda_k}{\sigma_k} \end{Bmatrix} \tag{56a}$$

where $[L^f_{\ell n}]$ is defined in Equation 50b.

Equation 56a can be solved for θ^w_{jk} and W^w_{jk} to yield

$$\theta^w_{jk} = - \frac{2a^2\bar{\alpha}_j^2 d_{24}}{m|L^f_{\ell n}|} \omega_k \left[d_{14}\eta'_j(2 - \sigma_k) + (d_{12} - d_{14})(\eta'_j + \sigma_k)\right] \quad (56b)$$

$$W^w_{jk} = - \frac{2(2 - \sigma_k)}{m \sin \lambda_k \, |L^f_{\ell n}|} \left[d_{14}(d_{12} - d_{14})\sigma_k + a^2\bar{\alpha}_j^2 d_{13}d_{24}\eta'_j(\gamma'_j + \sigma_k)\right] \quad (56c)$$

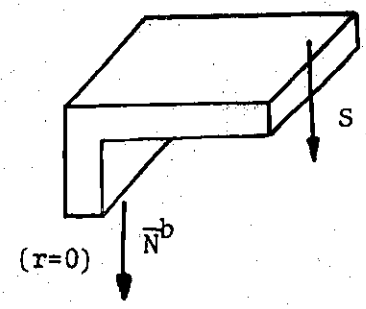

Figure 7. Boundary Rib Line Element for Flexural Analysis

The total solution for the deformations, Equation 44, will thus be complete with the evaluation of W^s_j and W^a_j for the case of flexible beam boundaries. These coefficients are determined by considering equilibrium at the beam boundaries, as shown in Figure 7, for example at r = 0

$$S_j(0) + \bar{N}^b_j(0) = 0 \quad (57)$$

where the superscript b indicates the boundary rib coefficient and $S_j(0)$ is the out-of-plane shear for the combined simple support and imposed unit deflection case. $S_j(0)$ and $\bar{N}^b_j(0)$ are given by Equations 11 and 34a, modified for boundary rib properties.

In terms of the displacements coefficients the boundary equilibrium equation at r = 0 becomes

$$-d_{14}(\Delta_r + \varepsilon_j')\theta_j^t(0) + a^2\bar{\alpha}_j^2 d_{24}(\Delta_r - \eta_j'^b)W_j^t(0) = 0 \tag{58a}$$

where

$$\varepsilon_j' = \frac{d_{14} + d_{12}}{d_{14}} \tag{58b}$$

and

$$\eta_j'^b = -1 + \frac{d_{22}}{d_{24}} - \frac{a}{D\bar{\alpha}_j^2 d_{24}}\left(\frac{\bar{K}}{\bar{a}}\frac{\bar{c}_{11}\bar{c}_{22} - \bar{c}_{12}^2}{\bar{c}_{22}}\right)^b \tag{58c}$$

Substitution of $\theta_j^t(0)$ and $W_j^t(0)$ from Equations 44a,b into Equation 58 yields

$$[\bar{S}_j^s(0) - a^2\bar{\alpha}_j^2 d_{24}\eta_j'^b]W_j^s = -S_j^s(0) \tag{59a}$$

$$[\bar{S}_j^s(0) - a^2\bar{\alpha}_j^2 d_{24}(\eta_j'^b + \frac{2}{m})]W_j^a = -S_j^a(0) \tag{59b}$$

where

$$S_j^s(0) = -d_{14}\sum_{k=1,3,\ldots}^{m}(\varepsilon_j' - \sigma_k)\theta_{jk} + a^2\bar{\alpha}_j^2 d_{24}\sum_{k=1,3,\ldots}^{m-1} W_{jk}\sin\lambda_k \tag{59c}$$

$$\bar{S}_j^s(0) = -d_{14}\sum_{k=1,3,\ldots}^{m}(\varepsilon_j' - \sigma_k)\theta_{jk}^w + a^2\bar{\alpha}_j^2 d_{24}\sum_{k=1,3,\ldots}^{m-1} W_k^w\sin\lambda_k \tag{59d}$$

and k takes on even values only for the anti-symmetric terms $S_j^a(0)$ and $\bar{S}_j^a(0)$. Note that the bar in $\bar{S}_j^s(0)$ and $\bar{S}_j^a(0)$ refers to imposed boundary displacements and not to rib properties.

Buckling Criteria for Rib Boundary Case

The stability criteria is obtained by determining values of the compressive stress for which the total deflection approaches infinity. It can be shown from an examination of Equation 44 that the buckling is governed by the coefficients of W_j^s and W_j^a in Equations 59a,b, that is, the stability equations are

$$\bar{S}_j^s(0) - a^2\bar{\alpha}_j^2 d_{24}\eta_j'^b = 0 \tag{60a}$$

$$\bar{S}_j^a(0) - a^2\bar{\alpha}_j^2 d_{24}(\eta_j'^b + \frac{2}{m}) = 0 \tag{60b}$$

The form of these equations is similar to that of Equation 51a (sides simply supported case) and it can be numerically solved by a similar incremental load procedure. However, note that the inclusion of summations on k require that all odd terms be used in determining symmetric roots and all even k terms be used for determining anti-symmetric roots.

This completes the micro stability analysis of non-composite flexural ribbed plates. Numerical examples are presented in Chapter VI.

3.2 Composite Membrane Analysis

The composite membrane model of ribbed plates includes the effects of membrane action and the two interactive forces between the membrane and the ribs shown in Figure 8, that is, shear forces in the

x and y-directions. The ribs are thus subjected to bending about the major and minor axis and to torsion.

This section complements and follows the same basic steps as the preceding one on the non-composite model. The explanations and derivations therefore will be more concise.

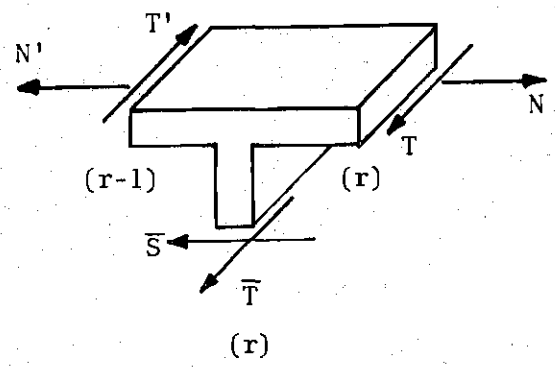

Figure 8. Rib Line Element for Membrane Analysis

Mathematical Model

Equilibrium of the membrane element requires the following relations between the series coefficients for rib line force resultants:

$$N_j(r) - N'_j(r-1) - \bar{S}_j(r) = 0 \tag{61a}$$

$$T_j(r) - T'_j(r-1) + \bar{T}_j(r) = 0 \tag{61b}$$

The force coefficients N_j, N'_j, T_j, T'_j are expressed in terms of the coefficients of the in-plane rib line deflections, Equation 25a. The stiffness coefficients used for the ribs, $\bar{S}_j$ and $\bar{T}_j$ are those given by Equations 30b and 34b. Displacement continuity requires that W_j

and V_j in these equations for the beam must be replaced by U_j and V_j for the membrane, respectively, for use in Equations 61a,b for the rib-line deflections, that is

$$\bar{a}\,\bar{V}_j(r) = a\,V_j(r) \tag{62a}$$

$$\bar{a}\,\bar{W}_j(r) = -a\,U_j(r) \tag{62b}$$

The continuity conditions are:

$$U'(r-1) = U(r) \tag{63a}$$

$$V'(r-1) = V(r) \tag{63b}$$

$$U'(r) = U(r+1) \tag{63c}$$

$$V'(r) = V(r+1) \tag{63d}$$

Substitution of the compatibility, continuity, and force-deformation relations into Equations 61a,b results in the following set of governing difference equations

$$\begin{bmatrix} b_{13}(\Delta_r - 2\gamma_j) & -2b_{14}\Xi_r \\ 2b_{14}\Xi_r & b_{24}(\Delta_r - 2\eta_j) \end{bmatrix} \begin{Bmatrix} U_j(r) \\ V_j(r) \end{Bmatrix} = \begin{Bmatrix} 0 \\ 0 \end{Bmatrix} \tag{64a}$$

in which

$$\gamma_j = -1 + \frac{b_{11}}{b_{13}} - \frac{a\bar{D}}{2\bar{a}\bar{K}b_{13}} \frac{\bar{e}_{11}\bar{e}_{22} + \bar{e}_{12}^{\,2}}{\bar{e}_{11}} \tag{64b}$$

$$\eta_j = -1 + \frac{b_{22}}{b_{24}} - \frac{a\bar{K}}{2\bar{a}\bar{K}b_{24}} \frac{\bar{c}_{11}\bar{c}_{22} - \bar{c}_{12}^2}{\bar{c}_{11}} \tag{64c}$$

Solution to the Mathematical Model

The general solution consists of superposition of the solutions for simple side supports and for imposed boundary deflections in the y-direction, V(0) and V(m), which are represented by their symmetric and anti-symmetric components

$$V^s = \frac{1}{2}[V(0) + V(m)] \qquad V^a = \frac{1}{2}[V(0) - V(m)] \tag{65a,b}$$

$$V(\overset{0}{m}) = \sum_{j=1}^{\infty} V_j(\overset{0}{m}) \sin \bar{\alpha}_j y \tag{65c}$$

For symmetric and anti-symmetric boundary conditions the total solutions therefore are

$$\begin{Bmatrix} U^t(r) \\ V^t(r) \end{Bmatrix} = \begin{Bmatrix} U_j(r) \\ V_j(r) \end{Bmatrix} + V_j^s \begin{Bmatrix} U_j^{vs} \\ V_j^{vs} \end{Bmatrix} \tag{66a}$$

and

$$\begin{Bmatrix} U^t(r) \\ V^t(r) \end{Bmatrix} = \begin{Bmatrix} U_j(r) \\ V_j(r) \end{Bmatrix} + V_j^a \begin{Bmatrix} U_j^{va} \\ V_j^{va} \end{Bmatrix} \tag{66b}$$

Simple Side Support Boundary Condition

A statement of the mathematical boundary conditions at y = 0,b is given in Chapter II, Equations 17a,b. For simple supports on the side boundaries, the deflection v and the force resultant n_x must be

zero at r = 0,m, that is, in terms of the coefficients

$$V_j(0) = V_j(m) = 0 \tag{67a,b}$$

$$N_j(0) - \bar{S}_j(0) = N_j'(m-1) + \bar{S}_j'(m) = 0 \tag{67c,d}$$

Substitution of the appropriate coefficients into Equations 67c,d yields the mathematical statement of the side boundary conditions as

$$b_{13}(\Delta_r - \gamma_j)U_j(0) - b_{14}(\Delta_r + \tau_j)V_j(0) = 0 \tag{68a}$$

$$-b_{13}(\nabla_r + \gamma_j)U_j(m) - b_{14}(\nabla_r - \tau_j)V_j(m) = 0 \tag{68b}$$

where γ_j, Δ_r, and ∇_r are as defined before and

$$\tau_j = 1 - \frac{b_{12}}{b_{14}} \tag{68c}$$

In order to utilize the classical finite series solution form, the governing and the boundary equations have to be conformable. It is therefore required that the boundaries be reinforced with ribs whose lateral bending stiffness is one-half that of the interior ribs, that is, $\bar{S}_j(r)$ in Equation 30b has to be modified to

$$\bar{S}_j\left(\begin{smallmatrix}0\\m\end{smallmatrix}\right) = \frac{1}{2}\frac{\bar{D}}{\bar{a}^2}\frac{\bar{e}_{11}\bar{e}_{22} + \bar{e}_{12}^2}{\bar{e}_{11}}\bar{W}_j\left(\begin{smallmatrix}0\\m\end{smallmatrix}\right) \tag{69a}$$

$$= -\frac{1}{2}\frac{a\bar{D}}{\bar{a}^3}\frac{\bar{e}_{11}\bar{e}_{22} + \bar{e}_{12}^2}{\bar{e}_{11}}U_j\left(\begin{smallmatrix}0\\m\end{smallmatrix}\right) \tag{69b}$$

The finite Fourier series solutions are

$$V_j(r) = \sum_{k=1}^{m-1} V_{jk} \sin \lambda_k r \tag{70a}$$

$$U_j(r) = \sum_{k=0}^{m} U_{jk} \cos \lambda_k r \tag{70b}$$

Substitution into the governing and boundary equations yields

$$[L^m_{\ell n}] \begin{Bmatrix} U_{jk} \\ V_{jk} \end{Bmatrix} = \begin{Bmatrix} 0 \\ 0 \end{Bmatrix} \tag{71a}$$

where

$$[L^m_{\ell n}] = \begin{bmatrix} b_{13}(\gamma_j + \sigma_k) & b_{14} \sin \lambda_k \\ b_{14} \sin \lambda_k & b_{24}(\eta_j + \sigma_k) \end{bmatrix} \tag{71b}$$

Buckling Criteria for Sides Simply Supported Case

From Equation 71a the buckling criteria is found by setting the determinant of coefficients equal to zero, that is,

$$|L^m_{\ell n}| = b_{13}b_{24}(\gamma_j + \sigma_k)(\eta_j + \sigma_k) - b_{14}^2\sigma_k(2 - \sigma_k) \tag{72}$$

This equation is solved for the critical stress in exactly the same manner as Equation 51a for the non-composite flexural model. Comparison of the critical stresses for the flexural and membrane models shows that they are of equal magnitude only for very narrow and thick plates. For all other plates the flexural plate buckling will govern,

that is, for all practical cases under consideration.

Rib Boundaries

The next step in the solution is to solve the membrane with imposed longitudinal boundary displacements, $V(^{0}_{m})$, represented by their symmetric and anti-symmetric components. The solution series for the deformations due to unit boundary displacements, V, are

$$V_j^{vs}(r) = 1 + \sum_{k=1,3,\ldots}^{m-1} V_{jk}^{v} \sin \lambda_k r \tag{73a}$$

$$U_j^{vs}(r) = \sum_{k=1,3,\ldots}^{m} U_{jk}^{v} \cos \lambda_k r \tag{73b}$$

$$V_j^{va}(r) = 1 - \frac{2r}{m} + \sum_{k=2,4,\ldots}^{m-1} V_{jk}^{v} \sin \lambda_k r \tag{73c}$$

$$U_j^{va}(r) = \sum_{k=0,2,\ldots}^{m} U_{jk}^{v} \cos \lambda_k r \tag{73d}$$

To find the Euler coefficients Equations 73a-d are substituted into Equation 64a. The algebraic terms that will arise on the right hand sides will be expanded into finite series as follows:

1. Symmetric terms

$$2(b_{14} - b_{12})(\delta_r^0 - \delta_r^m) = \frac{4}{m}(b_{14} - b_{12}) \sum_{k=1,3,\ldots}^{m} \omega_k \cos \lambda_k r \tag{74a}$$

$$2b_{24}\eta_j = \frac{4}{m} \cdot b_{24}\eta_j \sum_{k=1,3,\ldots}^{m-1} \frac{\sin \lambda_k}{\sigma_k} \sin \lambda_k r \tag{74b}$$

2. Anti-symmetric terms

$$(b_{14} - b_{12})(\delta_r^0 + \delta_r^m) - \frac{4}{m} b_{14} = \frac{4}{m} (b_{14} - b_{12}) \sum_{k=0,2,\ldots}^{m} \omega_k \cos \lambda_k r$$

$$- \frac{4}{m} b_{14} \sum_{k=0,2,\ldots}^{m} \delta_k^0 \cos \lambda_k r \qquad (74c)$$

$$2b_{24}\eta_j(1 - \frac{2r}{m}) = \frac{4}{m} b_{24}\eta_j \sum_{k=2,4,\ldots}^{m} \frac{\sin \lambda_k}{\sigma_k} \sin \lambda_k r \qquad (74d)$$

After matching like coefficients the resulting equations for the Euler coefficients for the displacements are

$$[L_{\ell n}^m] \begin{Bmatrix} U_{jk}^v \\ V_{jk}^v \end{Bmatrix} = \frac{4}{m} \begin{Bmatrix} (b_{14} - b_{12})\omega_k \\ b_{24}\eta_j \dfrac{\sin \lambda_k}{\sigma_k} \end{Bmatrix} \qquad (75)$$

where $[L_{\ell n}^m]$ is defined by Equation 71b. Equation 75 can be solved for U_{jk}^v and V_{jk}^v to yield

$$U_{jk}^v = \frac{2b_{24}\omega_k}{m\ |L_{\ell n}^m|} [b_{14}\eta_j(2 - \sigma_k) + (b_{12} - b_{14})(\eta_j + \sigma_k)] \qquad (76a)$$

$$V_{jk}^v = \frac{-2(2 - \sigma_k)}{m \sin \lambda_k\ |L_{\ell n}^m|} [b_{14}(b_{12} - b_{14})\sigma_k + b_{13}b_{24}\eta_j(\gamma_j + \sigma_k)] \qquad (76b)$$

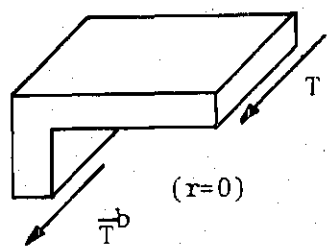

Figure 9. Boundary Rib Line Element for Membrane Analysis

For the total solution consider the equilibrium of forces in the y-direction at the boundaries as shown in Figure 9, for example, at r = 0

$$T_j(0) + \bar{T}_j^b(0) = 0 \tag{77}$$

where $T_j(0)$ is the in-plane shear for the combined simple support and imposed unit deflection cases and is given by Equation 25a. $\bar{T}_j^b(0)$ is given by Equation 34b, modified for boundary rib properties. In terms of the displacement coefficients the boundary equilibrium equation at r = 0 becomes

$$b_{14}(\Delta_r + \epsilon_j)U_j^t(0) + b_{24}(\Delta_r - \eta_j^b)V_j^t(0) = 0 \tag{78a}$$

where

$$\epsilon_j = \frac{b_{14} + b_{12}}{b_{14}} \tag{78b}$$

and

$$\eta_j^b = -1 + \frac{b_{22}}{b_{24}} - \frac{a}{\bar{K}b_{24}}\left(\frac{\bar{K}}{\bar{a}}\,\frac{\bar{c}_{11}\bar{c}_{22} - \bar{c}_{12}^2}{\bar{c}_{11}}\right)^b \tag{78c}$$

Substitution of $U_j^t(0)$ and $V_j^t(0)$ from Equations 66a,b into Equation 78a yields

$$[\bar{T}_j^s(0) - b_{24}\eta_j^b]V_j^s = -T_j^s(0) \tag{79a}$$

$$[\bar{T}_j^a(0) - b_{24}(\eta_j^b + \frac{2}{m})]V_j^a = -T_j^a(0) \tag{79b}$$

where

$$T_j^s(0) = b_{14} \sum_{k=1,3,\ldots}^{m} (\varepsilon_j - \sigma_k) U_{jk} + b_{24} \sum_{k=1,3,\ldots}^{m-1} V_{jk} \sin \lambda_k \quad (79c)$$

$$\overline{T}_j^s(0) = b_{14} \sum_{k=1,3,\ldots}^{m} (\varepsilon_j - \sigma_k) U_{jk}^v + b_{24} \sum_{k=1,3,\ldots}^{m-1} V_{jk}^v \sin \lambda_k \quad (79d)$$

and k takes on even values only for the anti-symmetric terms $T_j^a(0)$ and $\overline{T}_j^a(0)$.

Buckling Criteria for Rib Boundary Case

The buckling criteria is governed by the coefficients of V_j^s and V_j^a in Equations 79a,b, that is, the stability equations are

$$\overline{T}_j^s(0) - b_{24}\eta_j^b = 0 \quad (80a)$$

$$\overline{T}_j^a(0) - b_{24}(\eta_j^b + \frac{2}{m}) = 0 \quad (80b)$$

The form of and the solution to these equations is similar to that of the non-composite flexural model, Equations 60a,b.

This completes the micro stability analysis of composite membrane ribbed plates. Its solution will be included in the next section, the composite membrane-flexural model and in the numerical examples of Chapter VI.

3.3 Composite Membrane-Flexural Analysis

A completely general analysis of a ribbed plate must not only include both membrane and flexural plate effects but also the total interaction between ribs and plate. An element of the rib line

juncture is shown in Figure 10.

Formulas for the composite membrane and non-composite flexural analysis are included in the formulas for the composite membrane-flexural analysis as special cases. Therefore, the results of this section can be used to establish the range of applicability for the simpler models as well as for the approximate, empirical, and open form methods used by other investigators.

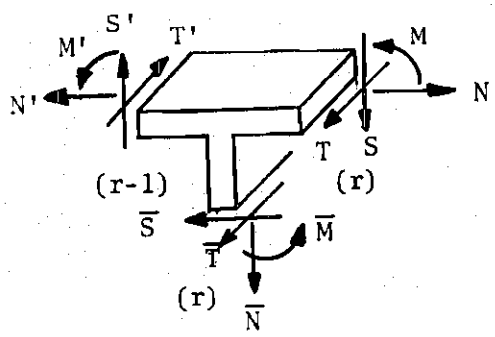

Figure 10. Rib Line Element for Composite Membrane-Flexural Analysis

Mathematical Model

The analysis requires the use of equilibrium equations of the two preceding sections. It will be necessary to refer back to those for definitions and symbols used.

The four equilibrium equations at the rib line juncture, in terms of the coefficients of the force resultants, are:

$$M_j(r) + M'_j(r-1) + \overline{M}_j(r) = 0 \tag{81a}$$

$$N_j(r) - N'_j(r-1) - \overline{S}_j(r) = 0 \tag{81b}$$

$$T_j(r) - T'_j(r-1) + \bar{T}_j(r) = 0 \tag{81c}$$

$$S_j(r) - S'_j(r-1) + \bar{N}_j(r) = 0 \tag{81d}$$

The unbarred force coefficients for the plate panel edges are expressed in terms of the deformation coefficients of the rib line deformations, that is, by use of Equations 11 and 25a. The barred force coefficients for the ribs are given by Equations 27a and 31a.

Substitution of the compatibility, continuity, and force-deformation relations into the equilibrium equations results in the following set of governing difference equations

$$\begin{bmatrix} \frac{D}{a^2} d_{13}(\Delta_r - 2\gamma'_j) & -\frac{\bar{D}}{\bar{a}^2}\bar{e}_{12} & 0 & -2d_{14}\frac{D}{a^2}\Delta_r \\ \frac{\bar{D}}{\bar{a}^2}\bar{e}_{12} & Kb_{13}(\Delta_r - 2\gamma_j) & -2Kb_{14}\Delta_r & 0 \\ 0 & 2Kb_{14}\Delta_r & Kb_{24}(\Delta_r - \eta_j) & \frac{a}{\bar{a}}\bar{c}_{12}\bar{K} \\ -2d_{14}\frac{D}{a^2}\Delta_r & 0 & \frac{a}{\bar{a}}\bar{c}_{12}\bar{K} & D\bar{\alpha}_j^2 d_{24}(\Delta_r - 2\eta'_j) \end{bmatrix} \begin{Bmatrix} \theta_j(r) \\ U_j(r) \\ V_j(r) \\ W_j(r) \end{Bmatrix} = \begin{Bmatrix} 0 \\ 0 \\ 0 \\ 0 \end{Bmatrix} \tag{82a}$$

where

$$\gamma_j = -1 + \frac{b_{11}}{b_{13}} - \frac{a\bar{D}e_{22}}{2\bar{a}^3 Kb_{13}} \tag{82b}$$

$$\gamma'_j = -1 - \frac{d_{11}}{d_{13}} - \frac{a\bar{D}e_{11}}{2\bar{a}Dd_{13}} \tag{82c}$$

$$\eta_j = -1 + \frac{b_{22}}{b_{24}} - \frac{a\overline{Kc}_{22}}{2\bar{a}Kb_{24}} \tag{82d}$$

$$\eta'_j = -1 + \frac{d_{22}}{d_{24}} - \frac{a\overline{Kc}_{11}}{2\overline{a\alpha}_j^2 Dd_{24}} \tag{82e}$$

and $\mathcal{V}_r$ and $\mathcal{E}_r$ are defined as before.

The above equations are completely general with respect to both membrane and flexural plate action and total interaction between plate and ribs.

Solution to the Mathematical Model

The general solution for beam side boundaries will be considered, including the effects of simple side supports superimposed by boundary deflections in the vertical and longitudinal directions. As for the simpler models presented in the two preceding sections, these boundary deflections are represented by their symmetric and anti-symmetric components. For the symmetric components the total solution is

$$\begin{Bmatrix} \theta_j^t(r) \\ U_j^t(r) \\ V_j^t(r) \\ W_j^t(r) \end{Bmatrix} = \begin{Bmatrix} \theta_j(r) \\ U_j(r) \\ V_j(r) \\ W_j(r) \end{Bmatrix} + V_j^s \begin{Bmatrix} \theta_j^V(r) \\ U_j^V(r) \\ V_j^V(r) \\ W_j^V(r) \end{Bmatrix} + W_j^s \begin{Bmatrix} \theta_j^W(r) \\ U_j^W(r) \\ V_j^W(r) \\ W_j^W(r) \end{Bmatrix} \tag{83}$$

For the anti-symmetric components, V_j^s and W_j^s in Equation 83 are replaced by V_j^a and W_j^a respectively.

Simple Side Support Boundary Condition

The first solution will be for simple supports, thus $V_j^s = V_j^a = W_j^s = W_j^a = 0$. Statements of the mathematical boundary conditions at $y = 0,b$ are given by Equations 2 and 17 in Chapter II. For simple supports on the side boundaries the deflections $W(^0_m) = V(^0_m) = 0$ and the force resultants $n_x(^0_m) = m_x(^0_m) = 0$. In terms of the appropriate force coefficients and after substitution of the force-deformation relations, the side boundary conditions are

$$\begin{bmatrix} \frac{D}{a^2} d_{13}(\Delta_r - \gamma_j') & -\frac{\bar{D}}{a^2} \bar{e}_{12} & 0 & -d_{14} \frac{D}{a^2} (\Delta_r + \tau_j') \\ \frac{\bar{D}}{a^2} \bar{e}_{12} & Kb_{13}(\Delta_r - \gamma_j) & -Kb_{14}(\Delta_r + \tau_j) & 0 \\ 0 & 0 & 1 & 0 \\ 0 & 0 & 0 & 1 \end{bmatrix} \begin{Bmatrix} \theta_j(0) \\ U_j(0) \\ V_j(0) \\ W_j(0) \end{Bmatrix} = \begin{Bmatrix} 0 \\ 0 \\ 0 \\ 0 \end{Bmatrix} \tag{84a}$$

$$\begin{bmatrix} -\frac{D}{a^2} d_{13}(\nabla_r + \gamma_j') & -\frac{\bar{D}}{a^2} \bar{e}_{12} & 0 & -d_{14} \frac{D}{a^2} (\nabla_r - \tau_j') \\ \frac{\bar{D}}{a^2} \bar{e}_{12} & -Kb_{13}(\nabla_r + \tau_j) & -Kb_{14}(\nabla_r - \tau_j) & 0 \\ 0 & 0 & 1 & 0 \\ 0 & 0 & 0 & 1 \end{bmatrix} \begin{Bmatrix} \theta_j(m) \\ U_j(m) \\ V_j(m) \\ W_j(m) \end{Bmatrix} = \begin{Bmatrix} 0 \\ 0 \\ 0 \\ 0 \end{Bmatrix} \tag{84b}$$

where γ_j and γ'_j are as defined by Equations 82b,c and all other terms are defined in the two preceding sections.

In order to utilize the classical finite series solution form, both the torsional and lateral bending stiffness of the boundary ribs are required to be one-half that of the interior ribs, see Equations 47 and 69b.

The finite series solutions are given by Equations 48 and 70. Substitution of these series into the governing and boundary equations yields

$$[L_{\ell n}] \begin{Bmatrix} \theta_{jk} \\ U_{jk} \\ V_{jk} \\ W_{jk} \end{Bmatrix} = \begin{Bmatrix} 0 \\ 0 \\ 0 \\ 0 \end{Bmatrix} \tag{85a}$$

where the coefficient matrix $[L_{\ell n}]$ is defined as

$$[L_{\ell n}] = \begin{bmatrix} -2\frac{D}{a^2} d_{13}(\sigma_k+\gamma'_j) & -\frac{\bar{D}}{a^2}\bar{e}_{12} & 0 & -2\frac{D}{a^2} d_{14} \sin \lambda_k \\ \frac{\bar{D}}{a^2}\bar{e}_{12} & -2Kb_{13}(\sigma_k+\gamma_j) & -2Kb_{14} \sin \lambda_k & 0 \\ 0 & -2Kb_{14} \sin \lambda_k & -2Kb_{24}(\sigma_k+\eta_j) & \frac{a}{a}\overline{Kc}_{12} \\ 2\frac{D}{a^2} d_{14} \sin \lambda_k & 0 & \frac{a}{a}\overline{Kc}_{12} & -2D\bar{\alpha}_j^2 d_{24}(\sigma_k+\eta'_j) \end{bmatrix} \tag{85b}$$

Buckling Criteria for Sides Simply Supported Case

From Equation 85a the stability criteria is found by setting the determinant of coefficients equal to zero, that is,

$$|L_{\ell n}| = (L_{11}L_{44} + L_{14}^2)(L_{22}L_{33} - L_{23}^2)$$

$$- L_{34}^2(L_{11}L_{22} + L_{12}^2) + L_{12}(L_{12}L_{33}L_{44} + 2L_{14}L_{23}L_{34}) = 0 \tag{86}$$

This equation is solved for the critical buckling stress in exactly the same manner as the buckling equations for the simpler models. Note the terms L_{12} and L_{34} which couple the effects of the flexural and membrane solutions. For $L_{12} = L_{34} = 0$ these effects are uncoupled and the stability equation reduces to the product of the stability equations for the simpler models.

Rib Boundaries

The solution series for the deformations due to unit boundary displacements in the y and z-directions can be written like those for the simpler models, that is, Equations 54 and 73. They are, for the symmetric behavior,

$$\begin{Bmatrix} \theta_j^{vs}(r) \\ U_j^{vs}(r) \\ \theta_j^{ws}(r) \\ U_j^{ws}(r) \end{Bmatrix} = \sum_{k=1,3,\ldots}^{m} \begin{Bmatrix} \theta_{jk}^{v} \\ U_{jk}^{v} \\ \theta_{jk}^{w} \\ U_{jk}^{w} \end{Bmatrix} \cos \lambda_k r \tag{87a}$$

$$\begin{Bmatrix} V_j^{vs}(r) \\ W_j^{vs}(r) \\ V_j^{ws}(r) \\ W_j^{ws}(r) \end{Bmatrix} = \begin{Bmatrix} 1 \\ 0 \\ 0 \\ 1 \end{Bmatrix} + \sum_{k=1,3,\ldots}^{m-1} \begin{Bmatrix} V_{jk}^{v} \\ W_{jk}^{v} \\ V_{jk}^{w} \\ W_{jk}^{w} \end{Bmatrix} \sin \lambda_k r \tag{87b}$$

To obtain the solution series for the anti-symmetric behavior the unit algebraic quantities in Equation 87b are replaced by $(1 - \frac{2r}{m})$ and the index k takes on even values only.

The Euler coefficients of displacement can be found by substituting separately the imposed v and w solution forms into Equation 85a, performing the indicated operations, expanding the algebraic terms as finite Fourier series (see Equations 55 and 74), and matching like coefficients. The resulting algebraic equations for Euler coefficients of displacement can then be determined from

$$[L_{\ell n}] \begin{Bmatrix} \theta_{jk}^{v} \\ U_{jk}^{v} \\ V_{jk}^{v} \\ W_{jk}^{v} \end{Bmatrix} = \frac{2}{m} \begin{Bmatrix} 0 \\ 2K(b_{14} - b_{12})\omega_k \\ 2Kb_{24}\eta_j \dfrac{\sin \lambda_k}{\sigma_k} \\ -\dfrac{a\overline{Kc}_{12}}{\bar{a}} \dfrac{\sin \lambda_k}{\sigma_k} \end{Bmatrix} \tag{88a}$$

$$[L_{\ell n}]\begin{Bmatrix} \theta^w_{jk} \\ U^w_{jk} \\ V^w_{jk} \\ W^w_{jk} \end{Bmatrix} = \frac{2}{m}\begin{Bmatrix} 2(d_{14} - d_{12})\,\frac{D}{a^2}\,\omega_k \\ 0 \\ -\frac{a\overline{kc}_{12}}{\overline{a}}\,\frac{\sin\lambda_k}{\sigma_k} \\ 2D\overline{\alpha}^2_j d_{24}\eta'_j\,\frac{\sin\lambda_k}{\sigma_k} \end{Bmatrix} \tag{88b}$$

Equations 88a,b represent sets of four simultaneous equations which can be routinely solved. Since numerical computations will require computer solutions, the lengthy explicit solutions for the coefficients θ^v_{jk} through W^w_{jk} are not presented here.

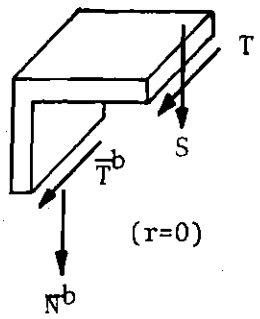

Figure 11. Boundary Rib Plate Element for Composite Membrane-Flexural Analysis

The total solutions for the deformations, Equation 83, will be complete with the evaluation of the coefficients of the imposed boundary deflections. The two simultaneous equilibrium equations used to determine these coefficients are Equations 57 and 77, repeated here for convenience

$$S_j(0) + \bar{N}_j^b(0) = 0 \tag{57}$$

$$T_j(0) + \bar{T}_j^b(0) = 0 \tag{77}$$

In terms of the displacement coefficients the equilibrium equations become

$$[R_{\ell n}] \begin{Bmatrix} V_j^s \\ W_j^s \end{Bmatrix} = - \begin{Bmatrix} T_j^s(0) \\ S_j^s(0) \end{Bmatrix} \tag{89a}$$

where

$$R_{11} = \bar{T}_j^s(0) - b_{24}\eta_j^b \tag{89b}$$

$$R_{12} = b_{14} \sum_{k=1,3,\ldots}^{m} (\varepsilon_j - \sigma_k) U_{jk}^w + b_{24} \sum_{k=1,3,\ldots}^{m-1} V_{jk}^w \sin \lambda_k + a\left(\frac{\overline{Kc}_{12}}{\bar{a}}\right)^b \tag{89c}$$

$$R_{21} = -d_{14} \sum_{k=1,3,\ldots}^{m} (\varepsilon_j' - \sigma_k) \theta_{jk}^v + a^{2-\bar{2}}\alpha_j d_{24} \sum_{k=1,3,\ldots}^{m-1} W_{jk}^w \sin \lambda_k + \frac{a^3}{D}\left(\frac{\overline{Kc}_{12}}{\bar{a}}\right)^b \tag{89d}$$

$$R_{22} = \bar{S}_j^s(0) - a^{2-\bar{2}}\alpha_j d_{24}\eta_j'^b \tag{89e}$$

and the terms $T_j^s(0)$, $\overline{T}_j^s(0)$, $S_j^s(0)$, and $\overline{S}_j^s(0)$ are as defined in Equations 79c,d and 59c,d respectively, except that the coefficients of deformations due to simple supports and imposed boundary deflections in those equations are derived from Equations 85 and 88.

Buckling Criteria for Rib Boundary Case

The stability criteria, in analogy to the two preceding sections, is that the determinant of coefficients equals zero, that is,

$$|R_{\ell n}| = 0 \tag{90}$$

This completes the micro stability analysis. Numerical examples are presented in Chapter VI.

CHAPTER IV

MACRO ANALYSIS--KERNEL FUNCTION AND IMPOSED BOUNDARY DEFORMATION SOLUTIONS FOR AXIALLY LOADED PLATES AND RIBS

For the discrete field macro analysis of a ribbed plate sets of solutions for the response to out-of-plane loads and in-plane loads are required. The formulas are for the plate deformations along the stringer center lines and for the side boundary shears for the cases of: (1) unit out-of-plane and in-plane loads and moments; and (2) imposed out-of-plane and in-plane boundary deflections.

4.1 Flexural Plate Solutions

For the analysis of a ribbed plate with significant out-of-plane and negligible in-plane stiffness one requires solutions for the flexural response to out-of-plane loads.

Mathematical Model

The same classical plate solution will be used for the macro analysis as for the micro analysis (see Chapter II and Figure 12). The governing differential equation is

$$[(D_{\sim x}^2 + D_{\sim y}^2)^2 + \frac{N}{D} D_{\sim y}^2]w(x,y) = \frac{1}{D} q(x,y) \qquad (91)$$

For both sets of solutions the boundary conditions at the ends are

$$w(x,{}^0_b) = m_y(x,{}^0_b) = 0 \qquad (92a,b)$$

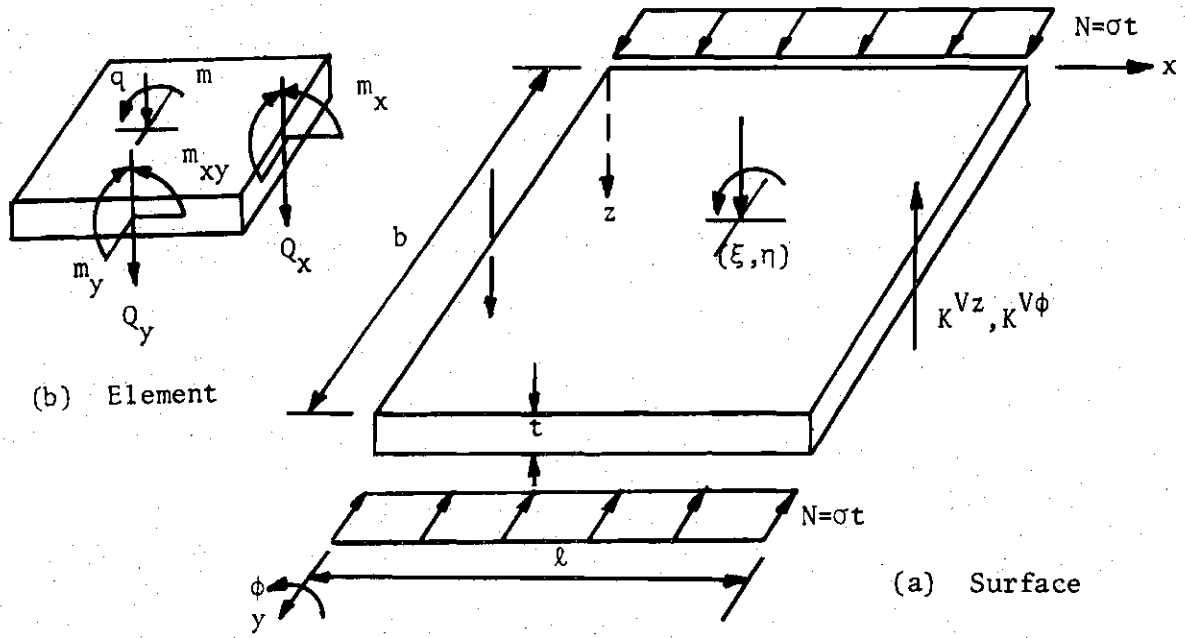

Figure 12. Flexural Plate Action

Simple Side Supports

The formulas for the deflections and shears will be derived for unit concentrated loads and moments, that is, kernel or Green's functions will be used. The kernel function is the particular solution for the displacement w at a point (x,y) due to a unit concentrated load or impulse load, applied at a point (ξ,η) in the z-direction. The unit impulse load is denoted by $\delta(x-\xi)\delta(y-\eta)$ where δ is the Dirac delta function in the continuous case. In other words, $K^{wz}(x,y,\xi,\eta)$ is found from

$$[(\underset{\sim}{D}_x^2 + \underset{\sim}{D}_y^2) + \frac{N}{D}\underset{\sim}{D}_y^2]K^{wz}(x,y,\xi,\eta) = \delta(x-\xi)\delta(y-\eta)\frac{1}{D} \qquad (93)$$

The kernel function for the displacement w due to a unit concentrated moment acting about an axis parallel to the y-axis, that is, parallel to the rib lines, is denoted by $K^{w\phi}(w,y,\xi,\eta)$. It can be obtained by differentiating the kernel function for w due to a concentrated load, that is,

$$K^{w\phi}(x,y,\xi,\eta) = \underset{\sim}{D}_{\xi} K^{wz}(x,y,\xi,\eta) \tag{94a}$$

The kernel functions for the rotation θ about an axis parallel to the y-axis due to unit concentrated loads and moments are denoted by $K^{\theta z}(x,y,\xi,\eta)$ and $K^{\theta\phi}(x,y,\xi,\eta)$. They can be obtained by differentiating the other two kernel functions, that is,

$$K^{\theta z}(x,y,\xi,\eta) = \underset{\sim}{D}_{x} K^{wz}(x,y,\xi,\eta) \tag{94b}$$

$$K^{\theta\phi}(x,y,\xi,\eta) = \underset{\sim}{D}_{x} K^{w\phi}(x,y,\xi,\eta) \tag{94c}$$

Since the plate is simple supported on the sides the side boundary conditions are

$$w(\overset{0}{\ell},y) = m_x(\overset{0}{\ell},y) = 0 \tag{95a,b}$$

In terms of the kernel functions these boundary conditions are

$$K^{wz}(\overset{0}{\ell},y,\xi,\eta) = (\underset{\sim}{D}_{x}^2 + \nu \underset{\sim}{D}_{y}^2) K^{wz}(\overset{0}{\ell},y,\xi,\eta) = 0 \tag{96a}$$

$$K^{w\phi}(\overset{0}{\ell},y,\xi,\eta) = (\underset{\sim}{D}_{x}^2 + \nu \underset{\sim}{D}_{y}^2) K^{w\phi}(\overset{0}{\ell},y,\xi,\eta) = 0 \tag{96b}$$

The kernel functions and the unit loads can be expressed as doubly infinite sinusoidal series as follows:

$$K^{wz}(x,y,\xi,\eta) = \frac{4}{\ell b} \sum_{j=1}^{\infty} \sum_{i=1}^{\infty} \overset{*}{C}_{ij} \sin\alpha_i\xi \sin\bar{\alpha}_j\eta \sin\alpha_i x \sin\bar{\alpha}_j y \tag{97a}$$

$$K^{w\phi}(x,y,\xi,\eta) = \frac{4}{\ell b} \sum_{j=1}^{\infty} \sum_{i=0}^{\infty} \overset{*}{\omega}_i \overset{*}{D}_{ij} \cos\alpha_i\xi \sin\bar{\alpha}_j\eta \sin\alpha_i x \sin\bar{\alpha}_j y \tag{97b}$$

$$K^{\theta z}(x,y,\xi,\eta) = \frac{4}{\ell b} \sum_{j=1}^{\infty} \sum_{i=0}^{\infty} \overset{*}{\omega}_i \overset{*}{D}_{ij} \sin\alpha_i\xi \sin\bar{\alpha}_j\eta \cos\alpha_i x \sin\bar{\alpha}_j y \quad (97c)$$

$$K^{\theta\phi}(x,y,\xi,\eta) = \frac{4}{\ell b} \sum_{j=1}^{\infty} \sum_{i=0}^{\infty} \overset{*}{\omega}_i \overset{*}{R}_{ij} \cos\alpha_i\xi \sin\bar{\alpha}_j\eta \cos\alpha_i x \sin\bar{\alpha}_j y \quad (97d)$$

$$q^z(x,y) = \delta(x-\xi)\delta(y-\eta)$$

$$= \frac{4}{\ell b} \sum_{j=1}^{\infty} \sum_{i=1}^{\infty} \sin\alpha_i\xi \sin\bar{\alpha}_j\eta \sin\alpha_i x \sin\bar{\alpha}_j y \quad (97e)$$

$$q^{\phi}(x,y) = \delta(x-\xi)\delta(y-\eta)$$

$$= \frac{4}{\ell b} \sum_{j=1}^{\infty} \sum_{i=1}^{\infty} \cos\alpha_i\xi \sin\bar{\alpha}_j\eta \sin\alpha_i x \sin\bar{\alpha}_j y \quad (97f)$$

where

$$\overset{*}{\omega}_i = 1 - \frac{1}{2}\delta_i^0 \quad ; \quad \alpha_i = \frac{i\pi}{\ell} \quad ; \quad \bar{\alpha}_j = \frac{j\pi}{b} \quad (97g,h,i)$$

Substitution of Equations 97a-f into Equation 91 and matching like coefficients yields

$$\overset{*}{C}_{ij} = \frac{1}{D} \cdot \frac{1}{(\alpha_i^2 + \bar{\alpha}_j^2)^2 - \frac{N}{D}\bar{\alpha}_j^2} \quad (98a)$$

$$\overset{*}{D}_{ij} = \alpha_i \overset{*}{C}_{ij} = \frac{1}{D} \frac{\alpha_i}{(\alpha_i^2 + \bar{\alpha}_j^2)^2 - \frac{N}{D}\bar{\alpha}_j^2} \quad (98b)$$

$$\overset{*}{R}_{ij} = \alpha_i \overset{*}{D}_{ij} = \frac{1}{D} \frac{\alpha_i^2}{(\alpha_i^2 + \bar{\alpha}_j^2)^2 - \frac{N}{D}\bar{\alpha}_j^2} \quad (98c)$$

where the * is used to indicate coefficients of doubly infinite series.

The kernel function solutions for the shear resultants due to unit impulse load and moment, physically identified only at the boundaries $x = 0,\ell$, are given by the force-deformation relations, see Chapter II, Equation 10f.

$$K^{Vz}(x,y,\xi,\eta) = -D\underset{\sim}{D}_x[\underset{\sim}{D}_x^2 + (2-\nu)\underset{\sim}{D}_y^2]K^{wz}(x,y,\xi,\eta) \tag{99a}$$

$$= \frac{4}{\ell b}\sum_{j=1}^{\infty}\sum_{i=1}^{\infty} Q_{ij}^{*z} \sin\alpha_i\xi \sin\bar{\alpha}_j\xi \cos\alpha_i x \sin\bar{\alpha}_j y \tag{99b}$$

$$K^{V\phi}(x,y,\xi,\eta) = -D\underset{\sim}{D}_x[\underset{\sim}{D}_x^2 + (2-\nu)\underset{\sim}{D}_y^2]K^{w\phi}(x,y,\xi,\eta) \tag{99c}$$

$$= \frac{4}{\ell b}\sum_{j=1}^{\infty}\sum_{i=1}^{\infty} Q_{ij}^{*\phi} \cos\alpha_i\xi \sin\bar{\alpha}_j\eta \cos\alpha_i x \sin\bar{\alpha}_j y \tag{99d}$$

The coefficients Q_{ij}^{z} and Q_{ij}^{ϕ} are obtained by substituting Equations 97a,b into Equations 99a,c respectively, making use of Equations 98a-c, and matching coefficients. This results in

$$Q_{ij}^{*z} = \frac{\alpha_i[\alpha_i^2 + (2-\nu)\bar{\alpha}_j^2]}{(\alpha_i^2 + \bar{\alpha}_j^2)^2 - \frac{N}{D}\bar{\alpha}_j^2} \tag{100a}$$

$$Q_{ij}^{*\phi} = \alpha_i Q_{ij}^{*z} = \frac{\alpha_i^2[\alpha_i^2 + (2-\nu)\alpha_j^2]}{(\alpha_i^2 + \bar{\alpha}_j^2)^2 - \frac{N}{D}\bar{\alpha}_j^2} \tag{100b}$$

By inspecting the coefficient $Q_{ij}^{*\phi}$ it is obvious that Equation 99d represents a diverging series with respect to i and therefore cannot be used. The problem arises, in effect, from a total of four

differentiations on a coefficient that was obtained from a fourth order differential equation. A solution to this problem lies in an improved loading term, Equation 97f, see Lee (14).

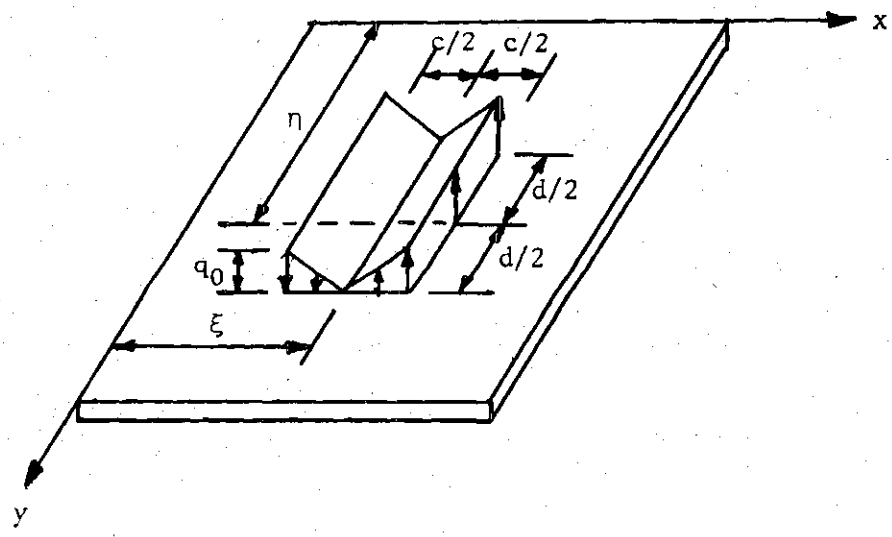

Figure 13. Loading Producing Moment About y Axis

Consider a loading such as shown in Figure 13. The resultant moment of this loading about an axis parallel to the y-axis is given by

$$M = \frac{1}{6} q_0 dc^2 \quad \text{or} \quad q_0 = \frac{6M}{dc^2} \tag{101a,b}$$

The loading can be expressed as doubly infinite series of the form

$$q(x,y) = \sum_{i=1}^{\infty} \sum_{j=1}^{\infty} q^*_{ij} \sin\alpha_i x \sin\bar{\alpha}_j y \tag{102a}$$

where $\overset{*}{q}_{ij}$ is given by

$$\overset{*}{q}_{ij} = \frac{4}{\ell b}\int_{\eta-\frac{d}{2}}^{\eta+\frac{d}{2}}\int_{\xi-\frac{c}{2}}^{\xi+\frac{c}{2}} \frac{2q_0}{c}(x-\xi)\ \sin\alpha_i x\ \sin\bar{\alpha}_j y\ dxdy \qquad (102b)$$

Integration and setting M = 1 results in

$$\overset{*}{q}_{ij} = \frac{192}{\ell b c^3 d}\cdot\frac{\sin\alpha_i\frac{c}{2} - \alpha_i\frac{c}{2}\cos\alpha_i\frac{c}{2}}{\alpha_i^2\bar{\alpha}_j}\sin\bar{\alpha}_j\frac{d}{2}\cos\alpha_i\xi\ \sin\bar{\alpha}_j\eta \qquad (102c)$$

Substitution of Equation 102c into Equation 102a, the result into Equation 91, and then using the same steps as outlined before results in the following new expressions for $\overset{*}{D}_{ij}$ and $\overset{*\phi}{Q}_{ij}$

$$\overset{*}{D}_{ij} = \frac{48(\sin\alpha_i\frac{c}{2} - \alpha_i\frac{c}{2}\cos\alpha_i\frac{c}{2})\sin\bar{\alpha}_j\frac{d}{2}}{Dc^3 d\alpha_i^2\bar{\alpha}_j\ [(\alpha_i^2+\bar{\alpha}_j^2)^2 - \frac{N}{D}\bar{\alpha}_j^2]} \qquad (103a)$$

$$\overset{*\phi}{Q}_{ij} = \frac{48}{c^3 d}(\sin\alpha_i\frac{c}{2} - \alpha_i\frac{c}{2}\cos\alpha_i\frac{c}{2})\sin\bar{\alpha}_j\frac{d}{2}$$

$$\times\frac{[\alpha_i^2 + (2-\nu)\bar{\alpha}_j^2]}{\alpha_i\bar{\alpha}_j[(\alpha_i^2+\bar{\alpha}_j^2)^2 - \frac{N}{D}\bar{\alpha}_j^2]} \qquad (103b)$$

Using Equation 103b the double series in Equation 99d will converge. If desired, $\overset{*}{R}_{ij}$ in Equation 98c can be redefined as $\overset{*}{R}_{ij} = \alpha_i\overset{*}{D}_{ij}$ using Equation 103a as the definition for $\overset{*}{D}_{ij}$, that is, the coefficient $\overset{*}{R}_{ij}$ will be

$$\overset{*}{R}_{ij} = \frac{48(\sin\alpha_i \frac{c}{2} - \alpha_i \frac{c}{2}\cos\alpha_i \frac{c}{2})\sin\bar{\alpha}_j \frac{d}{2}}{Dc^3 d\alpha_i \bar{\alpha}_j [(\alpha_i^2 + \bar{\alpha}_j^2)^2 - \frac{N}{D}\bar{\alpha}_j^2]} \tag{103c}$$

Imposed Boundary Displacements

The solution $w^h(x,y)$ for the deflection due to the imposed boundary displacements must satisfy the homogeneous Equation 91, that is, for $q(x,y) = 0$. The imposed boundary deflections can be written in series form as

$$w^h(\overset{0}{\ell},y) = \sum_{j=1}^{\infty} (W_j^s \pm W_j^a)\sin\bar{\alpha}_j y \tag{104}$$

The other side boundary condition is

$$m_x^h(\overset{0}{\ell},y) = (\underset{\sim}{D}_x^2 + \nu\underset{\sim}{D}_y^2)w^h(\overset{0}{\ell},y) = 0 \tag{105}$$

The solutions for $w^h(x,y)$ that satisfies these boundary conditions can be expressed as a doubly infinite series, plus algebraic terms to account for the inhomogeneous boundary conditions, as follows

$$w^h(x,y) = \frac{4}{\ell}\sum_{j=1}^{\infty}\sum_{i=1}^{\infty} \overset{*}{\bar{W}}_{ij}\,\overset{*}{\bar{C}}_{ij}\sin\alpha_i x \sin\bar{\alpha}_j y \tag{106a}$$

$$= \sum_{j=1}^{\infty} \{[1 - \frac{\nu}{2}\bar{\alpha}_j^2 x(\ell-x)]W_j^s + (1 - \frac{2x}{\ell})[1 - \frac{\nu}{6}\bar{\alpha}_j^2 x(\ell-x)]W_j^a$$

$$+ \frac{4}{\ell}\sum_{i=1}^{\infty} (\overset{*}{\bar{C}}_{ij} - \overset{*}{\bar{E}}_{ij})\overset{*}{\bar{W}}_{ij}\sin\alpha_i x\}\sin\bar{\alpha}_j y \tag{106b}$$

where

$$\overset{*}{\overline{W}}_{ij} = \begin{cases} W_j^s & \text{for i odd} \\ W_j^a & \text{for i even} \end{cases} \tag{106c}$$

The coefficients are determined through substitution of Equation 106b into Equation 91. The results are

$$\overset{*}{\overline{C}}_{ij} - \overset{*}{E}_{ij} = \frac{\overline{\alpha}_j^2\{\overline{\alpha}_j^2[(2\nu-1)\alpha_i^2 + \nu\overline{\alpha}_j^2] + \frac{N}{D}(\alpha_i^2 - \nu\overline{\alpha}_j^2)\}}{\alpha_i^3[(\alpha_i^2 + \overline{\alpha}_j^2)^2 - \frac{N}{D}\overline{\alpha}_j^2]} \tag{107a}$$

$$\overset{*}{E}_{ij} = \frac{1}{\alpha_i^3}(\alpha_i^2 - \nu\overline{\alpha}_j^2) \tag{107b}$$

$$\overset{*}{\overline{C}}_{ij} = \frac{\alpha_i[\alpha_i^2 + (2-\nu)\overline{\alpha}_j^2}{(\alpha_i^2 + \overline{\alpha}_j^2)^2 - \frac{N}{D}\alpha_j^2} = \overset{*}{Q}{}^z_{ij} \tag{107c}$$

$$\frac{4}{\ell}\sum_{i=1,3,\ldots}^{\infty} \overset{*}{E}_{ij} \sin\alpha_i x = 1 - \frac{\nu}{2}\overline{\alpha}_j^2 x(\ell-x) \tag{107d}$$

$$\frac{4}{\ell}\sum_{i=2,4,\ldots}^{\infty} \overset{*}{E}_{ij} \sin\alpha_i x = (1 - \frac{2x}{\ell})[1 - \frac{\nu}{6}\overline{\alpha}_j^2 x(\ell-x) \tag{107e}$$

The side boundary shear resultant $V_x^h(x,y)$ due to imposed side boundary deflections is also expressed as a double series and its coefficient is found through the use of Equations 10f, 106b, and 107a.

$$V_x^h(x,y) = \frac{4}{\ell}\sum_{j=1}^{\infty}\sum_{i=0}^{\infty} \overset{*}{\omega}_i \overset{*}{\overline{W}}_{ij} \overset{*}{\overline{S}}_{ij} \cos\alpha_i x \sin\overline{\alpha}_j y \tag{108a}$$

$$\overset{*}{\overline{S}}_{ij} = -D\frac{\{(1-\nu)\overline{\alpha}_j^4[(1+\nu)\alpha_i^2 + 2\overline{\alpha}_j^2] - \frac{N}{D}\overline{\alpha}_j^2[\alpha_i^2 + 2(1-\nu)\overline{\alpha}_j^2]\}}{(\alpha_i^2 + \overline{\alpha}_j^2)^2 - \frac{N}{D}\overline{\alpha}_j^2} \tag{108b}$$

The fact that the series for $V_x^h(x,y)$ does not converge with respect to the index j does not affect its use, as will be seen in the following chapter, since the summation has to be carried out only in the x direction, that is, with respect to the index i.

Transformation from Infinite to Finite Series

A fundamental requirement for the discrete field stability analysis of ribbed plates by the macro approach is the transformation from an infinite series, used to represent a continuous function, to a finite series, used to represent a discrete function. The finite series function thus coincides with the continuous function at the regularly spaced, discrete node points, the stringer center lines. A series that is finite with respect to r, denoting the stringer locations, is required, for example for $K^{wz}(\frac{a}{m}r,y,\frac{a}{m}\alpha,\eta)$ in which $r,\alpha = 1,(1),m-1$.

Derivations for the transformation of sine and cosine series are shown in references (7) and (14). For clarity, the major results are repeated here:

$$f(x) = \sum_{i=1}^{\infty} \overset{*}{F}_i \sin\alpha_i x \quad ; \quad \overset{*}{F}_i = \frac{2}{\ell}\int_0^{\ell} f(x)\sin\alpha_i x \qquad (109a,b)$$

$$f(\frac{\ell}{m}r) = \sum_{k=1}^{m-1} F_k \sin\frac{k\pi r}{m} \quad ; \quad F_k = \frac{2}{m}\sum_{r=1}^{m-1} f(\frac{\ell}{m}r)\sin\frac{k\pi r}{m} \qquad (109c,d)$$

$$\overset{*}{F}_i = -\overset{*}{F}_{-i} \quad ; \quad F_k = -F_{2Im-k} = F_{2Im+k} \quad ; \quad I = -\infty,(1),+\infty \qquad (109e,f,g)$$

$$F_k = \sum_{i=1}^{\infty} \overset{*}{F}_i(\pm\delta_i^{2Im+k}) = \sum_{I=-\infty}^{+\infty} \overset{*}{F}_{2Im+k} \qquad (109h,i)$$

$$g(x) = \sum_{i=0}^{\infty} {}^{*}\omega_i \, {}^{*}G_i \cos\alpha_i x \; ; \; {}^{*}G_i = \frac{2}{\ell} \int_0^{\ell} g(x) \cos\alpha_i x \, dx \qquad (110a,b)$$

$$g(\tfrac{\ell}{m} r) = \sum_{k=0}^{m} G_k \cos \frac{k\pi r}{m} \; ; \; G_k = \frac{2\omega_k}{m} \sum_{r=0}^{m} \omega_r \, g(\tfrac{\ell}{m} r) \cos \frac{k\pi r}{m} \qquad (110c,d)$$

$${}^{*}G_i = {}^{*}G_{-i} \; ; \; \omega_k = 1 - \frac{1}{2}\delta_k^0 - \frac{1}{2}\delta_k^m \; ; \qquad (110e,f)$$

$$G_k = G_{2Im\pm k} = \sum_{i=0}^{\infty} {}^{*}G_i \, \delta_i^{2Im\pm k} = \omega_k \sum_{I=-\infty}^{+\infty} G_{2Im+k} \qquad (110g,h,i)$$

Discrete-Continuous Flexural Kernel Functions

In order to represent the interior and boundary plate-stringer interactive forces and the boundary shear resultants, the doubly infinite series in Equations 97, 99, 106 and 108 have to be transformed to finite-infinite series that are valid only at the rib center lines, that is, at $x = \frac{\ell}{m} r$ and $\xi = \frac{\ell}{m} \alpha$. Equations 109i and 110i are used for the transformations.

The transformed finite-infinite series are as follows:

$$K^{wz}(\tfrac{\ell}{m} r, y, \tfrac{\ell}{m} \alpha, \eta) = \frac{4}{mb} \sum_{j=1}^{\infty} \sum_{k=1}^{m-1} C_{kj} \sin \lambda_k \alpha \sin\bar{\alpha}_j \eta \sin\lambda_k r \sin\bar{\alpha}_j y \qquad (111a)$$

$$K^{w\phi}(\tfrac{\ell}{m} r, y, \tfrac{\ell}{m} \alpha, \eta) = \frac{4}{mb} \sum_{j=1}^{\infty} \sum_{k=0}^{m} D_{kj} \cos\lambda_k \alpha \sin\bar{\alpha}_j \eta \sin\lambda_k r \sin\bar{\alpha}_j y \qquad (111b)$$

$$K^{\theta z}(\tfrac{\ell}{m} r, y, \tfrac{\ell}{m} \alpha, \eta) = \frac{4}{mb} \sum_{j=1}^{\infty} \sum_{k=0}^{m} D_{kj} \sin\lambda_k \alpha \sin\bar{\alpha}_j \eta \cos\lambda_k r \sin\bar{\alpha}_j y \qquad (111c)$$

$$K^{\theta\phi}\left(\frac{\ell}{m}r,y\ \frac{\ell}{m}\alpha,\eta\right) = \frac{4}{mb}\sum_{j=1}^{\infty}\sum_{k=0}^{m} R_{kj}\ \cos\lambda_k\alpha\ \sin\bar{\alpha}_j\eta\ \cos\lambda_k r\ \sin\bar{\alpha}_j y \tag{111d}$$

$$K^{Vz}\left(\frac{\ell}{m}r,y,\ \frac{\ell}{m}\alpha,\eta\right) = \frac{4}{mb}\sum_{j=1}^{\infty}\sum_{k=1}^{m} Q^{z}_{kj}\ \sin\lambda_k\alpha\ \sin\bar{\alpha}_j\eta\ \cos\lambda_k r\ \sin\bar{\alpha}_j y \tag{111e}$$

$$K^{V\phi}\left(\frac{\ell}{m}r,y,\ \frac{\ell}{m}\alpha,\eta\right) = \frac{4}{mb}\sum_{j=1}^{\infty}\sum_{k=1}^{m} Q^{\phi}_{kj}\ \cos\lambda_k\alpha\ \sin\bar{\alpha}_j\eta\ \cos\lambda_k r\ \sin\bar{\alpha}_j y \tag{111f}$$

$$w^{h}(r,y) = \frac{4}{m}\sum_{j=1}^{\infty}\sum_{k=1}^{m-1} \bar{W}_{kj}\ \bar{C}_{kj}\ \sin\lambda_k r\ \sin\bar{\alpha}_j y \tag{111g}$$

$$\bar{W}_{kj} = \begin{cases} W^{s}_{j} & \text{for k odd} \\ W^{a}_{j} & \text{for k even} \end{cases} \tag{111h}$$

$$V^{h}_{x}(r,y) = \frac{4}{m}\sum_{j=1}^{\infty}\sum_{k=0}^{m} \bar{W}_{kj}\ \bar{S}_{kj}\ \cos\lambda_k r\ \sin\bar{\alpha}_j y \tag{111i}$$

Owing to the definitions of the series solutions, the right hand sides of Equations 109i and 110i have to be multiplied by $\frac{m}{\ell}$, for example

$$C_{kj} = \frac{m}{\ell}\sum_{I=-\infty}^{\infty} \overset{*}{C}_{2Im+k,j} \tag{112}$$

Due to the complexity of the infinite series coefficients, no closed form expressions have been found for the finite series

coefficients, that is, for the infinite sums on I in Equations 109i and 110i. However, the convergence of these infinite series on I is very good and it improves for an increasing number of ribs, m. Since it is the plates with a large number of ribs that lack simple and rational solutions so far, this fact compensates for the shortcoming.

The boundary shears are of special interest and will be required in the following chapter.

$$V_x^h(\overset{0}{m},y) = \sum_{j=1}^{\infty} (W_j^s \bar{S}_j^s \pm W_j^a \bar{S}_j^a)\sin\bar{\alpha}_j y \qquad (113a)$$

The shear coefficients $\bar{S}_j^s$ and $\bar{S}_j^a$ can be found by performing the infinite sum on $\overset{*}{S}_{ij}$ with respect to i or by performing the finite sum on S_{kj} with respect to k. The summations must be for odd indices for $\bar{S}_j^s$ and for even indices for $\bar{S}_j^a$, that is,

$$\bar{S}_j^s \text{ , } \bar{S}_j^a = \sum_{\substack{i=1,3,\ldots \\ i=0,2,\ldots}}^{\infty} \overset{*}{\omega}_i \overset{*}{\bar{S}}_{ij} = \sum_{\substack{k=1,3,\ldots \\ k=0,2,\ldots}}^{m} \bar{S}_{kj} \qquad (113b,c)$$

This completes the two required sets of solutions for the axially loaded flexural plate: particular kernel function solutions and homogeneous solutions for imposed boundary displacements.

4.2 Membrane Plate Solutions

The purpose of this section is to derive solutions for the deformations and side boundary shears for axially loaded membranes. It will follow the same basic steps outlined in the preceding section for the flexural plate and therefore the presentation and the

explanations will be more concise. The main differences are that membrane theory will replace flexural plate theory and that the forces and displacements will be in-plane rather than out-of-plane.

Again two sets of solutions will be required for the response to in-plane loads, that is, for deflections in both in-plane directions and for side boundary shears for the cases of: (1) unit in-plane concentrated loads in both directions and simple side supports, and (2) imposed longitudinal side boundary deflections.

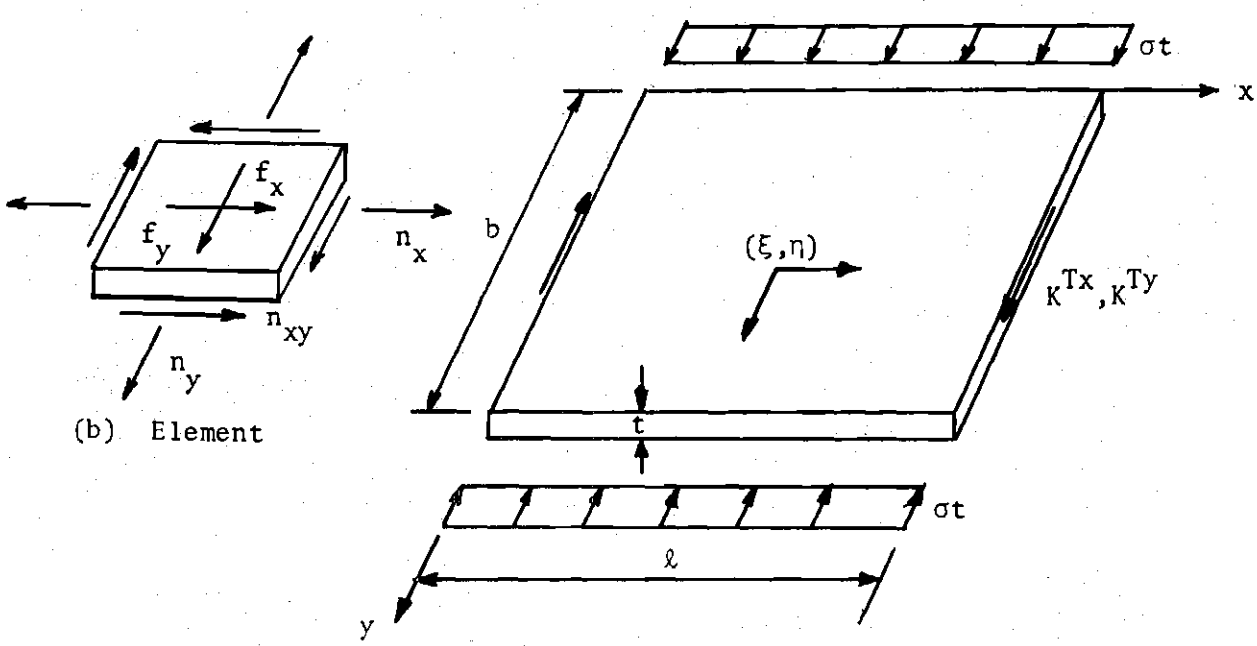

Figure 14. Membrane Plate Action

Mathematical Model

The same membrane solutions will be used for the macro analysis as for the micro analysis, see Chapter II and Figure 14. The governing differential equation is

$$K\begin{bmatrix} \underset{\sim}{D}_x^2 + \frac{1-\nu}{2}\lambda^2\underset{\sim}{D}_y^2 & \frac{1+\nu}{2}\underset{\sim}{D}_x\underset{\sim}{D}_y \\ \frac{1+\nu}{2}\underset{\sim}{D}_x\underset{\sim}{D}_y & \frac{1-\nu}{2}\underset{\sim}{D}_x^2 + \phi^2\underset{\sim}{D}_y^2 \end{bmatrix}\begin{Bmatrix} u(x,y) \\ v(x,y) \end{Bmatrix} = -\begin{Bmatrix} f_x(x,y) \\ f_y(x,y) \end{Bmatrix} \quad (114)$$

For both sets of solutions the boundary conditions at the ends are

$$u(x,{}^0_b) = 0 \quad ; \quad n_y(x,{}^0_b) = -\sigma t \quad (115a,b)$$

Simple Side Supports

The four required displacement kernel functions are the particular solutions for the displacements u(x,y) and v(x,y) due to unit concentrated loads applied at a point (ξ,η) in the x and y directions. The kernel functions are therefore obtained as solutions to

$$K\begin{bmatrix} \underset{\sim}{D}_x^2 + \frac{1-\nu}{2}\lambda^2\underset{\sim}{D}_y^2 & \frac{1+\nu}{2}\underset{\sim}{D}_x\underset{\sim}{D}_y \\ \frac{1+\nu}{2}\underset{\sim}{D}_x\underset{\sim}{D}_y & \frac{1-\nu}{2}\underset{\sim}{D}_x^2 + \phi^2\underset{\sim}{D}_y^2 \end{bmatrix}\begin{bmatrix} K^{ux}(x,y,\xi,\eta) & K^{uy}(x,y,\xi,\eta) \\ K^{vx}(x,y,\xi,\eta) & K^{vy}(x,y,\xi,\eta) \end{bmatrix}$$

$$= -\begin{bmatrix} \delta(x-\xi)\delta(y-\eta) & 0 \\ 0 & \delta(x-\xi)\delta(y-\eta) \end{bmatrix} \quad (116)$$

Since the membrane is simply supported at the sides, the boundary conditions are

$$v({}^0_\ell,y) = n_x({}^0_\ell,y) = 0 \quad (117a,b)$$

that is in terms of the kernel functions these boundary conditions are

$$\begin{bmatrix} \underset{\sim}{D}_x & \nu\underset{\sim}{D}_y \\ 0 & 1 \end{bmatrix} \begin{Bmatrix} K^{uy}(\overset{0}{\ell},y,\xi,\eta) \\ K^{vy}(\overset{0}{\ell},y,\xi,\eta) \end{Bmatrix} = \begin{Bmatrix} 0 \\ 0 \end{Bmatrix} \qquad (118a,b)$$

The kernel functions and the unit loads are expressed in the following doubly infinite series

$$K^{ux}(x,y,\xi,\eta) = \frac{4}{\ell b} \sum_{j=1}^{\infty} \sum_{i=0}^{\infty} \overset{*}{\omega}_i \overset{*}{F}_{ij} \cos\alpha_i\xi \sin\bar{\alpha}_j\eta \cos\alpha_i x \sin\bar{\alpha}_j y \qquad (119a)$$

$$K^{vx}(x,y,\xi,\eta) = \frac{4}{\ell b} \sum_{j=1}^{\infty} \sum_{i=1}^{\infty} \overset{*}{A}_{ij} \cos\alpha_i\xi \sin\bar{\alpha}_j\eta \sin\alpha_i x \cos\bar{\alpha}_j y \qquad (119b)$$

$$K^{uy}(x,y,\xi,\eta) = \frac{4}{\ell b} \sum_{j=1}^{\infty} \sum_{i=1}^{\infty} \overset{*}{A}_{ij} \sin\alpha_i\xi \cos\bar{\alpha}_j\eta \cos\alpha_i x \sin\bar{\alpha}_j y \qquad (119c)$$

$$K^{vy}(x,y,\xi,\eta) = \frac{4}{\ell b} \sum_{j=0}^{\infty} \sum_{i=1}^{\infty} \overset{*}{\omega}_j \overset{*}{B}_{ij} \sin\alpha_i\xi \cos\bar{\alpha}_j\eta \sin\alpha_i x \cos\bar{\alpha}_j y \qquad (119d)$$

$$f(x) = \delta(x-\xi)\delta(y-\eta) = \frac{4}{\ell b} \sum_{j=1}^{\infty} \sum_{i=0}^{\infty} \overset{*}{\omega}_i \cos\alpha_i\xi \sin\bar{\alpha}_j\eta \cos\alpha_i x \sin\bar{\alpha}_j y \qquad (119e)$$

$$f(y) = \delta(x-\xi)\delta(y-\eta) = \frac{4}{\ell b} \sum_{j=0}^{\infty} \sum_{i=1}^{\infty} \overset{*}{\omega}_j \sin\alpha_i\xi \cos\bar{\alpha}_j\eta \sin\alpha_i x \cos\bar{\alpha}_j y \qquad (119f)$$

Substitution of Equations 119a-f into Equation 116 and matching coefficients yields

$$\overset{*}{A}_{ij} = -\frac{1}{K}\frac{2(1+\nu)\alpha_i\bar{\alpha}_j}{\overset{*}{H}_{ij}} \tag{120a}$$

$$\overset{*}{B}_{ij} = \frac{2}{K}\frac{2\alpha_i^2 + (1-\nu)\lambda^2\bar{\alpha}_j^2}{\overset{*}{H}_{ij}} \tag{120b}$$

$$\overset{*}{F}_{ij} = \frac{2}{K}\frac{(1-\nu)\alpha_i^2 + 2\phi^2\bar{\alpha}_j^2}{\overset{*}{H}_{ij}} \tag{120c}$$

$$\overset{*}{H}_{ij} = 2(1-\nu)(\alpha_i^2 + \phi\lambda\bar{\alpha}_j^2)^2 + \alpha_i^2\bar{\alpha}_j^2\{[(1-\nu)\lambda - 2\phi]^2 - (1+\nu)^2\} \tag{120d}$$

The kernel function solutions for the in-plane shear resultants due to unit impulse loads in the x and y directions, physically identified only at the boundaries $x = 0,\ell$, are obtained by use of the force deformation relations (see Chapter II), Equation 22c, that is,

$$K^{Tx}(x,y,\xi,\eta) = \frac{1-\nu}{2} K\,[\underset{\sim}{D}_y K^{ux}(x,y,\xi,\eta) + \underset{\sim}{D}_x K^{vx}(x,y,\xi,\eta)] \tag{121a}$$

$$= \frac{4}{\ell b}\sum_{j=1}^{\infty}\sum_{i=0}^{\infty}\overset{*}{\omega}_i\,\overset{*x}{T}_{ij}\cos\alpha_i\xi\,\sin\bar{\alpha}_j\eta\,\cos\alpha_i x\,\cos\bar{\alpha}_j y \tag{121b}$$

$$K^{Ty}(x,y,\xi,\eta) = \frac{1-\nu}{2} K\,[\underset{\sim}{D}_y K^{uy}(x,y,\xi,\eta) + \underset{\sim}{D}_x K^{vy}(x,y,\xi,\eta)] \tag{121c}$$

$$= \frac{4}{\ell b}\sum_{j=0}^{\infty}\sum_{i=1}^{\infty}\overset{*}{\omega}_j\,\overset{*y}{T}_{ij}\sin\alpha_i\xi\,\cos\bar{\alpha}_j\eta\,\cos\alpha_i y\,\cos\bar{\alpha}_j y \tag{121d}$$

The coefficients T^x_{ij} and T^y_{ij} are obtained by substituting Equations 119a,b into 121a and Equations 119c,d into 121c, making use of Equations 120a-d, and matching like coefficients. This results in

$$T^{*x}_{ij} = \frac{2(1-\nu)}{H^*_{ij}} \bar{\alpha}_j \left(\phi^2 \bar{\alpha}^2_j - \nu \alpha^2_i\right) \tag{122a}$$

$$T^y_{ij} = \frac{2(1-\nu)}{H^*_{ij}} \alpha_i \left\{\alpha^2_i - \frac{1}{2}\left[(1+\nu) - (1-\nu)\lambda^2\right]\bar{\alpha}^2_j\right\} \tag{122b}$$

Imposed Boundary Displacements

The solutions $u^h(x,y)$ and $v^h(x,y)$ for the in-plane deflections due to imposed longitudinal boundary displacements must satisfy the homogeneous equation 114, that is for $f_x(x,y) = f_y(x,y) = 0$. The imposed boundary deflections can be written in the following series form

$$v^h(^0_\ell,y) = \sum_{j=0}^{\infty} (V^s_j \pm V^a_j)\cos\bar{\alpha}_j y \tag{123}$$

The other side boundary condition is

$$n^h_x(^0_\ell,y) = \underset{\sim}{D}_x u^h(^0_\ell,y) + \nu \underset{\sim}{D}_y v^h(^0_\ell,y) = 0 \tag{124}$$

The solutions for $u^h(x,y)$ and $v^h(x,y)$ will contain algebraic terms that satisfy the inhomogeneous boundary conditions and are expressed as follows

$$u^h(x,y) = \frac{4}{\ell} \sum_{j=1}^{\infty} \sum_{i=0}^{\infty} \omega^*_i \left(-\frac{\ell}{2}\nu\bar{\alpha}_j\right)\bar{V}^*_{ij}\,\bar{A}^*_{ij}\cos\alpha_i x \sin\bar{\alpha}_j y \tag{125a}$$

$$= \sum_{j=1}^{\infty} \left(-\frac{\ell}{2}\nu\bar{\alpha}_j\right) \{(1 - \frac{2x}{\ell})V_j^s + \frac{1}{2}(1 - \frac{2x}{\ell})^2 V_j^a$$

$$+ \frac{4}{\ell} \sum_{i=0}^{\infty} \omega_i \overset{*}{\bar{V}}_{ij} (\overset{*}{\bar{A}}_{ij} - \overset{*}{C}_i')\cos\alpha_i x\}\sin\bar{\alpha}_j y \qquad (125b)$$

$$v^h(x,y) = \frac{4}{\ell} \sum_{j=0}^{\infty} \sum_{i=1}^{\infty} \omega_j \overset{*}{\bar{V}}_{ij} \overset{*}{\bar{B}}_{ij} \sin\alpha_i x \cos\bar{\alpha}_j y \qquad (125c)$$

$$= \sum_{j=0}^{\infty} \overset{*}{\omega}_j \{V_j^s + (1 - \frac{2x}{\ell})V_j^a$$

$$+ \frac{4}{\ell} \sum_{i=1}^{\infty} \overset{*}{\bar{V}}_{ij} (\overset{*}{\bar{B}}_{ij} - \overset{*}{C}_i)\sin\alpha_i x\}\cos\bar{\alpha}_j y \qquad (125d)$$

where

$$\overset{*}{\bar{V}}_{ij} = \begin{cases} V_j^s \text{ for i odd} \\ V_j^a \text{ for i even} \end{cases} \qquad (125e)$$

The coefficients are determined through substitution of Equations 125b,d into Equation 114 which yields

$$(-\frac{\ell}{2}\nu\bar{\alpha}_j)(\overset{*}{\bar{A}}_{ij} - \overset{*}{C}_i') = \frac{\bar{\alpha}_j^3}{\alpha_i^2 \overset{*}{H}_{ij}} \{[\nu(1-\nu)^2\lambda^2 + 2(1+\nu)\phi^2 - \nu(1+\nu)^2]\alpha_i^2$$

$$+ 2\nu(1-\nu)\phi^2\lambda^2\bar{\alpha}_j^2\} \qquad (126a)$$

$$(\overset{*}{\bar{B}}_{ij} - \overset{*}{C}_i) = -\frac{2\bar{\alpha}_j^2}{\alpha_i \overset{*}{H}_{ij}} \{[2\phi^2 - \nu(1+\nu)]\alpha_i^2$$

$$+ (1-\nu)\phi^2\lambda^2\bar{\alpha}_j^2 \qquad (126b)$$

$$\overset{*}{C}{}'_i = \frac{2}{\ell\alpha_i^2} \quad ; \quad \overset{*}{C}{}'_0 = \frac{\ell}{24} \quad ; \quad \overset{*}{C}_i = \frac{1}{\alpha_i} \tag{126c,d,e}$$

$$-\frac{a}{2}\nu\bar{\alpha}_j \overset{*}{\bar{A}}_{ij} = \frac{2(1-\nu)}{\overset{*}{H}_{ij}}\bar{\alpha}_j\,(\phi^2\bar{\alpha}_j^2 - \nu\alpha_i^2) = \overset{*}{T}{}^x_{ij} \tag{126f}$$

$$\overset{*}{\bar{B}}_{ij} = \frac{2(1-\nu)}{\overset{*}{H}_{ij}}\alpha_i\{\alpha_i^2 - \frac{1}{2}[(1+\nu) - (1-\nu)\lambda^2]\bar{\alpha}_j^2\} = \overset{*}{T}{}^y_{ij} \tag{126g}$$

$$\frac{4}{\ell}\sum_{i=1,3,\ldots}^{\infty} \overset{*}{C}{}'_i \cos\alpha_i x = 1 - \frac{2x}{\ell} \tag{126h}$$

$$\frac{4}{\ell}\sum_{i=0,2,\ldots}^{\infty} \overset{*}{C}{}'_i \cos\alpha_i x = \frac{1}{2}\left(1 - \frac{2x}{\ell}\right)^2 \tag{126i}$$

$$\frac{4}{\ell}\sum_{i=1,3,\ldots}^{\infty} \overset{*}{C}_i \sin\alpha_i x = 1 \tag{126j}$$

$$\frac{4}{\ell}\sum_{i=0,2,\ldots}^{\infty} \overset{*}{C}_i \sin\alpha_i x = 1 - \frac{2x}{\ell} \tag{126k}$$

The side boundary in-plane shear resultant $n^h_{xy}(x,y)$ due to imposed boundary deflections and its coefficient, found through use of Equations 22c, 125, and 126 are as follows

$$n^h_{xy}(x,y) = \frac{4}{\ell}\sum_{j=1}^{\infty}\sum_{i=0}^{\infty} \overset{*}{\omega}_i \overset{*}{\bar{V}}_{ij} \overset{*}{\bar{T}}_{ij} \cos\alpha_i x \cos\bar{\alpha}_j y \tag{127a}$$

$$\overset{*}{\bar{T}}_{ij} = \frac{K(1-\nu)\bar{\alpha}_j^2}{\overset{*}{H}_{ij}}[(1-\nu)\phi^2(1-\lambda^2)\bar{\alpha}_j^2 - 2(\phi^2 - \nu^2)\alpha_i^2] \tag{127b}$$

Just as for the boundary shear resultant $V_x^h(x,y)$, for the flexural plate, the summations in Equation 127a are also carried out only with respect to i. Therefore, again, the fact that this series does not converge with respect to j does not affect its use.

Approximate Formulas for the Series Coefficients

All the coefficients in this section for membrane formulas can be greatly simplified by using an approximate formula for $\overset{*}{H}_{ij}$, Equation 120d. Substitution of Equations 16b,c into Equation 120d reveals that the second term in the definition of $\overset{*}{H}_{ij}$ contains only second and higher orders of ε. Since for all practical cases ε will be $\leq .001$ neglecting this second term has an almost unnoticeable effect on $\overset{*}{H}_{ij}$. Using only the first term in the definition of $\overset{*}{H}_{ij}$ from Equation 120d, that is,

$$\overset{*}{H}_{ij} = (\alpha_i^2 + \phi\lambda\bar{\alpha}_j^2)^2 \tag{128a}$$

the other coefficients simplify to

$$\overset{*}{A}_{ij} = -\frac{(1+\nu)}{K(1-\nu)} \frac{\alpha_i\bar{\alpha}_j}{(\alpha_i^2 + \phi\lambda\bar{\alpha}_j^2)^2} \tag{128b}$$

$$\overset{*}{B}_{ij} = \frac{1}{K(1-\nu)} \frac{2\alpha_i^2 + (1-\nu)\lambda^2\bar{\alpha}_j^2}{(\alpha_i^2 + \phi\lambda\bar{\alpha}_j^2)^2} \tag{128c}$$

$$\overset{*}{F}_{ij} = \frac{1}{K(1-\nu)} \frac{(1-\nu)\alpha_i^2 + 2\phi^2\bar{\alpha}_j^2}{(\alpha_i^2 + \phi\lambda\bar{\alpha}_j^2)^2} \tag{128d}$$

$$\overset{*x}{T}_{ij} = \frac{\bar{\alpha}_j(\phi^2\bar{\alpha}_j^2 - \nu\bar{\alpha}_i^2)}{(\alpha_i^2 + \phi\lambda\bar{\alpha}_j^2)^2} \tag{128e}$$

$$\overset{*y}{T}_{ij} = \frac{\alpha_i\{\alpha_i^2 - \frac{1}{2}[(1+\nu) - (1-\nu)\lambda^2]\bar{\alpha}_j^2}{(\alpha_i^2 + \phi\lambda\bar{\alpha}_j^2)^2} \tag{128f}$$

$$(-\frac{\ell}{2}\nu\bar{\alpha}_j)\overset{*}{\bar{A}}_{ij} = \overset{*x}{T}_{ij} \tag{128g}$$

$$\overset{*}{\bar{B}}_{ij} = T^y_{ij}$$

$$\overset{*}{\bar{T}}_{ij} = \frac{\bar{\alpha}_j^2 K}{(\alpha_i^2 + \phi\lambda\bar{\alpha}_j^2)^2}\left[\frac{1-\nu}{2}\phi^2(1-\lambda^2)\bar{\alpha}_j^2 - (\phi^2 - \nu^2)\alpha_i^2\right] \tag{128i}$$

Discrete-Continuous Membrane Kernel Functions

As in the flexural analysis, the membrane kernel functions are required in the form of finite-infinite series valid only at the rib lines. The transformed series are as follows

$$K^{ux}\left(\frac{\ell}{m}r,y,\frac{\ell}{m}\alpha,\eta\right) = \frac{4}{mb}\sum_{j=1}^{\infty}\sum_{k=0}^{m} F_{kj}\cos\lambda_k\alpha\sin\bar{\alpha}_j\eta\cos\lambda_k r\sin\bar{\alpha}_j y \tag{129a}$$

$$K^{vx}\left(\frac{\ell}{m}r,y,\frac{\ell}{m}\alpha,\eta\right) = \frac{4}{mb}\sum_{j=1}^{\infty}\sum_{k=1}^{m} A_{kj}\cos\lambda_k\alpha\sin\bar{\alpha}_j\eta\sin\lambda_k r\cos\bar{\alpha}_j y \tag{129b}$$

$$K^{uy}\left(\frac{\ell}{m}r,y,\frac{\ell}{m}\alpha,\eta\right) = \frac{4}{mb}\sum_{j=1}^{\infty}\sum_{k=1}^{m-1} A_{kj}\sin\lambda_k\alpha\cos\bar{\alpha}_j\eta\cos\lambda_k r\sin\bar{\alpha}_j y \tag{129c}$$

$$K^{vy}\left(\frac{\ell}{m}r,y,\frac{\ell}{m}\alpha,\eta\right) = \frac{4}{mb}\sum_{j=0}^{\infty}\sum_{k=1}^{m}{}^{*}\omega_j\, B_{kj}\,\sin\lambda_k\alpha\,\cos\bar{\alpha}_j\eta\,\sin\lambda_k r\,\cos\bar{\alpha}_j y \tag{129d}$$

$$K^{Tx}\left(\frac{\ell}{m}r,y,\frac{\ell}{m}\alpha,\eta\right) = \frac{4}{mb}\sum_{j=1}^{\infty}\sum_{k=0}^{m}T^{x}_{kj}\,\cos\lambda_k\alpha\,\sin\bar{\alpha}_j\eta\,\cos\lambda_k r\,\cos\bar{\alpha}_j y \tag{129e}$$

$$K^{Ty}\left(\frac{\ell}{m}r,y,\frac{\ell}{m}\alpha,\eta\right) = \frac{4}{mb}\sum_{j=0}^{\infty}\sum_{k=1}^{m}{}^{*}\omega_j\, T^{y}_{kj}\,\sin\lambda_k\alpha\,\cos\bar{\alpha}_j\eta\,\cos\lambda_k r\,\cos\bar{\alpha}_j y \tag{129f}$$

$$u^{h}(r,y) = \frac{4}{\ell}\sum_{j=1}^{\infty}\sum_{k=0}^{m}\bar{V}_{kj}\,\bar{A}_{kj}\,\cos\lambda_k r\,\sin\bar{\alpha}_j y \tag{129g}$$

$$v^{h}(r,y) = \frac{4}{\ell}\sum_{j=0}^{\infty}\sum_{k=1}^{m-1}{}^{*}\omega_j\,\bar{V}_{kj}\,\bar{B}_{kj}\,\sin\lambda_k r\,\cos\bar{\alpha}_j y \tag{129h}$$

$$n^{h}_{xy}(r,y) = \frac{4}{\ell}\sum_{j=1}^{\infty}\sum_{k=0}^{m}\bar{V}_{kj}\,\bar{T}_{kj}\,\cos\lambda_k r\,\cos\bar{\alpha}_j y \tag{129i}$$

where
$$\bar{V}_{kj} = \begin{cases} V^{s}_{j} & \text{for k odd} \\ V^{a}_{j} & \text{for k even} \end{cases} \tag{129j}$$

Again, as for the flexural analysis, the right hand sides of Equations 109i and 110i have to be multiplied by $\frac{m}{\ell}$ in order to obtain the correct finite series coefficients, for example

$$A_{kj} = \frac{m}{\ell}\sum_{I=-\infty}^{\infty}{}^{*}A_{2Im+k,j} \tag{130a}$$

$$\bar{A}_{kj} = \frac{m}{\ell} \sum_{I=-\infty}^{\infty} \left(-\frac{\ell}{2} \nu\alpha_j\right) \overset{*}{\bar{A}}_{2Im+k,j} \tag{130b}$$

The exact definitions of the infinite series coefficients are too complex for transformation into closed form finite series coefficients. However, using the approximate definitions of Equations 128a-i, it is possible to perform the infinite sum on I and obtain closed form expressions for the finite series coefficients. This is shown in Appendix B. The transformed coefficients are

$$A_{kj} = \frac{-\ell(1+\nu)}{4(1-\nu)mK\bar{D}_{kj}^2 \sqrt{\phi\lambda}} \sinh\lambda_j \sin\lambda_k \tag{131a}$$

$$B_{kj} = \frac{\ell}{4(1-\nu)mK\bar{D}_{kj}} \left\{\left[2 + (1-\nu)\frac{\lambda}{\phi}\right] \frac{\sinh\lambda_j}{\lambda_j} + \left[2 - (1-\nu)\frac{\lambda}{\phi}\right] \frac{1 - \cosh\lambda_j \cos\lambda_k}{\bar{D}_{kj}}\right\} \tag{131b}$$

$$F_{kj} = \frac{\ell\,\omega_k}{4(1-\nu)mK\bar{D}_{kj}} \left[(1-\nu+2\frac{\phi}{\lambda}) \frac{\sinh\lambda_j}{\lambda_j} + (1-\nu-2\frac{\phi}{\lambda}) \frac{1 - \cosh\lambda_j \cos\lambda_k}{\bar{D}_{kj}}\right] \tag{131c}$$

$$T^x_{kj} = \frac{\lambda_j \omega_k}{4\sqrt{\phi\lambda}\,\bar{D}_{kj}} \left[(\frac{\phi}{\lambda} - \nu) \frac{\sinh\lambda_j}{\lambda_j} - (\frac{\phi}{\lambda} + \nu) \frac{1 - \cosh\lambda_j \cos\lambda_k}{D_{kj}}\right] \tag{131d}$$

$$T^y_{kj} = \frac{\sin\lambda_k}{4\bar{D}_{kj}} \left\{2 - \left[1 + \frac{1+\nu-(1-\nu)\lambda^2}{2\phi\lambda}\right] \frac{\lambda_j \sinh\lambda_j}{\bar{D}_{kj}}\right\} \tag{131e}$$

$$\overline{A}_{kj} = T^{x}_{kj} \tag{131f}$$

$$\overline{B}_{kj} = T^{y}_{kj} \tag{131g}$$

$$\overline{T}_{kj} = -\frac{mK\lambda_j^2\omega_k}{4\ell\phi\lambda\overline{D}_{kj}}\{[\phi^2 - \nu^2 - \frac{1-\nu}{2}\frac{\phi}{\lambda}(1 - \lambda^2)]\frac{\sinh\lambda_j}{\lambda_j}$$

$$+ [\phi^2 - \nu^2 + \frac{1-\nu}{2}\frac{\phi}{\lambda}(1 - \lambda^2)]\frac{1 - \cosh\lambda_j \cos\lambda_k}{\overline{D}_{kj}} \tag{131h}$$

where

$$\lambda_j = \sqrt{\phi\lambda}\,\frac{\ell}{m}\,\overline{\alpha}_j \quad ; \quad \overline{D}_{kj} = \cosh\lambda_j - \cos\lambda_k \tag{131i,j}$$

The in-plane boundary shears due to imposed boundary displacements that will be required in the following chapter are

$$n^{h}_{xy}(\overset{0}{m},y) = \sum_{j=0}^{\infty}(V^{s}_{j}\,\overline{T}^{s}_{j} + V^{a}_{j}\,\overline{T}^{a}_{j})\cos\overline{\alpha}_j y \tag{132a}$$

The shear coefficients $\overline{T}^{s}_{j}$ and $\overline{T}^{a}_{j}$ can be found by performing the infinite sum on $\overset{*}{\overline{T}}_{ij}$ with respect to i or by performing the finite sum on $\overline{T}_{kj}$ with respect to k. The summations for $\overline{T}^{s}_{j}$ are for odd indices and for $\overline{T}^{a}_{j}$ are for even indices, that is,

$$\overline{T}^{s}_{j},\overline{T}^{a}_{j} = \sum_{\substack{i=1,3,\ldots\\ i=0,2,\ldots}}^{\infty}\overset{*}{\omega}_i\,\overset{*}{\overline{T}}_{ij} = \sum_{\substack{k=1,3,\ldots\\ k=0,2,\ldots}}^{m}\overline{T}_{kj} \tag{132b,c}$$

This completes the two required sets of solutions for the axially

loaded membrane.

4.3 Rib Formulas

The purpose of this section is to derive solutions for the deformations at the top of an axially loaded beam.

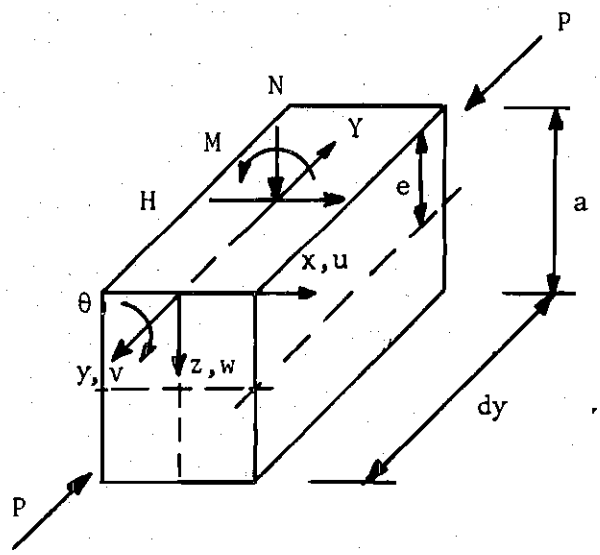

Figure 15. Rib Forces for Macro Solution

In addition to the axial load the beam is subjected to four loads applied at the top (see Figure 15). These loads can be separated into two sets. The first set, the in-plane loads N and Y, causes deflections in the y and z-directions, whereas the second set, the out-of-plane loads H and M, causes deflections in the x and ϕ-directions, that is, lateral deflection and rotation about the longitudinal axis.

The deflections will be derived for unit concentrated loads, that is, they will be written as kernel function solutions. The beam ends are simply supported.

Kernel Function Solutions for In-plane Loads

The governing differential equation for the beam subjected to in-plane loads and to axial compression has been shown in Chapter II, Equation 32, for the micro analysis. The following changes are made, however, to allow for the differences in notation for the macro analysis: (1) Y(y) replaces T(y), (2) N(y) changes sign, and (3) w(y) and v(y) replace the non-dimensionalized quantities U(y) and V(y) respectively. This results in

$$[L_{mn}] \begin{Bmatrix} w(y) \\ v(y) \end{Bmatrix} = \begin{Bmatrix} N(y) \\ -Y(y) \end{Bmatrix} \tag{133a}$$

where

$$[L_{mn}] = EA \begin{bmatrix} (\rho^2+e^2)D_{\sim y}^4 + \frac{P}{EA} D_{\sim y}^2 & -eD_{\sim y}^3 \\ eD_{\sim y}^3 & -D_{\sim y}^2 \end{bmatrix} \tag{133b}$$

To obtain the kernel function solutions the continuous loads N(y) and Y(y) are replaced alternately by unit concentrated loads $\delta(y-\eta)$, applied at point η, while the other load equals zero. That is, the kernel function solutions are found from

$$[L_{mn}] \; [K^{mn}] = \begin{bmatrix} 1 & 0 \\ 0 & 1 \end{bmatrix} \delta(y-\eta) \tag{134a}$$

where

$$[K^{mn}] = \begin{bmatrix} K^{wzs}(y,\eta) & K^{wys}(y,\eta) \\ K^{vzs}(y,\eta) & K^{vys}(y,\eta) \end{bmatrix} \tag{134b}$$

Both the kernel functions and the loads are expressed as infinite series as follows

$$[K^{mn}] = \frac{2}{b} \sum_{j=1}^{\infty} \begin{bmatrix} \overset{*}{C}_j \sin\bar{\alpha}_j\eta \sin\bar{\alpha}_j y & -\overset{*}{D}_j \cos\bar{\alpha}_j\eta \sin\bar{\alpha}_j y \\ \overset{*}{D}_j \sin\bar{\alpha}_j\eta \cos\bar{\alpha}_j y & -\bar{\omega}_j \overset{*}{B}_j \cos\bar{\alpha}_j\eta \cos\bar{\alpha}_j y \end{bmatrix} \tag{135a}$$

$$\begin{bmatrix} 1 & 0 \\ 0 & 1 \end{bmatrix} \delta(y-\eta) = \frac{2}{b} \sum_{j=1}^{\infty} \begin{bmatrix} \sin\bar{\alpha}_j\eta \sin\bar{\alpha}_j y & 0 \\ 0 & \overset{*}{\omega}_j \cos\bar{\alpha}_j\eta \cos\bar{\alpha}_j y \end{bmatrix} \tag{135b}$$

Substitution of Equations 135a,b into Equation 134a and matching like coefficients yields

$$\overset{*}{B}_j = \frac{e^2}{B\bar{\alpha}_j^2 - P} + \frac{1}{\bar{\alpha}_j^2 EA} \tag{136a}$$

$$\overset{*}{C}_j = \frac{1}{\bar{\alpha}_j^2 (B\bar{\alpha}_j^2 - P)} \tag{136b}$$

$$\overset{*}{D}_j = \frac{e}{\bar{\alpha}_j (B\bar{\alpha}_j^2 - P)} \tag{136c}$$

Kernel Function Solutions for Out-of-plane Loads

The governing differential equation for the beam subjected to

out-of-plane loads and to axial compression has been shown in Chapter II, Equation 28, for the micro analysis. The following changes are made to allow for the differences between macro and micro analysis: (1) H(y) replaces S(y), (2) M(y) changes signs, and (3) -u(y) replaces the non-dimensionalized quantity W(y). This results in the following governing differential equation for the macro analysis

$$[L_{mn}]\begin{Bmatrix}\theta(y)\\ u(y)\end{Bmatrix} = \begin{Bmatrix}-M(y)\\ H(y)\end{Bmatrix} \tag{137a}$$

where

$$[L_{mn}] = \begin{bmatrix} e^2(B'\underset{\sim}{D}_y^2 + P)\underset{\sim}{D}_y^2 - GJ\underset{\sim}{D}_y^2 & -e(B'\underset{\sim}{D}_y^2 + P)\underset{\sim}{D}_y^2 \\ -e(B'\underset{\sim}{D}_y^2 + P)\underset{\sim}{D}_y^2 & (B'\underset{\sim}{D}_y^2 + P)\underset{\sim}{D}_y^2 \end{bmatrix} \tag{137b}$$

The kernel function solutions are found by replacing the continuous loads M(y) and S(y) alternately by unit concentrated loads $\delta(y-\eta)$ while the other load equals zero, that is,

$$[L_{mn}]\ [K^{mn}] = \begin{bmatrix}1 & 0\\ 0 & 1\end{bmatrix}\delta(y-\eta) \tag{138a}$$

where

$$[K^{mn}] = \begin{bmatrix} K^{\theta\phi s}(y,\eta) & K^{\theta xs}(y,\eta) \\ K^{u\phi s}(y,\eta) & K^{uxs}(y,\eta) \end{bmatrix} \tag{138b}$$

Kernel functions and loads are expressed in the following series

$$[K^{mn}] = \frac{2}{b} \sum_{j=1}^{\infty} \begin{bmatrix} -\overset{*}{R}_j & \overset{*}{G}_j \\ -\overset{*}{G}_j & \overset{*}{F}_j \end{bmatrix} \sin\bar{\alpha}_j\eta \sin\bar{\alpha}_j y \tag{139a}$$

$$\begin{bmatrix} 1 & 0 \\ 0 & 1 \end{bmatrix} \delta(y-\eta) = \frac{2}{b} \sum_{j=1}^{\infty} \begin{bmatrix} 1 & 0 \\ 0 & 1 \end{bmatrix} \sin\bar{\alpha}_j\eta \sin\bar{\alpha}_j y \tag{139b}$$

Substitution of Equations 139a,b into Equation 138a and matching coefficients yields

$$\overset{*}{F}_j = \frac{e^2}{\bar{\alpha}_j^2 GJ} + \frac{1}{\bar{\alpha}_j^2 (B'\bar{\alpha}_j^2 - P)} \tag{140a}$$

$$\overset{*}{G}_j = \frac{e}{\bar{\alpha}_j^2 GJ} \tag{140b}$$

$$\overset{*}{R}_j = \frac{1}{\bar{\alpha}_j^2 GJ} \tag{140c}$$

This completes the kernel function solutions for ribs subjected to in-plane and out-of-plane loads.

CHAPTER V

MACRO STABILITY ANALYSIS OF RIBBED PLATES

The macro stability analysis is the second of the two methods developed in this thesis. The object is to arrive at simple stability equations for the same type of structures that were treated in the micro stability analysis in Chapter III. The solutions of this chapter will serve as an alternative and a check for the solutions of the micro stability analysis.

The method of solution will employ sets of compatibility equations for the plate and rib deformations at the rib lines. These deformations will be expressed in terms of the kernel function and imposed boundary deformation solutions presented in the preceding chapter. The plate deformations at a particular rib line are obtained by summing the effects of the plate-rib interactive forces for the discrete variable r and by integrating over the continuous variable y. The plate deformations due to the imposed boundary displacements, in the form of the transformed discrete-continuous series solution, must be added to the deformations due to the interactive forces.

The set of summation-integral equations are reduced to simple algebraic equations by use of the orthogonality properties of finite and infinite series. For the case of flexible side boundaries, the imposed deflections of the boundary ribs are matched with the deflections due to total plate edge shears arising from the sides simply supported case and the imposed boundary deflections.

5.1 Non-composite Flexural Analysis

The object of this section is a rational stability analysis of a ribbed plate under uniform longitudinal compression. The structure is proportioned and detailed such that the effects of the in-plane deformations and the T-beam action can be ignored, that is, the system (see Figure 16) acts as a flexural plate continuously supported by beam stringers that are neither longitudinally nor laterally constrained at the plate-stringer junction. This represents the simplest class of orthotropic plates.

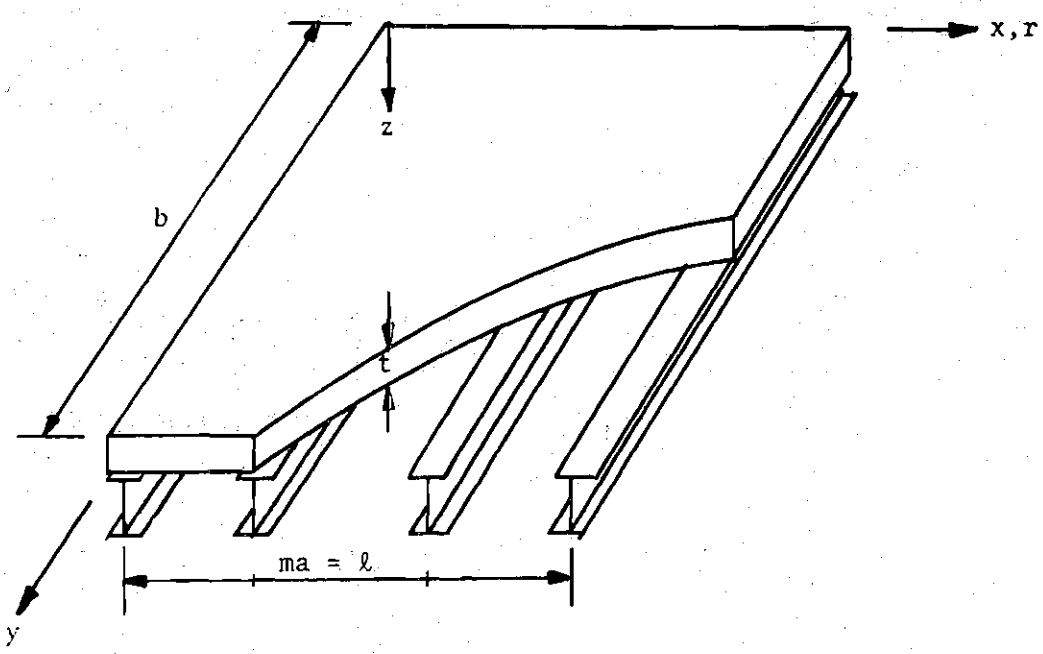

Figure 16. Non-composite Flexural Model

The system components are: (1) the plate, which is subjected to uniform in-plane longitudinal compression at the ends and to discrete-continuous plate-stringer interactive forces along the rib lines on its lower surface. The latter consist of vertical forces,

perpendicular to the plate, and bending moments about the longitudinal axis. The structural action of the plate is primarily flexural and admits of treatment by classical plate theory. The necessary formulas were developed in Chapter IV. (2) The interior ribs which are subjected to bending and torsion about their major and longitudinal axes caused by the distributed plate-stringer interactive forces. The necessary formulas were developed in Chapter IV. (3) The boundary stringers, which may have properties different from the interior stringers.

Mathematical Model

The approach will be a macro flexibility method leading to governing equations in the form of summation integral equations containing the unknown: (1) discrete-continuous plate-stringer interactive forces $N(r,y)$ and $M(r,y)$; and (2) continuous vertical boundary stringer deflections $w(\overset{0}{\ell},y)$ (see Equation 104).

The slab deformations along the stringer center lines, two dimensional discrete-continuous fields, are obtained by superposition of the deformations due to side boundary deformations $w^h(r,y)$ and $\theta^h(r,y)$ and plate-stringer interactive forces $N(r,y)$ and $M(r,y)$, that is,

$$w(r,y) = w^h(r,y) - \sum_{\alpha=0}^{m} \int_0^b [N(\alpha,\eta)K^{wz}(\frac{\ell}{m}r,y,\frac{a}{m}\alpha,\eta) - M(\alpha,\eta)K^{w\phi}(\frac{\ell}{m}r,y,\frac{a}{m}\alpha,\eta)]d\eta \qquad (141a)$$

$$\theta(r,y) = \theta^h(r,y) - \sum_{\alpha=0}^{m} \int_0^b [N(\alpha,\eta)K^{\theta z}(\frac{\ell}{m} r,y, \frac{a}{m} \alpha,\eta)$$

$$- M(\alpha,\eta)K^{w\phi}(\frac{\ell}{m} r,y, \frac{a}{m} \alpha,\eta)]d\eta \qquad (141b)$$

where $w^h(r,y)$ and $\theta^h(r,y)$ are given by Equation 111g and its partial derivative in the r direction and the kernel function solutions $K^{wz}(\frac{\ell}{m} r,y, \frac{\ell}{m} \alpha,\eta)$, $K^{w\phi}(\frac{\ell}{m} r,y, \frac{\ell}{m} \alpha,\eta)$, $K^{\theta z}(\frac{\ell}{m} r,y, \frac{\ell}{m} \alpha,\eta)$, $K^{\theta\phi}(\frac{\ell}{m} r,y, \frac{\ell}{m} \alpha,\eta)$ are given by Equations 111a-d.

Since the plate deformations before buckling are neglected, the terms $w(r,y)$ and $\theta(r,y)$ represent the additional deformations during buckling.

As the analysis will be through the use of finite-infinite Fourier series, the unknown interactive forces are expressed appropriately as

$$N(r,y) = \sum_{j=1}^{\infty} \sum_{k=1}^{m-1} N_{kj} \sin\lambda_k r \sin\bar{\alpha}_j y \qquad (142a)$$

$$M(r,y) = \sum_{j=1}^{\infty} \sum_{k=0}^{m} M_{kj} \cos\lambda_k r \sin\bar{\alpha}_j y \qquad (142b)$$

where

$$\lambda_k = \frac{k\pi}{m} \qquad (142c)$$

$$N_{kj} = \frac{4}{mb} \sum_{\alpha=1}^{m-1} \int_0^b N(r,y)\sin\lambda_k r \sin\bar{\alpha}_j y \qquad (142d)$$

$$M_{kj} = \frac{4}{mb} \sum_{\alpha=0}^{m} \int_{0}^{b} M(r,y)\cos\lambda_k r \, \sin\bar{\alpha}_j y \qquad (142e)$$

It should be noted that the coefficients N_{kj} and M_{kj} are cyclic on k outside the normal range k = 1,(1),m-1, see Equations 109, 110.

Substitution of the referenced series solutions into Equation 141a yields

$$\begin{aligned} w(r,y) = & \sum_{j=1}^{\infty} \sum_{k=1}^{m-1} \frac{4}{m} \bar{W}_{kj} \, \bar{C}_{kj} \, \sin\lambda_k r \, \sin\bar{\alpha}_j y \\ & - \sum_{\alpha=1}^{m-1} \int_{0}^{b} \left[\left(\sum_{j=1}^{\infty} \sum_{k=1}^{m-1} N_{kj} \, \sin\lambda_k \alpha \, \sin\bar{\alpha}_j \eta \right) \right. \\ & \times \left(\sum_{k=1}^{\infty} \sum_{k=1}^{m-1} \frac{4}{m} C_{kj} \, \sin\lambda_k \alpha \, \sin\bar{\alpha}_j \eta \, \sin\lambda_k r \, \sin\bar{\alpha}_j y \right) \\ & - \left(\sum_{j=1}^{\infty} \sum_{k=0}^{m} M_{kj} \, \cos\lambda_k \alpha \, \sin\bar{\alpha}_j \eta \right) \\ & \left. \times \left(\sum_{j=1}^{\infty} \sum_{k=0}^{m} \frac{4}{m} D_{kj} \, \cos\lambda_k \alpha \, \sin\bar{\alpha}_j \eta \, \sin\lambda_k r \, \sin\bar{\alpha}_j y \right) \right] d\eta \end{aligned} \qquad (143a)$$

Using the orthogonality properties of finite and infinite series simplifies this equation as follows

$$w(r,y) = \sum_{j=1}^{\infty} \sum_{k=1}^{m-1} \left(\frac{4}{m} \bar{W}_{kj} \, \bar{C}_{kj} - N_{kj} \, C_{kj} + M_{kj} \, D_{kj} \right) \sin\lambda_k r \, \sin\bar{\alpha}_j y \qquad (143b)$$

Substitution of the series solutions into Equation 141b and use of the

orthogonality properties yields

$$\theta(r,y) = \sum_{j=1}^{\infty} \sum_{k=0}^{m} \left(\frac{4}{m} \bar{W}_{kj}\ \lambda_k\ \bar{C}_{kj} - N_{kj}\ D_{kj} + M_{kj}\ R_{kj}\right) \cos\lambda_k r\ \sin\bar{\alpha}_j y \quad (143c)$$

The series coefficients $\bar{W}_{kj}$, $\bar{C}_{kj}$, C_{kj}, D_{kj}, and R_{kj} are given in Equations 111 and 112.

Equations 143b,c contain three unknown quantities, the coefficients of the plate-stringer interactive force series N_{kj} and M_{kj}, and the coefficients of the symmetric and anti-symmetric side boundary deflection series W_j^s and W_j^a, combined into the single symbol $\bar{W}_{kj}$ by use of Equation 111h.

The discrete continuous fields of stringer top deformations are given by

$$w_s(r,y) = \int_0^b N(r,\eta) K^{wzs}(y,\eta)\, d\eta \quad (144a)$$

$$\theta_s(r,y) = \int_0^b M(r,\eta) K^{\theta\phi s}(y,\eta)\, d\eta \quad (144b)$$

The continuous kernel functions for stringer deformations $K^{wzs}(y,\eta)$ and $K^{\theta\phi s}(y,\eta)$ are given by Equations 134b and 138b. Substitution of these equations and of Equations 142a,b into Equations 144a,b and use of the orthogonality properties yields the following finite-infinite series for the interior out-of-plane stringer top deformations

$$w_s(r,y) = \sum_{j=1}^{\infty} \sum_{k=1}^{m-1} N_{kj}\ \overset{*}{C}_j\ \sin\lambda_k r\ \sin\bar{\alpha}_j y \quad (145a)$$

$$\theta_s(r,y) = - \sum_{j=1}^{\infty} \sum_{k=0}^{m} M_{kj} \overset{*}{R}_j \cos\lambda_k r \sin\bar{\alpha}_j y \tag{145b}$$

Compatibility of plate and stringer top deformations along the stringer center lines provides the solution for the two unknown interactive force coefficients; that is, equating Equations 143b,c and 145a,b and matching coefficients yields

$$[Z_{kj}] \begin{Bmatrix} N_{kj} \\ M_{kj} \end{Bmatrix} = \frac{4}{m} \bar{W}_{kj} \bar{C}_{kj} \begin{Bmatrix} 1 \\ -\lambda_k \end{Bmatrix} \tag{146a}$$

where

$$[Z_{kj}] = \begin{bmatrix} C_{kj} + \overset{*}{C}_j & -D_{kj} \\ -D_{kj} & R_{kj} + \overset{*}{R}_j \end{bmatrix} \tag{146b}$$

and

$$\begin{Bmatrix} N_{kj} \\ M_{kj} \end{Bmatrix} = \frac{4}{m} \frac{\bar{W}_{kj} \bar{C}_{kj}}{|Z_{kj}|} \begin{Bmatrix} R_{kj} + \overset{*}{R}_j - \lambda_k D_{kj} \\ D_{kj} - \lambda_k (C_{kj} + \overset{*}{C}_j) \end{Bmatrix} \tag{146c}$$

The solution for $\bar{W}_{kj}$ is found by expressing the vertical deflections $w(^0_m,y)$ of the boundary stringers in terms of the plate edge shears $P(^0_m,y)$ applied to it. These edge shears consist of the reactions $V^h(^0_m,y)$ due to edge deflections $w^h(^0_m,y)$, and reactions due to the interactive forces, that is

$$P\binom{0}{m},y) = V_x^h\binom{0}{m},y) - \sum_{\alpha=0}^{m} \int_0^b [N(\alpha,\eta)K^{Vz}\binom{0}{m},y, \frac{\ell}{m}\alpha,\eta)$$

$$- M(\alpha,\eta)K^{V\phi}\binom{0}{m},y, \frac{\ell}{m}\alpha,\eta)]d\eta \qquad (147)$$

where $V_x^h\binom{0}{m},y)$, $K^{Vz}\binom{0}{m},y, \frac{a}{m}\alpha,\eta)$ and $K^{V\phi}\binom{0}{m},y, \frac{a}{m}\alpha,\eta)$ are given in Equations 113a, 111e, and 111f.

The deflections of the boundary stringers due to the plate edge shears are

$$w\binom{0}{m},y) = \int_0^b P\binom{0}{m},\eta)K^{wzb}(y,\eta)d\eta \qquad (148)$$

where $K^{wzb}(y,\eta)$ is given by Equations 135a and 136b, modified for boundary stringer properties, that is,

$$C_j^{*b} = \frac{1}{\bar{\alpha}_j^2(B^b\bar{\alpha}_j^2 - P^b)} \qquad (149)$$

Substitution of Equation 147 into Equation 148, expansion of the symmetric and anti-symmetric components, use of the orthogonality properties, and matching like coefficients yields

$$W_j^s[(C_j^{*b})^{-1} - \bar{S}_j^s + \bar{S}_j^{es}] = 0 \qquad (150a)$$

$$W_j^a[(C_j^{*b})^{-1} - \bar{S}_j^a + \bar{S}_j^{ea}] = 0 \qquad (150b)$$

where $\bar{S}_j^s$ and $\bar{S}_j^a$ are given by Equations 113b,c and

$$\bar{S}_j^{es}, \bar{S}_j^{ea} = \sum_{\substack{k=1,3,\ldots \\ k=0,2,\ldots}}^{m} \frac{4}{m} \frac{\bar{C}_{kj}}{|Z_{kj}|} \{[(R_{kj} + \overset{*}{R}_j) - \lambda_k D_{kj}]\bar{C}_{kj}$$

$$- [D_{kj} - \lambda_k (C_{kj} + \overset{*}{C}_j)]Q_{kj}^{\phi}\} \qquad (150c,d)$$

The series coefficient Q_{kj}^{ϕ} is given by Equations 103b and 112.

Buckling Criteria for Simple Side Supports

For the case of simple side supports the solution for the non-composite flexural model is given by Equation 146a, modified for zero deflections, that is, $\bar{W}_{kj} = 0$. The buckling stress is the lowest compressive stress σ, associated with the buckling mode (k,j), for which the determinant of coefficients equals zero, that is

$$|Z_{kj}| = (C_{kj} + \overset{*}{C}_j)(R_{kj} + \overset{*}{R}_j) - D_{kj}^2 = 0 \qquad (151)$$

Buckling Criteria for Beam Boundaries

For this case $\bar{W}_{kj} \neq 0$. The solution is given by Equations 150a,b for arbitrary W_j^s and W_j^a. Both equations must be checked separately for the lowest stress σ, associated with the jth longitudinal buckling mode, that is

$$1 - \overset{*b}{C}_j(\bar{S}_j^s - S_j^{es}) = 0 \qquad (152a)$$

or

$$1 - \overset{*b}{C}_j(\bar{S}_j^a - S_j^{ea}) = 0 \qquad (152b)$$

In contrast to the solution for simple side supports, the buckling mode in the transverse direction cannot be determined except for being either symmetric or anti-symmetric, depending on whether the

lowest buckling stress was obtained From Equation 152a or 152b, which represent summations in the r direction over odd or even values of k respectively.

This completes the theoretical basis for the non-composite flexural stability analysis of a ribbed plate by the macro approach. Numerical examples will be presented in Chapter VI.

3.2 Composite Membrane Analysis

The object of this section is a rational stability analysis of a ribbed plate under uniform longitudinal compression, proportioned and detailed such that the T-beam or composite action between the plate and stringers is significant (see Figure 17). The out-of-plane or flexural stiffness of the plate is negligible, that is, the plate behaves according to membrane theory.

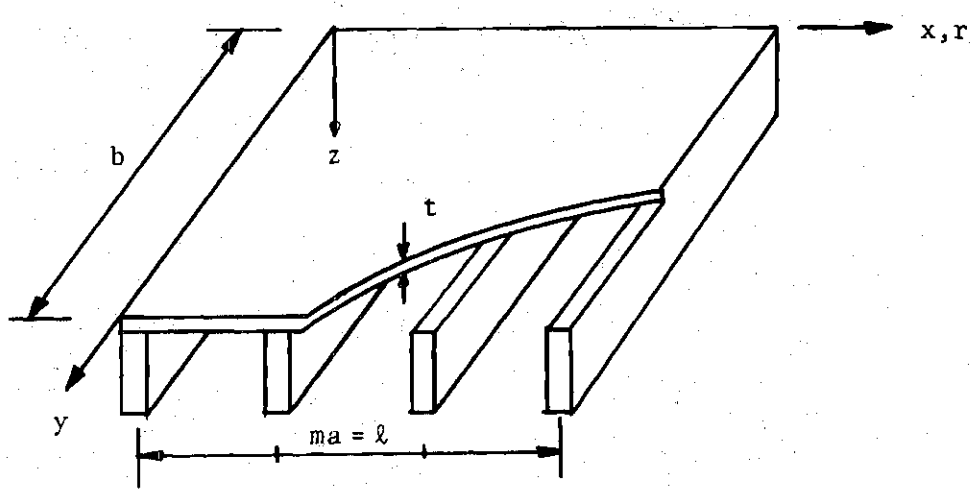

Figure 17. Composite Membrane Model

The composite membrane analysis complements the non-composite flexural analysis and serves as the second step towards the composite

membrane-flexural analysis, the most comprehensive model treated in the following section.

The system components are: (1) the plate, which is subjected to uniform longitudinal compression applied at the ends and to longitudinal and lateral discrete-continuous plate-stringer interactive forces along the rib lines at its lower surface. Its structural action is primarily that of a membrane and admits of treatment by plane stress elasticity theory. The necessary formulas were developed in Chapter IV; (2) the interior ribs, which are subjected to bending about their major and minor axes caused by the distributed plate-stringer longitudinal and lateral interactive forces. The necessary formulas were developed in Chapter IV; and (3) the boundary stringers, which may have properties different from the interior stringers.

Mathematical Model

The approach used for the composite membrane analysis is similar to that used for the non-composite flexural analysis in the previous section. The major differences are that plane stress formulas replace flexural plate formulas and that the plate-stringer interactive forces act in-plane rather than out-of-plane. Because of the conceptual similarities with the non-composite flexural analysis the representation and explanations in this section will be more concise.

The unknown quantities are: (1) the discrete-continuous plate stringer interactive shear forces $Y(r,y)$ and $H(r,y)$; (2) the continuous longitudinal boundary stringer displacements $v(\overset{0}{\ell},y)$ (see Equation 123).

The in-plane plate displacements along the stringer center lines, two dimensional discrete-continuous fields, are given by

$$u(r,y) = u^h(r,y) + \sum_{\alpha=0}^{m} \int_0^b [Y(\alpha,\eta)K^{uy}(\frac{\ell}{m} r,y, \frac{\ell}{m} \alpha,\eta)$$

$$- H(\alpha,\eta)K^{ux}(\frac{\ell}{m} r,y, \frac{\ell}{m} \alpha,\eta)]d\eta \qquad (153a)$$

$$v(r,y) = v^h(r,y) + \sum_{\alpha=0}^{m} \int_0^b [Y(\alpha,\eta)K^{vy}(\frac{\ell}{m} r,y, \frac{\ell}{m} \alpha,\eta)$$

$$- H(\alpha,\eta)K^{vx}(\frac{\ell}{m} r,y, \frac{\ell}{m} \alpha,\eta)]d\eta \qquad (153b)$$

where $u^h(r,y)$, $v^h(r,y)$, $K^{ux}(\frac{\ell}{m} r,y, \frac{\ell}{m} \alpha,\eta)$, $K^{uy}(\frac{\ell}{m} r,y, \frac{\ell}{m} \alpha,\eta)$, $K^{vx}(\frac{\ell}{m} r,y, \frac{\ell}{m} \alpha,\eta)$, $K^{vy}(\frac{\ell}{m} r,y, \frac{\ell}{m} \alpha,\eta)$ are given by Equations 129g,h and 129a-d respectively.

Since the prebuckling deformations are neglected, the terms $u(r,y)$ and $v(r,y)$ represent the additional deformations during buckling.

The series for the interactive shear forces are given by

$$Y(r,y) = \sum_{j=1}^{\infty} \sum_{k=1}^{m-1} Y_{kj} \sin\lambda_k r \cos\bar{\alpha}_j y \qquad (154a)$$

$$H(r,y) = \sum_{j=1}^{\infty} \sum_{k=0}^{m} H_{kj} \cos\lambda_k r \sin\bar{\alpha}_j y \qquad (154b)$$

$$Y_{kj} = \frac{4}{mb} \sum_{\alpha=1}^{m-1} \int_0^b Y(r,y) \sin\lambda_k r \cos\bar{\alpha}_j y \qquad (154c)$$

$$H_{kj} = \frac{4}{mb} \sum_{\alpha=0}^{m} \int_0^b H(r,y) \cos\lambda_k r \sin\bar{\alpha}_j y \qquad (154d)$$

Substitution of the referenced series solutions into Equations 154a,b and use of the orthogonality properties yields

$$u(r,y) = \sum_{j=1}^{\infty} \sum_{k=0}^{m} (\frac{4}{m} \overline{V}_{kj} \overline{A}_{kj} - H_{kj}F_{kj} + Y_{kj}A_{kj})\cos\lambda_k r \sin\overline{\alpha}_j y \tag{155a}$$

$$v(r,y) = \sum_{j=0}^{\infty} \sum_{k=1}^{m-1} \overset{*}{\omega}_j (\frac{4}{m} \overline{V}_{kj} \overline{B}_{kj} - H_{kj}A_{kj} + Y_{kj}B_{kj})\sin\lambda_k r \cos\overline{\alpha}_j y \tag{155b}$$

where the coefficients of the symmetric and anti-symmetric side boundary deflection series V_j^s and V_j^a have been combined into the single symbol $\overline{V}_{kj}$. The coefficients $\overline{V}_{kj}$, $\overline{A}_{kj}$, $\overline{B}_{kj}$, A_{kj}, B_{kj}, F_{kj} are given in Equations 129j, 131f,g,a,b, and c respectively.

The discrete continuous fields of stringer lateral and longitudinal deflections are

$$u_s(r,y) = \int_0^b H(r,\eta)K^{uxs}(y,\eta)d\eta \tag{156a}$$

$$v_s(r,y) = \int_0^b Y(r,\eta)K^{vys}(y,\eta)d\eta \tag{156b}$$

The continuous kernel functions for the stringer deformations $K^{uxs}(y,\eta)$ and $K^{vys}(y,\eta)$ are given by Equations 139 and 135. Substitution of these equations and Equations 154a,b into Equations 156a,b yields the finite-infinite series for the interior in-plane stringer top deformations

$$u_s(r,y) = \sum_{j=1}^{\infty} \sum_{k=0}^{m} H_{kj} \overset{*}{F}_j \cos\lambda_k r \sin\bar{\alpha}_j y \tag{157a}$$

$$v_s(r,y) = - \sum_{j=0}^{\infty} \sum_{k=1}^{m-1} Y_{kj} \overset{*}{B}_j \sin\lambda_k r \cos\bar{\alpha}_j y \tag{157b}$$

The plate-stringer compatibility equations result from equating Equations 155 and 157 and matching like coefficients

$$[X_{kj}] \begin{Bmatrix} H_{kj} \\ Y_{kj} \end{Bmatrix} = \frac{4}{m} \bar{V}_{kj} \begin{Bmatrix} \bar{A}_{kj} \\ -\bar{B}_{kj} \end{Bmatrix} \tag{158a}$$

where

$$[X_{kj}] = \begin{bmatrix} \bar{F}_{kj} + \overset{*}{F}_j & -A_{kj} \\ -A_{kj} & B_{kj} + \overset{*}{B}_j \end{bmatrix} \tag{158b}$$

and

$$\begin{Bmatrix} H_{kj} \\ Y_{kj} \end{Bmatrix} = \frac{4}{m} \frac{\bar{V}_{kj}}{|X_{kj}|} \begin{Bmatrix} (B_{kj} + \overset{*}{B}_j)\bar{A}_{kj} - A_{kj}\bar{B}_{kj} \\ A_{kj}\bar{B}_{kj} - (F_{kj} + \overset{*}{F}_j)\bar{B}_{kj} \end{Bmatrix} \tag{158c}$$

The solution for $\bar{V}_{kj}$ is found by expressing the longitudinal deflections $v(\overset{0}{m},y)$ of the boundary stringers in terms of the longitudinal plate edge shears applied to it. These edge shears consist of the reactions $n^h_{xy}(\overset{0}{m},y)$ due to longitudinal edge deflections and reactions due to the interactive forces $Y(r,y)$ and $H(r,y)$, that is,

$$T(^{0}_{m},y) = n^{h}_{xy}(^{0}_{m},y) + \sum_{\alpha=0}^{m} \int_{0}^{b} [Y(\alpha,\eta)K^{Ty}(^{0}_{m},y, \frac{\ell}{m}\alpha,\eta)$$

$$- H(\alpha,\eta)K^{Tx}(^{0}_{m},y, \frac{\ell}{m}\alpha,\eta)]d\eta \qquad (159)$$

where $n^{h}_{xy}(^{0}_{m},y)$, $K^{Tx}(^{0}_{m},y, \frac{\ell}{m}\alpha,\eta)$, $K^{Ty}(^{0}_{m},y, \frac{\ell}{m}\alpha,\eta)$ are given by Equations 132a, 129e, and 129f respectively. The longitudinal deflections of the boundary stringers due to the plate edge shears are

$$V(^{0}_{m},y) = - \int_{0}^{b} T(^{0}_{m},y)K^{vyb}(y,\eta)d\eta \qquad (160)$$

where $K^{vyb}(y,\eta)$ is given by Equations 135a and 136a, modified for boundary stringer properties, that is,

$$\overset{*b}{B}_{j} = \frac{(e^{b})^{2}}{B^{b}\bar{\alpha}_{j}^{2} - P^{b}} + \frac{1}{\bar{\alpha}_{j}^{2}E^{b}A^{b}} \qquad (161)$$

Substitution of Equation 159 into Equation 160, expansion of the symmetric and anti-symmetric components, use of the orthogonality properties, and matching like coefficients yields

$$V^{s}_{j}\,[(\overset{*b}{B}_{j})^{-1} - \bar{T}^{s}_{j} + \bar{T}^{es}_{j}] = 0 \qquad (162a)$$

$$V^{a}_{j}\,[(\overset{*b}{B}_{j})^{-1} - \bar{T}^{a}_{j} + \bar{T}^{ea}_{j}] = 0 \qquad (162b)$$

where $\bar{T}^{s}_{j}$ and $\bar{T}^{a}_{j}$ are given by Equations 132b,c and

$$\bar{T}^{es}_{j},\bar{T}^{ea}_{j} = \sum_{\substack{k=1,3,\ldots \\ k=0,2,\ldots}}^{m} \frac{4}{m}\{[(B_{kj} + \overset{*}{B}_{kj})\bar{A}_{kj} - A_{kj}\bar{B}_{kj}]T^{x}_{kj}$$

$$- [A_{kj}\bar{A}_{kj} - (F_{kj} + \overset{*}{F}_{j})\bar{B}_{kj}]\bar{B}_{kj}\} \qquad (162c,d)$$

The series coefficient T^x_{kj} is given by Equation 131d.

Buckling Criteria for Simple Side Supports

For the case of simple side supports, the solution for the composite-membrane model is given by Equation 158a, modified for zero loading, that is $\overline{V}_{kj} = 0$. The buckling stress is the lowest stress σ associated with the in-plane buckling mode (k,j), for which the determinant of coefficients equals zero, that is

$$|X_{kj}| = (F_{kj} + \overset{*}{F}_j)(B_{kj} + \overset{*}{B}_j) - A^2_{kj} = 0 \tag{163}$$

Buckling Criteria for Beam Boundaries

For this case $\overline{V}_{kj} \neq 0$. The solution is given by Equations 162a,b for arbitrary V^s_j and V^a_j. Both equations must be checked separately for the lowest stress σ associated with the jth longitudinal in-plane buckling mode, that is

$$1 - \overset{*b}{B}_j(\overline{T}^s_j - \overline{T}^{es}_j) = 0 \tag{164a}$$

or

$$1 - \overset{*b}{B}_j(\overline{T}^a_j - \overline{T}^{ea}_j) = 0 \tag{164b}$$

Again, as in the non-composite flexural analysis, the buckling mode for flexural beam boundaries can only be determined to be symmetric or anti-symmetric.

This completes the theoretical basis for the composite membrane stability analysis of a ribbed plate by the macro analysis. Its solutions will be included in the next section, the composite membrane-flexural analysis and in the numerical examples of Chapter VI.

3.3 Composite Membrane-Flexural Analysis

In this section the analysis will include simultaneously the out-of-plane and in-plane effects considered separately in the two preceding sections. There will be four plate-stringer interactive forces acting along the rib lines and two boundary displacements. Formulas for the composite membrane-flexural analysis include formulas for the non-composite flexural and composite membrane models as special cases. Therefore, the results of this section can be used to establish the range of applicability for the simpler models as well as for the empirical, approximate, and open form methods used by other investigators.

Mathematical Model

The analysis requires the simultaneous solution of the compatibility conditions of the two preceding sections and it will be necessary to refer back to those for definitions and symbols used.

The unknown dependent quantities are: (1) the out-of-plane plate-stringer interactive forces $M(r,y)$ and $N(r,y)$; (2) the in-plane plate-stringer interactive forces $Y(r,y)$ and $H(r,y)$; (3) the out-of-plane vertical boundary stringer deflections $w(^{0}_{m},y)$; and (4) the in-plane longitudinal displacements of the top of the boundary stringers, $v(^{0}_{m},y)$.

The discrete continuous fields of out-of-plane and in-plane plate deformations at the stringer center lines are given by Equations 141a,b and 153a,b. The unknown interactive forces are given by Equations 142a,b and 154a,b, and the kernel function solutions for the plate deformations by Equations 111 and 129.

Substitution of these series solutions into Equations 141 and 153, using orthogonality properties, and matching like coefficients yields Equations 143 and 155, repeated here for clarity

$$w(r,y) = \sum_{j=1}^{\infty} \sum_{k=1}^{m-1} (\frac{4}{m} \overline{W}_{kj} \overline{C}_{kj} - N_{kj} C_{kj} + M_{kj} D_{kj}) \sin\lambda_k r \sin\overline{\alpha}_j y \qquad (143b)$$

$$\theta(r,y) = \sum_{j=1}^{\infty} \sum_{k=0}^{m} (\frac{4}{m} \overline{W}_{kj} \lambda_k \overline{C}_{kj} - N_{kj} D_{kj} + M_{kj} R_{kj}) \cos\lambda_k r \sin\overline{\alpha}_j y \qquad (143c)$$

$$u(r,y) = \sum_{j=1}^{\infty} \sum_{k=0}^{m} (\frac{4}{m} \overline{V}_{kj} \overline{A}_{kj} - H_{kj} F_{kj} + Y_{kj} A_{kj}) \cos\lambda_k r \sin\overline{\alpha}_j y \qquad (155a)$$

$$v(r,y) = \sum_{j=1}^{\infty} \sum_{k=1}^{m-1} (\frac{4}{m} \overline{V}_{kj} \overline{B}_{kj} - H_{kj} A_{kj} + Y_{kj} B_{kj}) \sin\lambda_k r \sin\overline{\alpha}_j y \qquad (155b)$$

The discrete-continuous fields of stringer top deformations for the composite membrane-flexural model include the effects of one in-plane and one out-of-plane interactive force each, in contrast to the simpler models treated in the two preceding sections. They are:

$$u_s(r,y) = \int_0^b [H(r,\eta)K^{uxs}(y,\eta) + M(r,\eta)K^{u\phi s}(y,\eta)]d\eta \qquad (165a)$$

$$v_s(r,y) = \int_0^b [Y(r,\eta)K^{vys}(y,\eta) + N(r,\eta)K^{vzs}(y,\eta)]d\eta \qquad (165b)$$

$$w_s(r,y) = \int_0^b [Y(r,\eta)K^{wys}(y,\eta) + N(r,\eta)K^{wzs}(y,\eta)]d\eta \qquad (165c)$$

$$\theta_s(r,y) = \int_0^b [H(r,\eta)K^{\theta xs}(y,\eta) + MK^{\theta\phi s}(y,\eta)]d\eta \qquad (165d)$$

where the continuous kernel functions for stringer deformations are given in Equations 135 and 139.

Substitution of these equations and of Equations 142 and 154 into Equations 165a-d, use of orthogonality properties, and matching like coefficients yields

$$u_s(r,y) = \sum_{j=1}^{\infty} \sum_{k=1}^{m-1} (H_{kj} \overset{*}{F}_j - M_{kj} \overset{*}{G}_j)\cos\lambda_k r \sin\bar{\alpha}_j y \tag{166a}$$

$$v_s(r,y) = \sum_{j=1}^{\infty} \sum_{k=1}^{m-1} (N_{kj} \overset{*}{D}_j - Y_{kj} \overset{*}{B}_j)\sin\lambda_k r \cos\bar{\alpha}_j y \tag{166b}$$

$$w_s(r,y) = \sum_{j=1}^{\infty} \sum_{k=1}^{m-1} (N_{kj} \overset{*}{C}_j - Y_{kj} \overset{*}{D}_j)\sin\lambda_k r \sin\bar{\alpha}_j y \tag{166c}$$

$$\theta_s(r,y) = \sum_{j=1}^{\infty} \sum_{k=1}^{m-1} (H_{kj} \overset{*}{G}_j - M_{kj} \overset{*}{R}_j)\cos\lambda_k r \sin\bar{\alpha}_j y \tag{166d}$$

The plate stringer compatibility equations are obtained by equating Equations 166 with Equations 143 and 155, which, after arranging in matrix form, yields

$$\begin{bmatrix} F_{kj}+\overset{*}{F}_j & -A_{kj} & 0 & -\overset{*}{G}_j \\ -A_{kj} & B_{kj}+\overset{*}{B}_j & -\overset{*}{D}_j & 0 \\ 0 & -\overset{*}{D}_j & C_{kj}+\overset{*}{C}_j & -D_{kj} \\ -\overset{*}{G}_j & 0 & -D_{kj} & R_{kj}+\overset{*}{R}_j \end{bmatrix} \begin{Bmatrix} H_{kj} \\ Y_{kj} \\ N_{kj} \\ M_{kj} \end{Bmatrix} = \frac{4}{m} \begin{bmatrix} \bar{V}_{kj} & \bar{A}_{kj} \\ -\bar{V}_{kj} & \bar{B}_{kj} \\ \bar{W}_{kj} & \bar{C}_{kj} \\ -\bar{W}_{kj}\lambda_k & \bar{C}_{kj} \end{bmatrix} \tag{167a}$$

where

$$\begin{Bmatrix} H_{kj} \\ Y_{kj} \\ N_{kj} \\ M_{kj} \end{Bmatrix} = \frac{4}{m} \begin{bmatrix} \beta_{11} & \beta_{12} & \beta_{13} & \beta_{14} \\ \beta_{21} & \beta_{22} & \beta_{23} & \beta_{24} \\ \beta_{31} & \beta_{32} & \beta_{33} & \beta_{34} \\ \beta_{41} & \beta_{42} & \beta_{43} & \beta_{44} \end{bmatrix} \begin{Bmatrix} \overline{V}_{kj} & \overline{A}_{kj} \\ -\overline{V}_{kj} & \overline{B}_{kj} \\ \overline{W}_{kj} & \overline{C}_{kj} \\ -\overline{W}_{kj} & \lambda_k \ \overline{C}_{kj} \end{Bmatrix} \tag{167b}$$

$$\begin{bmatrix} \overline{\beta}_{11} & \beta_{12} & \beta_{13} & \beta_{14} \\ \beta_{21} & \beta_{22} & \beta_{23} & \beta_{24} \\ \beta_{31} & \beta_{32} & \beta_{33} & \beta_{34} \\ \beta_{41} & \beta_{42} & \beta_{43} & \beta_{44} \end{bmatrix} = \begin{bmatrix} F_{kj}+\overset{*}{F}_j & -A_{kj} & 0 & -\overset{*}{G}_j \\ -A_{kj} & B_{kj}+\overset{*}{B}_j & -\overset{*}{D}_j & 0 \\ 0 & -\overset{*}{D}_j & C_{kj}+\overset{*}{C}_j & -D_{kj} \\ -\overset{*}{G}_j & 0 & -D_{kj} & R_{kj}+\overset{*}{R}_j \end{bmatrix}^{-1} \tag{167c}$$

The two boundary stringer conditions must be satisfied simultaneously. The out-of-plane and in-plane edge shears $P(^0_m,y)$ and $T(^0_m,y)$ are the same as for the simpler models, Equations 147 and 159. The boundary stringers, however, now are subjected to two interactive forces simultaneously and their deflections $v(^0_m,y)$ and $w(^0_m,y)$ at the top become

$$v(^0_m,y) = \int_0^b [P(^0_m,\eta)K^{vzb}(y,\eta) - T(^0_m,\eta)K^{vyb}(y,\eta)]d\eta \tag{168a}$$

$$w(^0_m,y) = \int_0^b [P(^0_m,\eta)K^{wzb}(y,\eta) - T(^0_m,\eta)K^{wyb}(y,\eta)]d\eta \tag{168b}$$

Substitution of Equations 147, 159 and 135 and 136, modified for boundary rib properties, into Equations 168a,b, expansion of the symmetric and anti-symmetric components, use of the orthogonality properties, matching like coefficients, and solving for W_j^s, V_j^s and W_j^a, V_j^a respectively, yields

$$\begin{bmatrix} L_j^s - \bar{S}_j^s \overset{*b}{C}_j + 1 & X_j^s - \bar{T}_j^s \overset{*b}{D}_j \\ E_j^s - \bar{S}_j^s \overset{*b}{D}_j & Z_j^s - \bar{T}_j^s \overset{*b}{B}_j + 1 \end{bmatrix} \begin{Bmatrix} W_j^s \\ V_j^s \end{Bmatrix} = \begin{Bmatrix} 0 \\ 0 \end{Bmatrix} \tag{169a}$$

and

$$\begin{bmatrix} L_j^a - \bar{S}_j^a \overset{*b}{A}_j + 1 & X_j^s - \bar{T}_j^a \overset{*b}{D}_j \\ E_j^a - \bar{S}_j^a \overset{*b}{D}_j & Z_j^s - \bar{T}_j^a \overset{*b}{B}_j + 1 \end{bmatrix} \begin{Bmatrix} W_j^a \\ V_j^a \end{Bmatrix} = \begin{Bmatrix} 0 \\ 0 \end{Bmatrix} \tag{169b}$$

where the new series coefficients are defined as follows

$$L_j^s, L_j^a = \frac{4}{m} \sum_{\substack{k=1,3,\ldots \\ k=0,2,\ldots}}^{m} \bar{C}_{kj} \{ [(\beta_{13} - \lambda_k \beta_{14}) T_{kj}^x - (\beta_{23} - \lambda_k \beta_{24}) \bar{B}_{kj}] \overset{*b}{D}_j$$

$$+ [\beta_{33} - \lambda_k \beta_{34}) \bar{C}_{kj} - (\beta_{43} - \lambda_k \beta_{44}) Q_{kj}^{\phi}] \overset{*b}{C}_j \} \tag{169c,d}$$

$$X_j^s, X_j^a = \frac{4}{m} \sum_{\substack{k=1,3,\ldots \\ k=0,2,\ldots}}^{m} \{ [(\beta_{11} \bar{A}_{kj} - \beta_{12} B_{kj}) T_{kj}^x - (\beta_{21} \bar{A}_{kj} - \beta_{22} \bar{B}_{kj}) \bar{B}_{kj}] \overset{*b}{D}_j$$

$$+ [(\beta_{31} \bar{A}_{kj} - \beta_{32} \bar{B}_{kj}) \bar{C}_{kj} - (\beta_{41} \bar{A}_{kj} - \beta_{42} \bar{B}_{kj}) Q_{kj}^{\phi}] \overset{*b}{C}_j \} \tag{169e,f}$$

$$E_j^s, E_j^a = \frac{4}{m} \sum_{\substack{k=1,3,\ldots \\ k=0,2,\ldots}}^{m} \overline{C}_{kj}\{[(\beta_{13}-\lambda_k\beta_{14})T_{kj}^x - (\beta_{23}-\lambda_k\beta_{24})\overline{B}_{kj}]\overset{*b}{B}_j$$

$$+ [(\beta_{33}-\lambda_k\beta_{34})\overline{C}_{kj} - (\beta_{43}-\lambda_k\beta_{44})Q_{kj}^{\phi}]\overset{*b}{D}_j\} \qquad (169g,h)$$

$$Z_j^s, Z_j^a = \frac{4}{m} \sum_{\substack{k=1,3,\ldots \\ k=0,2,\ldots}}^{m} [(\beta_{11}\overline{A}_{kj} - \beta_{12}\overline{B}_{kj})T_{kj}^x - (\beta_{21}\overline{A}_{kj} - \beta_{22}\overline{B}_{kj})\overline{B}_{kj}]\overset{*b}{B}_j$$

$$+ [(\beta_{31}\overline{A}_{kj} - \beta_{32}\overline{B}_{kj})\overline{C}_{kj} - (\beta_{41}\overline{A}_{kj} - \beta_{43}\overline{B}_{kj})Q_{kj}^{\phi}]\overset{*b}{D}_j\} \qquad (169i,j)$$

Buckling Criteria for Simple Side Supports

For the case of simple side supports the solution for the composite membrane-flexural model is given by Equation 167a, modified for zero loading, that is $\overline{W}_{kj} = \overline{V}_{kj} = 0$. The buckling stress is the lowest compressive stress σ, associated with the buckling mode (k,j), i.e., for k halfwaves in the transverse, and j halfwaves in the longitudinal direction, for which the determinant of coefficients of the interactive forces equals zero. In terms of the coefficients, the criteria is:

$$|X_{kj}||Z_{kj}| + \overset{*2}{D}_j\overset{*2}{G}_j - \overset{*2}{G}_j(B_{kj} + \overset{*}{B}_j)(C_{kj} + \overset{*}{C}_j)$$

$$- \overset{*2}{D}_j(F_{kj} + \overset{*}{F}_j)(R_{kj} + \overset{*}{R}_j) + 2\overset{*}{D}_j\overset{*}{G}_j A_{kj}D_{kj} = 0 \qquad (170)$$

The coupling of the flexural and membrane actions is through the coefficients $\overset{*}{D}_j$ and $\overset{*}{G}_j$ of the stringer deflection kernel functions,

K^{wy}, K^{vz}, $K^{u\phi}$, and $K^{\theta x}$. For $\overset{*}{D}_j = \overset{*}{G}_j = 0$ the solution reduces to the product of the determinants of the two simpler models and the flexural and membrane actions are uncoupled.

Buckling Criteria for Beam Boundaries

For the most general case of flexible side boundary stringers, the solution is given by Equations 169a,b. For arbitrary $\overline{W}_{kj}$ and $\overline{V}_{kj}$ the determinants equal zero:

$$(L_j^s - \overline{S}_j^s \overset{*b}{C}_j + 1)(Z_j^s - \overline{T}_j^s \overset{*b}{B}_j + 1) - (X_j^s - \overline{T}_j^s \overset{*b}{D}_j)(E_j^s - \overline{S}_j^s \overset{*b}{D}_j) = 0 \tag{171a}$$

$$(L_j^a - \overline{S}_j^a \overset{*b}{C}_j + 1)(Z_j^a - \overline{T}_j^a \overset{*b}{B}_j + 1) - (X_j^a - \overline{T}_j^a \overset{*b}{D}_j)(E_j^a - \overline{S}_j^a \overset{*b}{D}_j) = 0 \tag{171b}$$

Both equations must be checked for buckling into symmetric or anti-symmetric modes k, associated with the jth longitudinal mode.

This completes the theoretical basis for the composite membrane-flexural stability analysis of a ribbed plate by the macro approach. Numerical examples will be presented in Chapter VI.

CHAPTER VI

NUMERICAL ILLUSTRATIONS

Because of the multiple parameters involved, there is an endless number of graphical presentations which would be useful to the practicing designer. Large portions of books (12,13) and several papers (17,18) have been devoted to detailed graphical results of this nature. The lengthy and costly computation time and/or the intimate knowledge of the analysis formulation (especially with regard to approximate schemes), combined with the inherent problem of determining the lowest buckling mode for any ribbed plate related problem, have all contributed to the need for graphical or tabular presentations.

The author feels that the formulas developed by the discrete field stability analyses outlined here will enable designers to efficiently and accurately study ribbed plate buckling behavior without relying on charts or tables. While the computer programs developed in the preparation of this thesis were research programs and not intended to be user oriented, their use could easily be extended for such purposes. The factors leading to this assessment are: (1) the generality of the formulation requiring no program modifications for various boundary conditions, number or properties of ribs, etc.; (2) the efficiency of using formulas which require run times of only a few seconds (Univac 1108 and CDC CYBER 74 computers) for large systems; and (3) the ease of finding the lowest buckling load which requires one run for most cases and at most one additional run for corroborative purposes since the

solutions to the stability equations are not generally sensitive. Therefore, rather than presenting extensive numerical examples, only examples which illustrate the effect of various problem parameters will be shown.

The stability equations used are those for the non-composite flexural and the composite membrane-flexural models. For the case of sides simply supported ribbed plates they are Equations 51a and 86 for the micro approach, and Equations 151 and 171 for the macro approach. For the case of flexible side boundaries the stability equations are Equations 60a,b and 90 for the micro approach and Equations 152a,b and 172a,b for the macro approach. The stability equations that result from the composite membrane analysis were found not to govern in the whole range of problem parameters that were investigated. This was to be expected since ribbed plates always are proportioned such as to buckle out-of-plane, that is, in flexural modes.

The basic input required to solve the stability equations for the lowest buckling load are the geometrical and material properties of the plate and ribs. For the plate these are the dimensions b, ℓ, and t, and the properties E and ν, that is, Young's modulus and Poissons' ratio. By specifying the number of interior ribs, m-1, the rib spacing is determined as $a = \ell/m$. If the ribs are flat strips they may be defined in two ways for the solution by the micro approach, that is, either as plates with one free edge or as ordinary beams. The solution by the macro approach presently only allows for ribs treated as ordinary beams.

Ribs defined as plates require the input of their depth and

thickness, $\bar{a}$ and $\bar{t}$, and their properties $\bar{E}$ and $\bar{\nu}$. Ribs defined as ordinary beams may have any shape and they are defined by their cross-sectional area, Young's modulus, moment of inertia about major and minor axes, torsional stiffness, and eccentricity of their shear center from the stiffener top. For the case of beam side boundaries the boundary ribs properties may be different from those of the interior ribs.

In the research programs used to generate numerical examples, loops were specified for ranges of j and k, the number of halfwaves of the buckling modes in the longitudinal and transverse directions, to be searched for the lowest K_{cr}. That is, lower and upper limits, along with particular values, were given as input data for j and k. This can be readily done by the engineer with knowledge of the limits associated with unstiffened plate buckling behavior. For flexible beam boundaries only the longitudinal modes, j, need to be specified since each value of j is associated with just two solutions, symmetric and anti-symmetric, for transverse buckling modes.

The number of longitudinal modes j to be searched theoretically extends from one to the integer nearest the panel aspect ratio b/a. However, for torsionally stiff ribs one or more additional modes should be searched. The number of modes k to be investigated in the transverse direction for the sides simply supported case extends the whole range from 1 to m. The roots K_{cr} for $k > m$ are greater than or equal to the results for $1 \leq k \leq m$.

For the case of simple side supports the total number of possible buckling modes increases geometrically with increasing number of panels

m, and increasing panel aspect ratios, b/a. However, a pattern can easily be established in trial runs for the range of j-k combinations that yields the lowest roots K_{cr}. For most of the parameter combinations presented in Figures 19-24, the buckling occurred either in or near the local configuration, i.e., $j = b/a \pm 1$, $k = m$, or in the overall mode $j = k = 1$. Attention is called to the fact that there is almost always a sudden transition from the (near) local to the overall mode, or vice versa, for gradual changes in one or more of the problem parameters. Therefore, these two basic modes should always be investigated.

An efficient method of establishing the range for the governing buckling mode is to hold j fixed and vary k over the whole range $1 \leq k \leq m$ (or vice versa). For an arbitrary set of problem parameters the lowest K_{cr} (j,k) for a number of buckling modes (j,k) is plotted in Figure 18. The values K_{cr} corresponding to some fixed longitudinal modes, j, are connected by dotted lines for clarity. For each j there exists a lowest value for K_{cr}, that is, $K_{cr}(j) = \min K_{cr}(j,k)$ for some k. This value of k was observed to remain constant over a large range of j, that is, the pattern of the dotted lines in Figure 18 changes only slightly for each new value of j. Therefore, it is sufficient to check only the $K_{cr}(j)$, in addition to the overall buckling modes. It was also found that the buckling pattern will remain fairly constant over large ranges of the problem parameters.

All numerical results for the critical buckling stress are plotted in terms of K_{cr} which is defined as

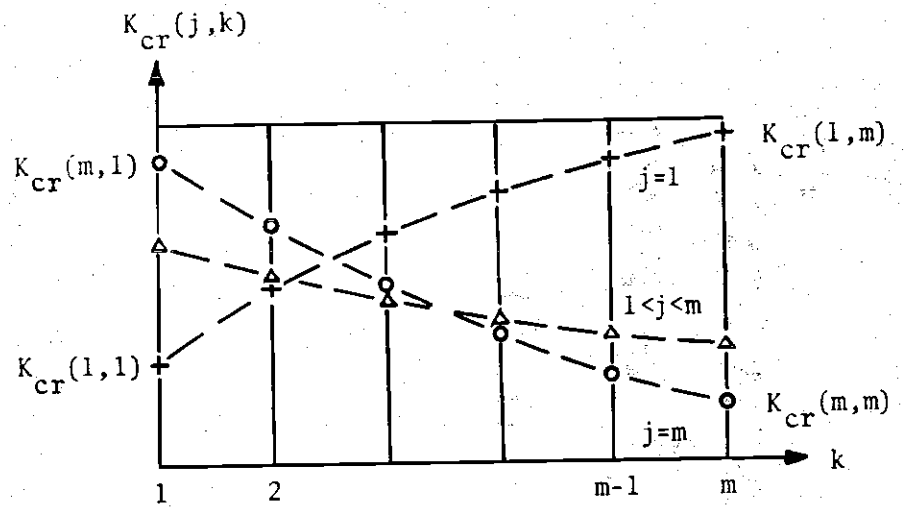

Figure 18. Buckling Coefficient K_{cr} as a Function of the Buckling Modes (j,k) for Simple Side Supports

$$K_{cr} = \sigma_{cr} \frac{a^2 t}{\pi^2 D} \tag{172}$$

that is, the buckling coefficient for the ribbed plate is directly related to the buckling coefficient for an unstiffened rectangular plate of width "a". It should be recalled that for a simply supported unstiffened plate the buckling coefficient has a minimum value of 4. Expressing the buckling coefficient K_{cr} in terms of the panel width "a" clearly defines the range of K_{cr}. Since the largest possible buckling load for a panel with both side boundaries fixed is well known, see Timoshenko (19), a safe upper limit of max $K_{cr} = 10$ can be established. The lower limit on K_{cr} is zero, since for overall buckling of systems with weak beam boundaries and large aspect ratios column type buckling will govern, that is, the results are closely approximated by an Euler hyperbola.

For the case of flexible beam boundaries an upper limit for K_{cr} is established by the solution for the simple side support case. The solution to the stability equations involves summations over all odd k for symmetric and all even k for anti-symmetric buckling modes. The number of possible buckling modes for beam boundaries, therefore, is smaller than for simple side supports, whenever the number of panels is greater than two. For plates stiffened by many ribs and having small aspect ratios b/ℓ the influence of the side boundaries is small. The results for flexible boundaries will closely approach those for simple supports.

For every combination of j and k there will be an infinite

number of roots, of which only the lowest is of interest here. The lowest root K_{cr} for any combination of j and k is found by trial and error, starting with K = 0 and increasing K by initially fixed increments ΔK. The lowest root will either fall in the range $0 < K < 10$ or be of no interest when higher than 10. The stability functions for the sides simply supported cases are continuous over the whole range from K equals zero to K equals K_{cr}. A routine has been developed to search for sign changes in this function and then establishing constantly increasing lower and decreasing upper bounds on K until K_{cr} has been determined to any desired degree of accuracy.

The stability function for the case of beam boundaries exhibits vertical asymptotes at the roots for the sides simply supported plate. Since these asymptotes may fall very close to the roots, special routines must be used to detect the asymptotes and avoid iterations up to the second or higher roots.

While the routines necessary to locate the lowest buckling load are the same for both the micro and the macro approaches, there is a marked difference in the routines that compute the coefficients of the stability equations. For the micro approach closed form expressions are used throughout. However, the various coefficients often contain stiffness parameters for plate, interior, and boundary ribs simultaneously. Great care was necessary to correctly organize the computer program in order to keep these terms distinct. For the macro approach some of the major expressions in the stability equations are not available in closed form but have to be numerically evaluated by separate routines. It was found, however, that most of these open

form expressions converge rapidly and that the final results for the buckling load can be determined to the same degree of accuracy and as efficiently as for the micro solution.

Extensive comparisons of the numerical results for the micro and macro analyses revealed that the solutions are identical. The curves presented in Figures 19-24 were first developed using the micro analysis solutions and then verified by the solutions for the macro analysis. The micro stability equations were programmed and run on the Univac 1108 computer using double precision (16 significant digits) to avoid possible sensitivities due to the transcendental terms in the stiffness coefficients of the boundary force-deformation relations. These sensitivities only occur for the case of flexible side supports and only for particular combinations of problem parameters.

The macro stability equations were programmed and run on the CDC CYBER 74 computer using single precision (14 significant digits). The convergence of the open form summations in the transformation of doubly infinite to finite-infinite series (Equations 109 and 110) was very good with but one exception (Equation 103). Even for the most numerically sensitive case of very few ribs, i.e., for small m, the finite series terms were sufficiently accurate after summing only 10 to 20 terms. Sufficient accuracy is defined here as three significant digits for the buckling coefficient.

The convergence for Q^{ϕ}_{kj} is very slow and requires up to and over 1000 terms depending on the selection of the ratio c/ℓ (see Figure 13). The exact value of Q^{ϕ}_{kj} is approached from above for decreasing ratios c/ℓ with satisfactory results obtained for $c/\ell \approx 1/50$

and about 100 terms used in the summation. Selecting smaller ratios c/ℓ also requires using more terms in order for the summation of Q^{ϕ}_{kj} to stabilize.

For the case of rectangular stiffeners the solutions for stiffener response were obtained by using two methods, the flat plate panel with one free edge and the ordinary beam theory. In general, the results for the flat plate panel are slightly lower than those for ordinary beams. However, since in many cases stiffeners will not be of rectangular shape, the ordinary beam theory solutions were used for all figures except Figure 24, in which solutions for the two stiffeners are compared to each other.

The solutions for the non-composite flexural model correspond to the classical solutions available for simple side supports. Except for Wah (20), rib torsional stiffness was not included by other investigators. Its inclusion increases the buckling loads appreciably. The buckling for torsionally stiff ribs occurs in longitudinal half-waves that are shorter than the stiffener spacing. The effect of flexible beam boundaries is clearly demonstrated even with the simple non-composite flexural model. Whenever the buckling occurs in the overall mode and the aspect ratio $b/\ell > 1$, the loss of buckling load due to flexible side boundaries is substantial. For increased rib stiffnesses the buckling occurs in local or near local modes and the effect of flexible beam boundaries is reduced.

The composite membrane analysis yields solutions for the buckling load that are far above those for the flexural model in all practical cases. Its main purpose is to provide an intermediate step for the

solution to the higher order model.

The results for the composite membrane-flexural model show several effects that cannot be obtained by lower order models. Most pronounced is the effect of stiffener eccentricity. It is seen that the effective stiffener moment of inertia cannot be taken about an axis at the rib-plate juncture. Rather, the effective stiffener eccentricity decreases with increasing width-to-thickness ratio. The optimum stiffener design calls for large values for the bending stiffnesses about both axes and for the torsional rigidity, whereas the cross-sectional area should be kept as small as possible.

In the presentation of the numerical results the following ratios of problem parameters were used for all figures:

$$\gamma = \frac{\overline{EA\rho^2}}{aD} \quad ; \quad \delta = \frac{\overline{A}}{at} \quad ; \quad \tau = \frac{\overline{GJ}}{aD} \qquad (173a,b,c)$$

$$\gamma^b = \frac{(\overline{EA\rho^2})^b}{aD} \quad ; \quad \delta^b = \frac{\overline{A}^b}{at} \qquad (173d,e)$$

that is, the individual rib properties are related to those of a plate strip of width a, the rib spacing.

Figure 19 shows the effect of plate aspect ratios b/ℓ and of flexible beam boundaries. For reasons of comparison to the classical simple side support solution, the effects of torsional rigidity and eccentricity were neglected. As long as the aspect ratio remains well below unity, local buckling controls, independent of the side boundary supports. The curve for K_{cr} displays the typical wave pattern for buckling into different modes with a minimum value for K_{cr} of 4.

For larger aspect ratios overall buckling governs. The ribs are no longer stiff enough to remain straight and buckle with the plate. The classical solution for simple side supports still displays a wave pattern, however, and its results are identical with the solutions given by Klöppel (12), Seide (18), and Wah (20).

For flexible side boundaries the wave pattern is maintained only for very stiff boundary ribs. For increasing plate aspect ratios and for weak boundary ribs the buckling curves approach the typical Euler hyperbola.

Another illustration of the effect of beam boundaries is given in Figure 20. As expected the results for simple side supports and for beam boundaries differ most for small values of γ but become nearly identical for large γ's near the transition from overall to local buckling. Note that for cases where local buckling controls, the boundary conditions do not influence K_{cr}. Further increases in major axis bending stiffness, I_z, after local buckling modes govern, will not increase the buckling load.

When large bending stiffnesses about the minor axis, I_x, are included, buckling will occur in the overall mode up to much higher values of γ than for negligible I_x, that is, the transition from overall to local buckling modes is shifted towards higher values of γ. This is accompanied by substantial increases in the buckling coefficient K_{cr}.

Figure 20 also illustrates the effect of stiffener eccentricity. For both the simple support and beam boundary case, K_{cr} is increased substantially over the concentrically placed stiffener case until local

buckling controls. Then K_{cr} is higher for the concentric stiffeners than for the eccentric ones. Since the major axis moment of inertia, I_z, and the eccentricity, $\bar{e}$, are independent input parameters one can determine the effective moment of inertia which will be smaller than if taken about an axis through the top of the rib, that is, $I_{eff} < I_z + \bar{A}\bar{e}^2$. For a better illustration of that reduction see Figure 21.

Figure 21 assumes ribs of rectangular shape, that is, the ribs are described by their depth and thickness alone. While the thickness is held constant the depth is increased gradually from $\bar{a} = a/6$ to $\bar{a} = a$. On the left hand side of the curves the transition is shown from buckling in the overall mode to local buckling. While the eccentricity, $\bar{e}$, for a rectangular rib is equal to one-half of its depth, the effective moment of inertia, I_{eff}, is less than assumed in the classical approximation. The upper curve is based on the input for I_{eff} computed as $I_{eff} = I_z + \bar{A}(\bar{a}/2)^2$, that is, about the top of the stiffener. The lower curve is based on inputs of I_z and $\bar{e} = \bar{a}/2$ as independent quantities. For increasing rib depths, or depth-to-thickness ratios, the actual effect of eccentricity results in a sharply reduced K_{cr}. The classical solution thus greatly overestimates the effect of rib bending stiffness. The exact solution presented in this dissertation can, therefore, be used to determine the actual effect of eccentricity.

Figures 22 and 23 deal with the effect of rib torsional rigidity. The cross-sectional area is held constant in both figures. The bending stiffness is also constant in Figure 22 but varies in Figure 23. There

is a marked increase of K_{cr} for high ratios of τ in the case of simple side supports. As seen from Figure 22 this increase is only moderate for the case of beam boundaries. Figure 23, with the area held constant, shows the effect of varying depth-to-thickness ratios. For small $\bar{a}$, that is, small ratios $\bar{a}/\bar{t}$, the increase in K_{cr} for the inclusion of the torsional rigidity is substantial. This effect is reduced for increasing ratios $\bar{a}/\bar{t}$. More important, however, is the associated reduction of the effective moment of inertia.

Figure 24 well demonstrates the advantages of the solutions presented here for plates with many ribs. For reasons of comparison rectangular ribs were used with the total rib area and the rib thickness held constant, i.e., $m\bar{A}$ and $\bar{t}$ equal constants, while the number of ribs was varied. The ribs were treated utilizing both ordinary beam theory and plate theory. Since the rib thickness and the total area are fixed an increase in the number of ribs corresponds to a reduction of rib depth and bending stiffness. Ordinary beam theory and plate theory differ most for large depth-to-thickness ratios (few ribs), while yielding nearly identical results for small depth-to-thickness ratios (many ribs). The overall load carrying capacity of the plate is proportional to m^2K_{cr}. This quantity has a marked peak which indicates the optimum number of ribs. For the parameters chosen and for m up to and including the peak value, the plate buckles in local or near-local modes. The ribs thus represent nodal lines and the longitudinal half-waves are equal to or slightly greater than the rib spacing. For m greater than the peak values, the plates buckle in the overall mode with one half-wave in each direction.

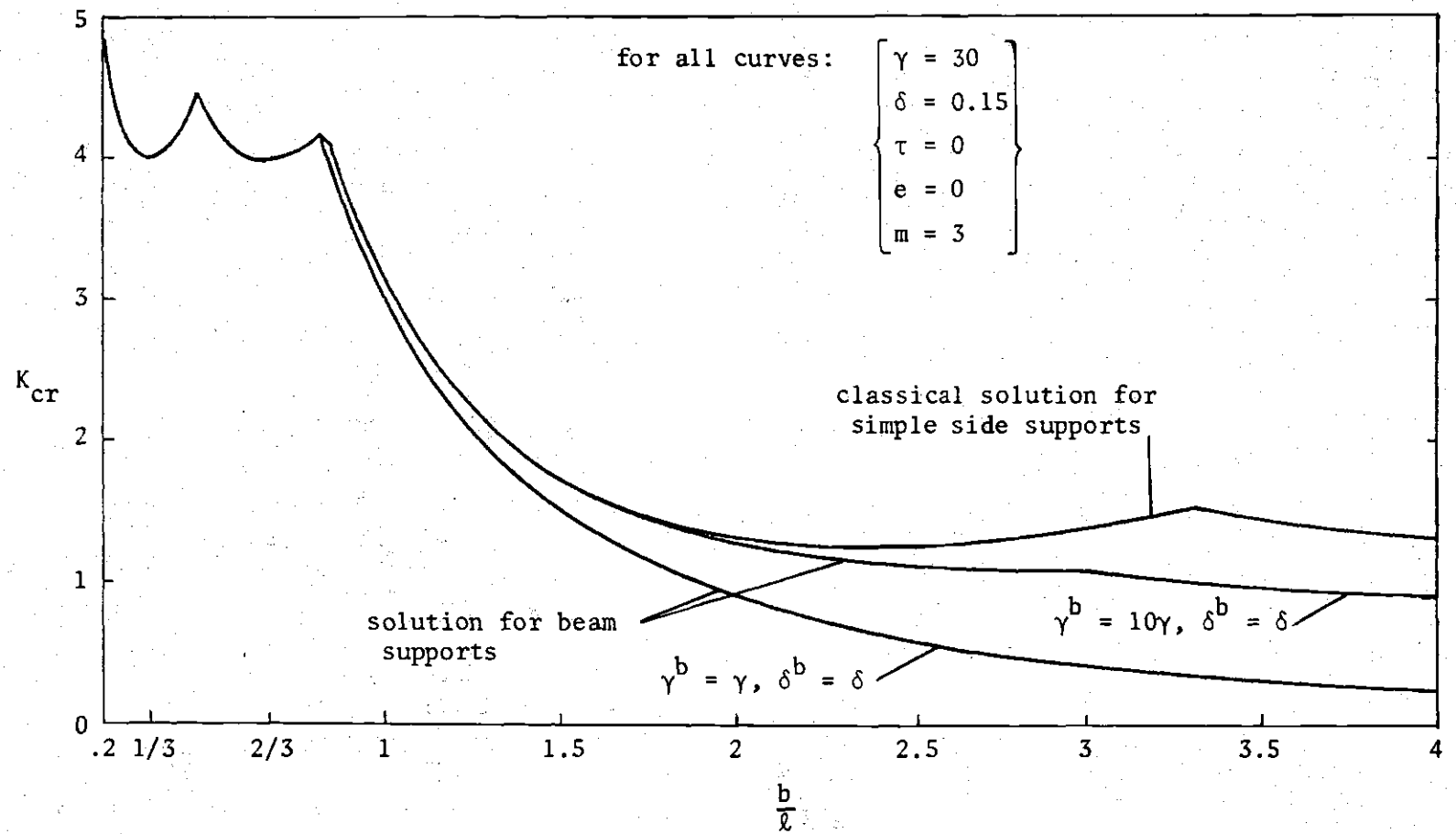

Figure 19. Classical Solution for Simple Side Supports and for Varying Beam Boundaries

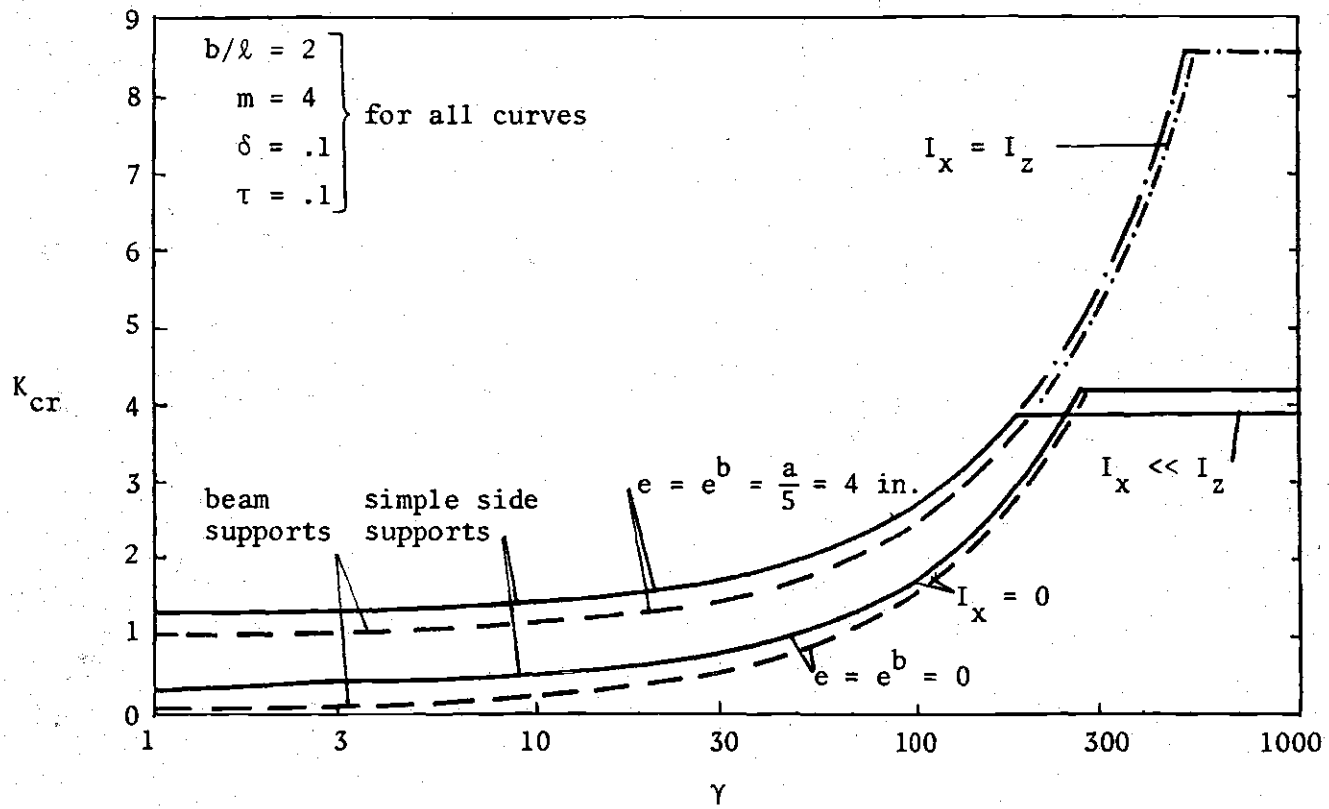

Figure 20. Effect of Boundary Conditions, Stiffener Eccentricity, and Lateral Bending Stiffness

$\bar{t} = t/2 = .5$ in.

$m = 2$

$b/\ell = 1$

$a = 30$ in.

$e = \bar{a}/2$

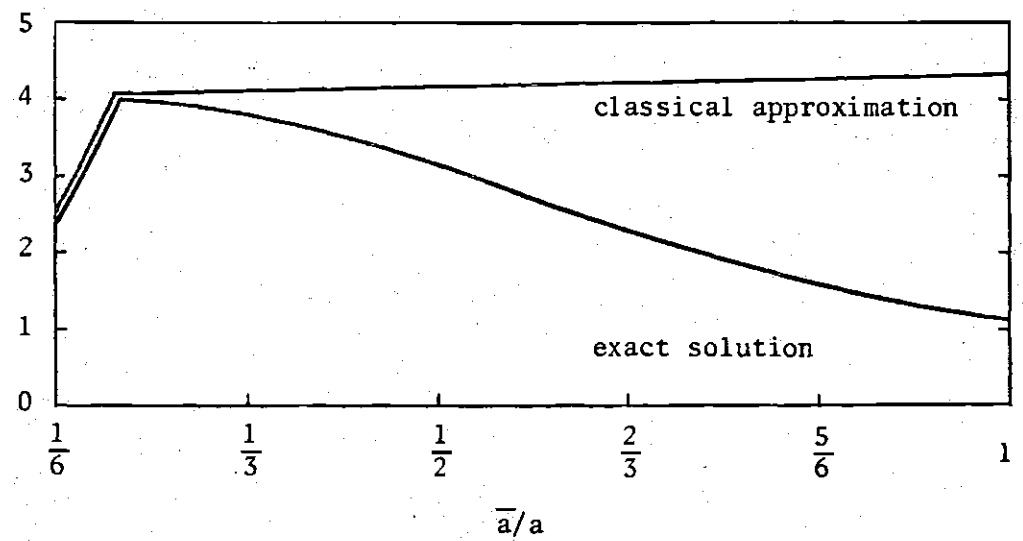

Figure 21. Effect of Rib Eccentricity for Rectangular Stiffeners of Varying Depth and Simple Side Supports

$m = 4$

$b/\ell = 2$

$\delta = \delta^b = 0.1$

$\gamma = \gamma^b = 100$

$\tau^b = \tau/2$

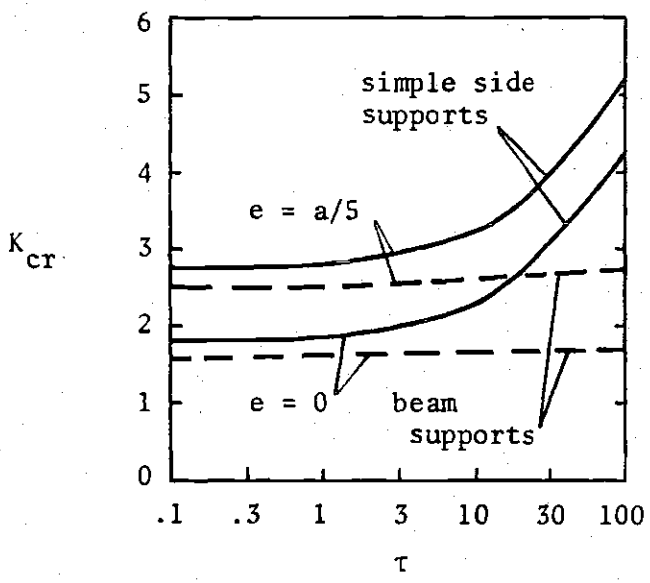

Figure 22. Effects of Rib Torsional Rigidity and Eccentricity

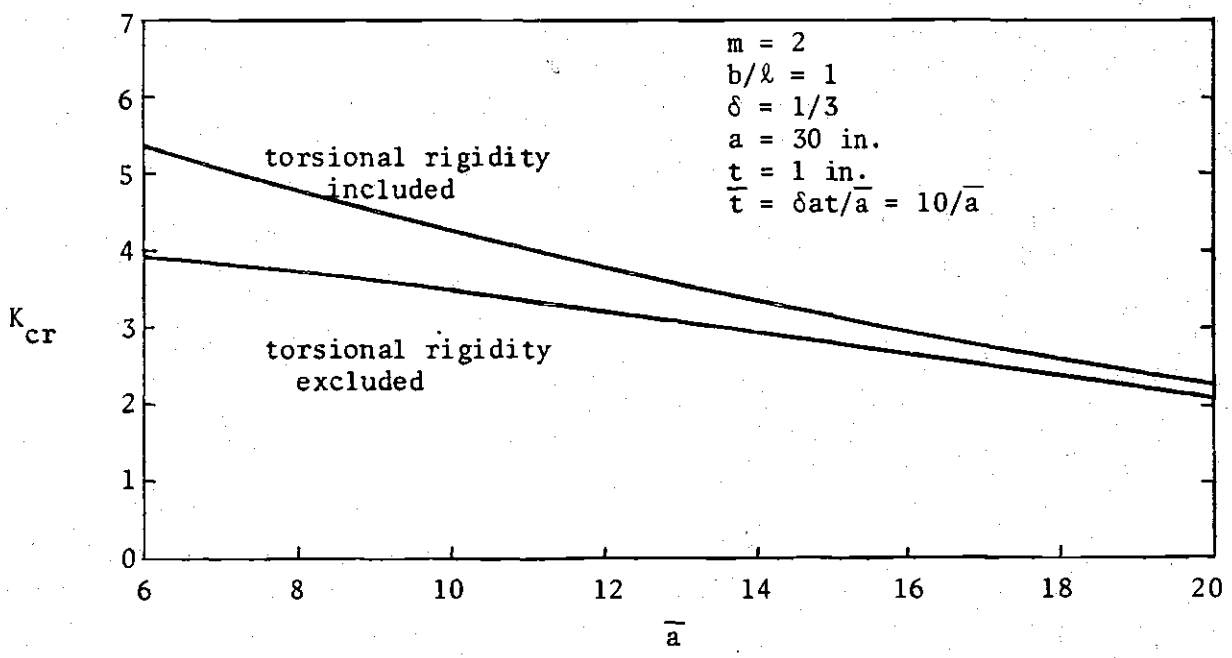

Figure 23. Influence of Torsional Rigidity and Depth-to-Thickness Ratio for Rectangular Stiffeners and Simple Side Supports

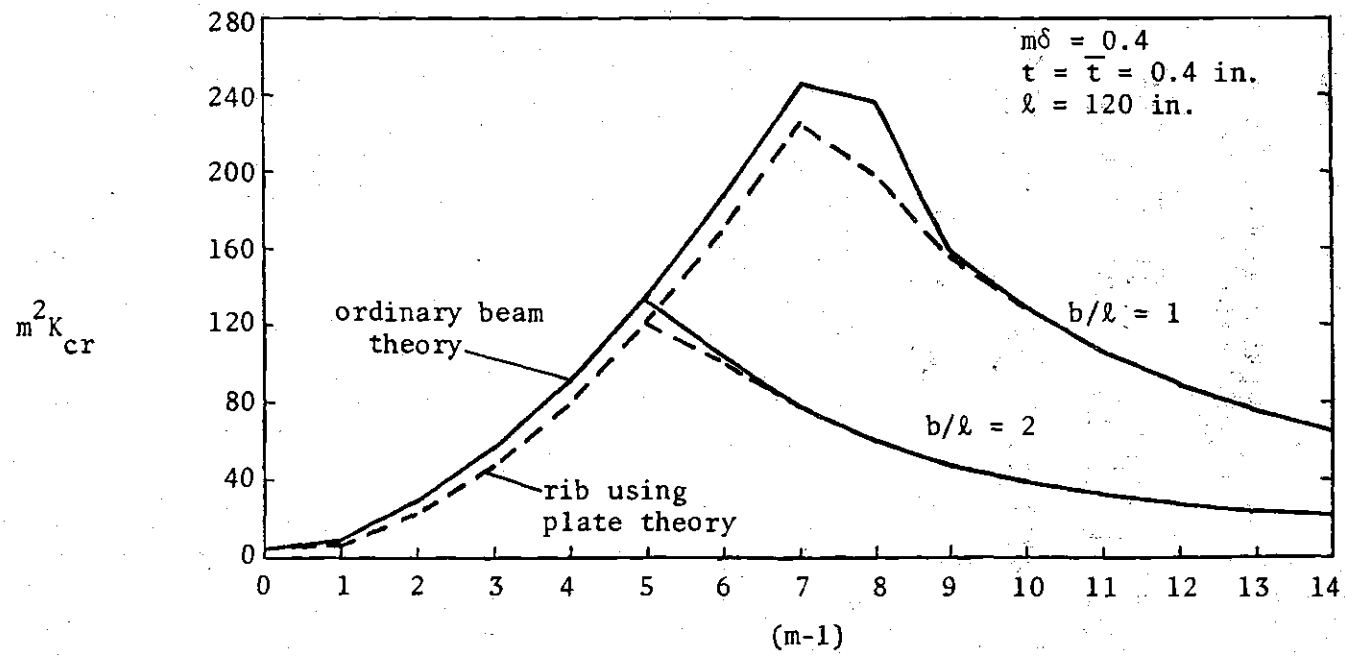

Figure 24. Effect of the Number of Stiffeners (m-1) with Total Stiffener Area Held Constant and Simple Side Supports

The results of discrete field stability analysis were also used in comparisons to several laboratory tests by other investigators, for example to tests conducted by Dubas (9), see Table 1. For most ribbed plate designs the elastic-plastic material properties and the post-buckling strength will have some effect on the initial and ultimate buckling load. Dubas suggested to use separate design criterias for the buckling of ribbed plates, one for the initial buckling and another for the ultimate strength. Since linear elastic theory was used in this dissertation it must be expected that its result will best predict initial buckling, but with marked improved accuracy over previously available methods.

The tests prepared by Dubas used flat strip stiffeners and very deep and strong boundary ribs. Theoretical results based on simple side supports and on beam boundaries therefore are nearly identical. The loads were applied in pure bending to the overall system, resulting in practically uniform compression across the plate and rib depth. Since the ultimate stresses were not published in (9) but only the corresponding ultimate moments, a theoretical ultimate stress was computed, using linear stress distribution across the depth of the boundary beams, for reasons of comparison to the stresses obtained from the discrete field stability equations. These two stresses are shown in columns 12 and 13 of Table 1. Column 14 shows the stresses obtained by Dubas in his linear elastic analysis. Very stiff ribs were used for tests A1 and B1 that force the plate into local buckling. The higher ultimate stress reflexts post-buckling strength. Tests A2 and B2, with weak ribs, yield much lower buckling stresses. The plates

Table 1. Comparison of Test Results to Results of the Discrete Field Stability Analysis

(a) Plate and Rib Properties (units mm)

1	2	3	4	5	6	7	8	9
Test	b	ℓ	m	a	t	$\bar{a}$	$\bar{t}$	γ
A1	900	800	4	200	3.2	60	2.9	87
A2	900	800	4	200	3.3	37	3.3	21
B1	900	600	3	200	4.0	77	3.8	165
B2	900	600	3	200	4.0	37	3.1	15

(b) Measured and Computed Stresses (units tons/cm^2)

10	11	12	13	14
Test	Yield Stress	Ultimate Stress	σ_{cr} by Author	σ_{cr} by Dubas (9)
A1	2.95	2.28	1.95	1.95
A2	3.0	1.47	1.64	1.87
B1	2.9	2.79	2.85	2.50
B2	2.9	1.78	1.63	1.82

buckle in the overall mode. The linear theory in (9) overpredicts both results. The discrete field stability analysis serves as a much better model. It predicts the result for test A2 much better and actually underestimates the strength of test plate B2.

CHAPTER VII

CONCLUSIONS

Two discrete field methods of analysis are presented for determining critical buckling loads of ribbed plate systems. The analysis includes eccentric stiffeners, flexural and membrane plate behavior, general boundary conditions on two opposite sides, and complete interaction between plate and ribs. Infinite-finite Fourier series solution forms are utilized to generate stability equations whose forms are independent of the number of ribs in the system. The stability equations are solved by an incremental load procedure which is efficient and generally not numerically sensitive.

Two methods of analysis are used, the micro and the macro approaches. In the micro analysis, equilibrium of the plate-rib juncture element is considered and leads to sets of difference equations after early uncoupling of the continuous and discrete variables. In the macro analysis, compatibility of deformations at the rib lines with the rib deformations is used in arriving at sets of summation-integral equations. Both methods lead to identical results. Closed form solutions are found for all coefficients of the series solutions for deformations in the micro analysis but only for some of the corresponding coefficients in the macro analysis. However, the convergence of the open form summations is generally very good.

The simple model of the non-composite flexural analysis serves to illustrate the classical solutions to the ribbed plate stability

problem and also serves as a preliminary step toward the more complex composite membrane-flexural model. This last model can be used to measure the validity of the simpler model treated here as well as the approximate and numerical solutions used by other investigators.

Numerical results illustrate to what extent flexible side supports reduce the buckling load, that the effective eccentricities of the ribs depend on their shape, and that the torsional and lateral rigidities have pronounced effects on the buckling loads. The solution forms presented here are attractive alternatives to approximate analyses since the only assumptions utilized are those associated with linear elastic behavior. In addition, the analyses and the solution techniques are no more complex than approximate solutions which involve replacing the actual system by an equivalent continuum. The procedures outlined here were also found to be computationally efficient with computer time being an order of magnitude less for small systems and several orders of magnitude less for large systems when compared to open form simultaneous equation approaches. The macro solution for the side simply supported case and for the simpler flexural model is so compact and numerically insensitive that it is believed that the buckling loads can be found using only programmable desk-top calculators.

It is believed that the analyses presented here are the first general discrete field stability analyses for any type of ribbed plate or other discrete two-dimensional structure and that they will have applications in many areas of structural analysis.

APPENDIX A

LIST OF SYMBOLS

A, B, B'	rib area and flexural rigidity about major and minor axis
A^b, B^b	boundary rib area and flexural rigidity about major axis
a, b	panel dimensions
$\bar{a}, \bar{a}^b$	depth of rib and boundary panels
$\overset{*}{A}_{ij}, \overset{*}{B}_{ij}, \overset{*}{C}_{ij}, \overset{*}{D}_{ij}, \overset{*}{F}_{ij}$	coefficients of continuous kernel functions for plate
$A_{kj}, B_{kj}, C_{kj}, D_{kj}, F_{kj}$	coefficients of discrete kernel functions for plate
$\overset{\pm}{A}_{ij}, \overset{\pm}{B}_{ij}, \overset{\pm}{C}_{ij}$	coefficients of continuous homogeneous solutions for plate
$\bar{A}_{kj}, \bar{B}_{kj}, \bar{C}_{kj}$	coefficients of discrete homogeneous solutions for plate
$\overset{*}{B}_j, \overset{*}{C}_j, \overset{*}{D}_j, \overset{*}{F}_j, \overset{*}{G}_j, \overset{*b}{B}_j, \overset{*b}{D}_j$	coefficients for continuous kernel functions for ribs and boundary ribs
$b_{11} - b_{22}$	plate panel membrane stiffness coefficients
$\overset{*}{C}_i, \overset{*}{C}'_i, \overset{*}{E}_{ij}$	coefficients of continuous homogeneous solutions for plate
$c_{11} - c_{12}$	rib panel membrane stiffness coefficients
$D, \bar{D}$	flexural plate panel and rib panel stiffness coefficients
$\underset{\sim}{D}_x, \underset{\sim}{D}_y$	differential operators
$\bar{D}_{kj}$	series parameter
$d_{11} - d_{22}$	plate panel flexural stiffness coefficients

E, E^b	Young's modulus for interior and boundary ribs
$E_j^s, E_j^a, L_j^s, L_j^a$	special boundary coefficients
e, e^b	eccentricity of interior and boundary ribs
$e_{11} - e_{22}$	rib panel flexural stiffness coefficients
F_j	membrane stress function
f_x, f_y	applied in-plane plate forces
GJ	torsional rigidity
$H(r,y), H_{kj}$	plate-stringer interactive lateral force and coefficient
I, i, j, k	series indices
I_j, I_j', J_j	constants in plate solution
$K, \overline{K}$	membrane plate and rib panel stiffness coefficients
K_{cr}	ribbed plate buckling coefficient
$K^{ux}, K^{uy}, K^{vx}, K^{vy}$ $K^{wz}, K^{w\phi}, K^{\theta z}, K^{\theta\phi}$	plate and membrane kernel functions for displacements
$K^{uxs}, K^{u\phi s}, K^{vys}, K^{vzs}$ $K^{wys}, K^{wzs}, K^{\theta xs}, K^{\theta\phi s}$	rib kernel functions for displacements
$K^{Tx}, K^{Ty}, K^{Vx}, K^{Vy}$	plate kernel functions for edge force resultants
$L_{\ell n}, L_{\ell n}^f, L_{\ell n}^m$	solution matrix coefficients
ℓ	plate width
$M(r,y), M_{kj}$	plate-stringer interactive moment and coefficient
$M_j, M_j', \overline{M}_j$	coefficients of plate and rib boundary moments
$m-1$	number of interior ribs
m_x, m_y, m_{xy}	plate panel stress resultants
$m_1 - m_4$	plate panel solution arguments
N	plate panel axial compressive stress resultant
$N(r,y), N_{kj}$	plate-stringer interactive normal force and coefficient

$N_j, N'_j, \bar{N}_j$	coefficients of plate and rib boundary forces
n_x, n_y, n_{xy}	plate panel stress resultants
n^h_{xy}	in-plane boundary shear resultant for homogeneous solution
P, P^b	axial compression resultant on interior and boundary rib
$P(0,y), P(\ell,y)$	resultant out-of-plane edge shear
$\overset{*z}{Q}_{ij}, \overset{*\phi}{Q}_{ij}, Q^z_{kj}, Q^\phi_{kj}$	coefficients of continuous and discrete kernel functions of plate boundary shear
$q, \overset{*}{q}_{ij}$	out-of-plane load and coefficient
$\overset{*}{R}_{ij}, R_{kj}$	coefficient for continuous and discrete kernel function for plate
$\overset{*}{R}_j$	coefficient for continuous kernel function for rib
$R_{\ell m}$	beam boundary solution coefficients
r	discrete coordinate axis numbering rib lines
$S_j, S'_j, \bar{S}_j$	coefficients of plate and rib out-of-plane shears
$\overset{*}{\bar{S}}_{ij}, \bar{S}_{kj}$	homogeneous plate shear coefficients
$\bar{S}^s_j, \bar{S}^a_j, \bar{S}^{es}_j, \bar{S}^{as}_j$	coefficients of out-of-plane boundary shear
$T_j, T'_j, \bar{T}_j$	coefficients of plate and rib in-plane shears
$\overset{*x}{T}_{ij}, \overset{*y}{T}_{ij}, T^x_{kj}, T^y_{kj}$	coefficients of continuous and discrete kernel functions for plate
$\overset{*}{T}_{ij}, T_{kj}$	membrane shear coefficients
$\overset{*}{\bar{T}}_{ij}, \bar{T}_{kj}$	homogeneous membrane shear coefficients
$\bar{T}^s_j, \bar{T}^a_j, \bar{T}^{es}_j, \bar{T}^{ea}_j$	coefficients of in-plane boundary shear
$T(0,y), T(\ell,y)$	resultant in-plane edge shears
$t, \bar{t}, \bar{t}^b$	thickness of plate panel, rib and boundary rib
u_s, v_s, w_s, θ_s	displacements of ribs
u, U_j, U_{jk}	displacement x or r direction and coefficients

$U_i^t, U_i^v, U_{ik}^v, U_i^w, U_{ik}^w$	coefficients of x direction displacements
v, V_j, V_{jk}	displacement in y direction and coefficients
$V_j^t, V_j^v, V_{jk}^v, V_j^w, V_{jk}^w$	coefficients of y direction displacements
V_x^h	out-of-plane boundary shear resultant for homogeneous solution
$V_j^s, V_j^a, \overline{V}_{ij}, \overline{V}_{kj}$	coefficients of in-plane boundary displacement
w, W, W_k	displacements in z direction and coefficients
$W^t, W^v, W_k^v, W^w, W_k^w$	coefficients of z direction displacement
$W_j^s, W_j^a, \overline{\overline{W}}_{ij}, \overline{W}_{kj}$	coefficients of out-of-plane boundary displacement
$X_j^s, X_j^a, Z_j^s, Z_j^a$	special boundary coefficients
x_{kj}, Z_{kj}	coefficient determinants
x, y, z	continuous coordinates
$Y(r,y), Y_{kj}$	plate-stringer interactive shear force and coefficient
α, β	discrete load coordinates
$\alpha_i, \overline{\alpha}_j, \beta_j$	plate series solution arguments
$\beta_{11} - \beta_{44}$	coefficients in membrane-flexural macro analysis
γ_j, γ_j'	ribbed plate coefficients
γ, δ, τ	ratios of rib bending stiffness, cross section area, and torsional stiffness
δ_i^α	Kronecker delta function, discrete impulse function
$\delta(x-\xi)$	Dirac delta function, continuous impulse function
ε	strain due to compressive stress σ
ϵ_j, ϵ_j'	beam boundary solution coefficients
ζ, ψ	plate panel solution coefficients
η_j, η_j'	ribbed plate coefficients

$\theta, \theta_j, \theta_{jk}$	plate panel rib line rotation and coefficients
$\theta_j^t, \theta_j^v, \theta_{jk}^v, \theta_j^w, \theta_{jk}^w$	coefficients of rib line rotations
λ, ϕ	plate strain coefficients
λ_j, λ_k	series parameters
ν	Poisson's ratio
ξ, η	continuous impulse load coordinates
π	standard ratio
ρ, ρ^b	radius of gyration of interior and boundary ribs
σ	plate compressive stress
σ_k	parameter in finite series
τ_j, τ_j'	ribbed plate coefficients
ϕ	coordinate for rib line moments and rotations
$\omega_j, \omega_k, \omega_r$	weighting functions
Δ_r, ∇_r	first forward and backward difference operators
$\boxtimes_r, \boxminus_r$	second central difference and mean operators

APPENDIX B

SUMMATION OF INFINITE SERIES

In the discrete field macro analysis the deformations and side boundary shears of flexural plates and membranes are expressed as doubly infinite series. These series then have to be transformed into finite-infinite series valid only at the rib lines. The necessary transformations are defined by Equations 109 and 110. The basic relation between coefficients of finite-infinite and doubly infinite series is

$$F_{kj} = \sum_{I=-\infty}^{\infty} \overset{*}{F}_{2Im+k,j} \tag{174}$$

For ease, speed, and accuracy of calculation it is desirable to find closed form expressions for the infinite series on Equation 172. For the approximate membrane kernel function coefficients, that is Equations 128a-i, it is possible to perform these summations, as will be shown in this appendix.

The basic equation used for the summations on I is given by Jolley (10, Equation 858), that is,

$$\sum_{n=-\infty}^{\infty} \frac{1}{(n+x)^2 + y^2} = \frac{\pi}{y} \frac{\sinh 2\pi y}{\cosh 2\pi y - \cos 2\pi x} \tag{175a}$$

Other important infinite summations required for the transformation of doubly infinite into finite-infinite series can be obtained through

partial derivatives of both sides of Equation 175a Using the results from these partial derivatives, the following three infinite summations can be written

$$\sum_{-\infty}^{\infty} \frac{1}{[(n+x)^2 + y^2]^2} = \frac{\pi}{2y}\left[\frac{\sinh 2\pi y}{y(\cosh 2\pi y - \cos 2\pi x)} - 2\pi \frac{1 - \cosh 2\pi y \cos 2\pi x}{(\cosh 2\pi y - \cos 2\pi x)^2}\right] \tag{175b}$$

$$\sum_{-\infty}^{\infty} \frac{(n+x)y}{[(n+x)^2 + y^2]^2} = \pi^2 \frac{\sinh 2\pi y \sin 2\pi x}{(\cosh 2\pi y - \cos 2\pi x)^2} \tag{175c}$$

$$\sum_{-\infty}^{\infty} \frac{(n+x)^3}{[(n+x)^2 + y^2]^2} = \frac{\pi}{2} \frac{\sin 2\pi x}{\cosh 2\pi y - \cos 2\pi x}\left(2 - \frac{2\pi y \sinh 2\pi y}{\cosh 2\pi y - \cos 2\pi x}\right) \tag{175d}$$

Transformations of Coefficients

All summations follow the same basic pattern of rewriting the infinite series coefficients in order for them to conform to one of the Equations 175a-d.

Summation of $\overset{*}{A}_{kj}$

The coefficient $\overset{*}{A}_{ij}$ is defined in Equation 128b as

$$\overset{*}{A}_{ij} = \frac{1+\nu}{K(1-\nu)} \frac{\alpha_i \bar{\alpha}_j}{(\alpha_i^2 + \phi\lambda\bar{\alpha}_j^2)^2} \tag{176a}$$

therefore A_{kj} is obtained by use of Equation 174 from

$$A_{kj} = - \frac{1+\nu}{K(1-\nu)} \frac{m}{a} \sum_{I=-\infty}^{\infty} \frac{\alpha_{2Im+k} \bar{\alpha}_j}{(\alpha_{2Im+k}^2 + \phi\lambda\bar{\alpha}_j^2)^2} \tag{176b}$$

Substitution of $\alpha_{2Im+k} = (2Im+k)\frac{\pi}{a}$, division by $\sqrt{\phi\lambda}$, and division of enumerator and denominator by appropriate powers of $2m\pi/a$ yields

$$A_{kj} = - \frac{1+\nu}{K(1-\nu)} \frac{m}{a} \left(\frac{a}{2m\pi}\right)^2 \frac{1}{\sqrt{\phi\lambda}} \sum_{-\infty}^{\infty} \frac{(I + \frac{k}{2m}) \sqrt{\phi\lambda} \frac{a}{2m\pi} \bar{\alpha}_j}{[(I + \frac{k}{2m})^2 + (\sqrt{\phi\lambda} \frac{a}{2m\pi} \bar{\alpha}_j)^2]^2} \tag{176c}$$

By setting $x = \frac{k}{2m}$ and $y = \sqrt{\phi\lambda} \frac{a\bar{\alpha}_j}{2\pi m}$ Equation 176c will have the same form as Equation 173c and A_{kj} can be written as

$$A_{kj} = - \frac{1+\nu}{K(1-\nu)} \frac{a}{4m\sqrt{\phi\lambda}} \frac{\sinh 2\pi y \sin 2\pi x}{(\cosh 2\pi y - \cos 2\pi x)^2} \tag{176d}$$

Introducing the parameters $\lambda_j = 2\pi y = \sqrt{\phi\lambda} \frac{a\bar{\alpha}_j}{m}$ and $\bar{D}_{kj} = \cosh\lambda_j - \cos\lambda_k$ where $\lambda_k = 2\pi x = \frac{k\pi}{m}$ as defined in Equation 48b, the final form for A_{kj} will be

$$A_{kj} = \frac{-a(1+\nu)}{4(1-\nu)mK\bar{D}_{kj}^2 \sqrt{\phi\lambda}} \sinh\lambda_j \sin\lambda_k \tag{176e}$$

Summation of $\overset{*}{B}_{ij}$

The coefficient $\overset{*}{B}_{ij}$ is defined in Equation 128c as

$$\overset{*}{B}_{ij} = \frac{1}{K(1-\nu)} \frac{2\alpha_i^2 + (1-\nu)\lambda^2\bar{\alpha}_j^2}{(\alpha_i^2 + \phi\lambda\bar{\alpha}_j^2)^2} \tag{177a}$$

which can be written as

$$\overset{*}{B}_{ij} = \frac{1}{K(1-\nu)} \left\{ \frac{2}{\alpha_i^2 + \phi\lambda\bar{\alpha}_j^2} - \frac{[2 - (1-\nu)\frac{\lambda}{\phi}]\phi\lambda\bar{\alpha}_j^2}{(\alpha_i^2 + \phi\lambda\bar{\alpha}_j^2)^2} \right\} \tag{177b}$$

Proceeding in the same manner as in the summation of $\overset{*}{A}_{ij}$ and using Equations 175a for the first term and 175b, multiplied by $[2 - (1-\nu)\frac{\lambda}{\phi}]\phi\lambda\bar{\alpha}_j^2$, for the second term of Equation 177b yields

$$B_{kj} = \frac{a}{4(1-\nu)m\bar{K}\bar{D}_{kj}} \left\{ [2 + (1-\nu)\frac{\lambda}{\phi}] \frac{\sinh\lambda_j}{\lambda_j} \right.$$

$$\left. + [2 - (1-\nu)\frac{\lambda}{\phi}] \frac{1 - \cosh\lambda_j \cos\lambda_k}{\bar{D}_{kj}} \right\} \tag{177c}$$

Summation of $\overset{*}{F}_{ij}$

The coefficient $\overset{*}{F}_{ij}$ is defined in Equation 128d as

$$\overset{*}{F}_{ij} = \frac{1}{K(1-\nu)} \frac{(1-\nu)\alpha_i^2 + 2\phi^2\bar{\alpha}_j^2}{(\alpha_i^2 + \phi\lambda\bar{\alpha}_j^2)^2} \tag{178a}$$

which is rewritten as

$$\overset{*}{F}_{ij} = \frac{1}{K(1-\nu)} \left[\frac{1-\nu}{\alpha_i^2 + \phi\lambda\bar{\alpha}_j^2} - \frac{(1-\nu-2\frac{\phi}{\lambda}\bar{\alpha}_j^2)}{(\alpha_i^2 + \phi\lambda\bar{\alpha}_j^2)^2} \right] \tag{178b}$$

From here on the summation of $\overset{*}{F}_{ij}$ follows the same steps as the summation of $\overset{*}{B}_{ij}$ with the result

$$F_{kj} = \frac{a}{4(1-\nu)mK\overline{D}_{kj}} \left[(1-\nu+2\ \frac{\phi}{\lambda})\ \frac{\sinh\lambda_j}{\lambda_j} + (1-\nu-2\ \frac{\phi}{\lambda})\ \frac{1 - \cosh\lambda_j\ \cos\lambda_k}{\overline{D}_{kj}} \right] \tag{178c}$$

Summation of T^{*x}_{ij}

The coefficient T^{*x}_{ij} is defined in Equation 128e as

$$T^{*x}_{ij} = \frac{\overline{\alpha}_j(\phi^2\overline{\alpha}_j^2 - \nu\alpha_i^2)}{(\alpha_i^2 + \phi\lambda\overline{\alpha}_j^2)^2} \tag{179a}$$

which is rewritten as

$$T^{*x}_{ij} = \frac{\phi(\phi+\nu\lambda)\overline{\alpha}_j^2}{(\alpha_i^2 + \phi\lambda\overline{\alpha}_j^2)^2} - \frac{\nu\overline{\alpha}_j}{\alpha_i^2 + \phi\lambda\overline{\alpha}_j^2} \tag{179b}$$

Using Equation 175b, multiplied by $\phi(\phi+\nu\lambda)\overline{\alpha}_j^2$, for the first part and Equation 175a, multiplied by $\nu\overline{\alpha}_j$, for the second part of Equation 179b, and then following the same steps as outlined in the summations above, yields

$$T^{x}_{kj} = \frac{\lambda_j}{4\sqrt{\phi\lambda}\ \overline{D}_{kj}} \left[(\frac{\phi}{\lambda} - \nu)\ \frac{\sinh\lambda_j}{\lambda_j} - (\frac{\phi}{\lambda} + \nu)\ \frac{1 - \cosh\lambda_j\ \cos\lambda_k}{\overline{D}_{kj}} \right] \tag{179c}$$

Summation of T^{y}_{ij}

The coefficient T^{y}_{ij} is defined in Equation 128f as

$$\overset{*y}{T}_{ij} = \frac{\alpha_i\{\alpha_i^2 - \frac{1}{2}[1+\nu-(1-\nu)\lambda^2]\bar{\alpha}_j^2\}}{(\alpha_i^2 + \phi\lambda\bar{\alpha}_j^2)^2} \tag{180a}$$

which is rewritten as

$$\overset{*y}{T}_{ij} = \frac{\alpha_i^3}{(\alpha_i^2 + \phi\lambda\bar{\alpha}_j^2)^2} - \frac{1}{2}[1+\nu-(1-\nu)\lambda^2]\frac{\alpha_i\bar{\alpha}_j^2}{(\alpha_i^2 + \phi\lambda\bar{\alpha}_j^2)^2} \tag{180b}$$

Using Equation 175d and Equation 175c multiplied by $\frac{1}{2}[1+\nu-(1-\nu)\lambda^2]\bar{\alpha}_j$, for the first and second parts of Equation 180b respectively, yields

$$T^y_{kj} = \frac{\sin\lambda_k}{4\bar{D}_{kj}}\left\{2 - [1 + \frac{1+\nu-(1-\nu)\lambda^2}{2\phi\lambda}]\frac{\lambda_j \sinh\lambda_j}{\bar{D}_{kj}}\right\} \tag{180c}$$

The coefficients $\bar{A}_{kj}$ and $\bar{B}_{kj}$ follow directly from T^x_{kj} and T^y_{kj}.

Summation of $\overset{*}{\bar{T}}_{ij}$

The coefficient $\overset{*}{\bar{T}}_{ij}$ is defined in Equation 128i as

$$\overset{*}{\bar{T}}_{ij} = \frac{\bar{\alpha}_j^2 K}{(\alpha_i^2 + \phi\lambda\bar{\alpha}_j^2)^2}[\frac{1-\nu}{2}\phi^2(1-\lambda^2)\bar{\alpha}_j^2 - (\phi^2 - \nu^2)\alpha_i^2] \tag{181a}$$

which can be written as

$$\overset{*}{\bar{T}}_{ij} = [\phi\lambda(\phi^2 - \nu^2) + \frac{1-\nu}{2}\phi^2(1-\lambda^2)]K\frac{1}{(\alpha_i^2 + \phi\lambda\bar{\alpha}_j^2)^2}$$

$$- (\phi^2 - \nu^2)K\frac{\bar{\alpha}_j^2}{\alpha_i^2 + \phi\lambda\bar{\alpha}_j^2} \tag{181b}$$

Using Equations 175a and 175b, multiplied by the appropriate factors, for the two terms of Equation 181b yields

$$\overline{T}_{kj} = \frac{-mK\lambda_j^2}{4a\phi\lambda\overline{D}_{kj}} \{[\phi^2 - \nu^2 - \frac{1-\nu}{2}\frac{\phi}{\lambda}(1-\lambda^2)] \frac{\sinh\lambda_j}{\lambda_j}$$

$$+ [\phi^2 - \nu^2 + \frac{1-\nu}{2}\frac{\phi}{\lambda}(1-\lambda^2)] \frac{1 - \cosh\lambda_j \cos\lambda_k}{\overline{D}_{kj}} \} \qquad (181c)$$

BIBLIOGRAPHY

1. Barbré, R., "Stabilität Gleichmässig Gedrückter Rechteckplatten mit Längs-und Quersteifen," Ingenieur-Archiv, Vol. 8 (1937), pp. 117.

2. Bleich, F., Buckling Strength of Metal Structures, McGraw-Hill, New York (1952).

3. Bounin, D., "Buckling of Ribbed Plates," thesis presented to the Georgia Institute of Technology, in 1971, in partial fulfillment of the requirements for the degree Master of Science in Civil Engineering.

4. Dean, D. L., Discrete Field Analysis of Structural Systems, Lecture notes of a short course sponsored by the International Centre for Mechanical Sciences, Udine, Italy (1973).

5. Dean, D. L. and Abdel-Malek, R. A., "Rational Analysis of Orthotropic Bridge Decks," International Journal of Mechanical Sciences, Pergamon Press, Vol. 16, 1974, pp. 173-192.

6. Dean, D. L. and Avent, R. R., "Analysis of Metal Plate-Stringer-Diaphragm Bridge Decks, Intl. Assn. for Bridge and Structural Engineering, Vol. 35-I, 1975, pp. 45-64.

7. Dean, D. L. and GangaRao, H. V. S., "Macro Approach to Discrete Field Analysis," Jr. of the Engrg. Mech. Div., ASCE, Vol. 96, No. EM4, Proc. Paper 7463, August 1970, pp. 377-394.

8. Dean, D. L., Omid'varan, C., "Analysis of Ribbed Plates," Journal of the Structural Division, ASCE, Vol. 95 (March, 1969), pp. 411-440.

9. Dubas, Pierre, "Versuche über das überkritische Verhalten längsversteifter Kastenträger," Berichte der Arbeitskommissionen der IVBH, Band 11, Seminar London, 1971, pp. 367.

10. Jolley, L. B. W., Summation of Series, Dover Publications, Inc., New York, 1961.

11. Kapur, K. K., Hartz, B. J., "Stability of Plates Using the Finite Element Method," Journal of the Engineering Mechanics Division, ASCE, Vol. 92, (April 1966), p. 177.

12. Klöppel, K., Scheer, J., Beulwerte Ausgesteifter Rechteckplatten, Vol. 1, Wilhelm Ernst u. Sohn, Berlin (1960).

13. Klöppel, K., Scheer, J., Beulwerte Ausgesteifter Rechteckplatten, Vol. 2, Wilhelm Ernst u. Sohn, Berlin (1968).

14. Lee, D. N., "Analysis of Flat Plate Continuous Over Column Supports," thesis presented to North Carolina State Univ., in 1969, in partial fulfillment of the requirements for the degree Master of Science.

15. Lokshin, A. S., "On Calculation of Plates with Ribs," Journal of Applied Mathematics and Mechanics, 1st Series, Vol. 2, (1935), pp. 225-240, Moscow (in Russian).

16. Pflüger, A., "Zum Beulproblem der Anistropen Rechteckplatte," Ingenieur-Archiv, Vol. 16, (1947), pp. 111.

17. Ratay, R. T., "Buckling of Simply Supported Stiffened Compression Panels," ASCE National Structures Engineering Meeting, Preprint No. 2272, (April, 1974).

18. Seide, P., "The Effect of Longitudinal Stiffeners Located on One Side of a Plate on the Compressive Buckling Stress of the Plate-Stiffener Combination," NACA TN 2873 (January, 1953).

19. Timoshenko, S. P., Gere, J. M., Theory of Elastic Stability, McGraw Hill, New York, 2nd edition (1961).

20. Wah, T., "Buckling of Longitudinally Stiffened Plates," Aeronautical Quarterly, (February, 1967), pp. 85-99.

21. Wittrick, W. H., "A Unified Approach to the Initial Buckling of Stiffened Panels in Compression," Aeronautical Quarterly, Vol. 19, (August, 1968), pp. 265.

VITA

The author was born on June 12, 1942 in Stuttgart, Germany. He graduated from high school in 1961 and from the University of Stuttgart in 1968 with the degree Dipl.-Ing. in civil engineering. He then worked as a structural engineer.

In September, 1969 the award of a graduate research assistantship enabled him to continue his education at the Georgia Institute of Technology where he received his Master of Science in Civil Engineering in 1971.

Employed again as a structural engineer in 1972, the author continued his studies for the doctoral degree at the Georgia Institute of Technology.

In 1969 he married Miss Irina Mende of Stuttgart. They have two children, Lars and Yvonne.

He is a member of the society of Sigma Xi and an associate member of the American Society of Civil Engineers.